AD

USAAVLABS TECHNICAL REPORT 65-82

A THEORY FOR PREDICTING THE ROTATIONAL NOISE OF LIFTING ROTORS IN FORWARD FLIGHT, INCLUDING A COMPARISON WITH EXPERIMENT

By

R. G. Loewy

L. R. Sutton

January 1966

U. S. ARMY AVIATION MATERIEL LABORATORIES

FORT EUSTIS, VIRGINIA

CONTRACT DA 44-177-AMC-204(T)

ROCHESTER APPLIED SCIENCE ASSOCIATES, INC.

ROCHESTER, NEW YORK

Disclaimers

The findings in this report are not to be construed as an official Department of the Army position unless so designated by other authorized documents.

When Government drawings, specifications, or other data are used for any purpose other than in connection with a definitely related Government procurement operation, the United States Government thereby incurs no responsibility nor any obligation whatsoever; and the fact that the Government may have formulated, furnished, or in any way supplied the said drawings, specifications, or other data is not to be regarded by implication or otherwise as in any manner licensing the holder or any other person or corporation, or conveying any rights or permission, to manufacture, use, or sell any patented invention that may in any way be related thereto.

Disposition Instructions

Destroy this report when no longer needed. Do not return it to originator.

DEPARTMENT OF THE ARMY
U. S. ARMY AVIATION MATERIEL LABORATORIES
FORT EUSTIS, VIRGINIA 23604

This report has been reviewed by the U. S. Army Aviation Materiel Laboratories and is considered to be technically sound. The report is published for the exchange of information and the stimulation of ideas.

Task 1P121401A14801
Contract DA 44-177-AMC-204(T)
USAAVLABS Technical Report 65-82
January 1966

A THEORY FOR PREDICTING THE ROTATIONAL NOISE OF LIFTING ROTORS IN FORWARD FLIGHT, INCLUDING A COMPARISON WITH EXPERIMENT

RASA Report 65-10

by

Robert G. Loewy
Lawrence R. Sutton

Prepared by

Rochester Applied Science Associates, Inc.
Rochester, New York

for

U. S. ARMY AVIATION MATERIEL LABORATORIES
FORT EUSTIS, VIRGINIA

ABSTRACT

A theory and resultant calculations are presented, predicting the noise generated by a lifting rotor in forward flight. With suitable adjustments in parameters, this theory reproduced (by numerical integration) the closed form results of Garrick and Watkins in their investigation of noise produced by a propeller. The theory presented here accounts for (1) asymmetry of inflow, lift, and drag; (2) non-linear section characteristics, compressibility, and reverse flow; (3) first harmonic and steady rigid blade flapping and pitching; (4) rotor shaft tilt; and (5) chordwise distribution of lift and drag forces. Sound pressure levels were evaluated for up to 20 harmonics at a general field point translating with the rotor hub, for the H-34 and HU-1 helicopters. A comparison with experiment is also presented.

PREFACE

This program was conducted by Rochester Applied Science Associates, Inc., under Contract DA 44-177-AMC-204(T) and was carried out under the technical cognizance of Mr. John E. Yeates, U. S. Army Aviation Materiel Laboratories, Fort Eustis, Virginia. The principal investigator, at RASA, was Dr. Robert G. Loewy; associated with him was Mr. Lawrence R. Sutton. The RASA subcontractor for machine computation was Scientific Calculations, Inc. Mr. H. Sternfeld, of the Vertol Division, Boeing Company, provided a special narrow-band sound spectrum analysis for use in the comparison of theory and test.

CONTENTS

ILLUSTRATIONS

SYMBOLS

a, d, f, g, l	pulse shape variables, see Fig. 4
a_{oi}, a_{mi}, b_{mi}	normalized Fourier coefficients of general pulse shape
ASL	aerodynamic section loading, i.e. force normal to the blade chord per unit span
B	number of blades in the rotor
C	velocity of sound, ft/sec
C_i	blade chord at radius station i, ft
$C_i' = C_i \cos\theta_i$	steady part of the projection of blade chord on the swept surface
C_N or $C_{N_{ij}}$	blade element normal force coefficient at source point ij
$C_{L_{ij}}, C_{D_{v_{ij}}}, C_{D_{w_{ij}}}, C_{D_{ij}}$	coefficients of lift, incompressible drag, compressibility drag, total drag at source point ij
$c_{m_i}, d_{m_i}, e_{m_i}$	amplitude coefficients of Fourier cosine series for lift, incompressible drag, compressibility drag, at radius station i
$db = 20 \log_{10} \frac{P_{rms}}{P_{ref}}$	where $P_{ref} = 0.0002$ dyne/cm^2
e	flapping hinge offset, ft
$F_{m_{x,y,z_{ij}}}$	complex amplitude of force acting on the fluid in the x,y, z direction, at the frequency of the m^{th} harmonic, at the source point ij
$f_i, \bar{f}_i, \bar{\bar{f}}_i, \bar{\bar{\bar{f}}}_i$	normalized pulse shape at radial station i, in general, for lift, for incompressible drag, for compressibility drag

$i = \sqrt{-1}$	imaginary number
k or $k_m = \frac{mB\Omega}{C}$	inverse of wave length of m^{th} harmonic
$L_{ij}, D_{v_{ij}}, D_{w_{ij}}, D_{ij}$	lift, incompressible drag, compressible drag, total drag acting on incremental span length at source point ij
m	harmonic number
$M = \frac{V}{C}$	Mach number
$M_{ij} = \frac{V_{ij}}{C}$	Mach number of a blade element at source point ij
n	maximum number of azimuthal increments
P	sinusoidally varying pressure
$P_{\omega,m}$	complex amplitude of pressure sinusoidally varying at frequency ω or harmonic m
q	blade twist angle, radians, per fraction of blade length from flap hinge to tip, positive when decreasing with increasing radius
r_i	blade radius at station i, measured from shaft axis along unflapped blade
R	total rotor radius, ft
R_e	indicates the operation of taking the real part
S or S_{ij}	amplitude radius, see Eq 2a
t	time, sec, measured from $\psi_j=0$
T	fundamental period, sec
U_{ij}	resultant relative air velocity perpendicular to a blade leading edge at source point ij

U_p	component of U_{ij} perpendicular to the swept surface, positive up
U_T	component of U_{ij} tangent to the swept surface
v	averaged induced velocity assumed constant over the rotor, positive down
V	aircraft velocity
x,y,z or x_{ij},y_{ij},z_{ij}	coordinates of "source points" at radial station i, azimuthal station j, in a translating Cartesian system with origin at the center of the rotor, see Fig. 1
x_o,y_o,z_o	coordinates of "field points" in the same translating Cartesian system as defines the "source point" locations
α_{ij}	blade element aerodynamic angle of attack at source point ij
α_s	tilt of rotor shaft relative to vertical, positive aft
$\beta_j = \beta_o - \beta_1 \cos\psi_j - \beta_2 \sin\psi_j$	blade flapping angle at azimuth angle ψ_j, positive up
β_o	coning angle, positive up
β_1	coefficient of longitudinal flapping positive so as to make rotor tilt aft
β_2	coefficients of lateral flapping positive so as to make rotor tilt to port
$\gamma = \sqrt{1-M^2}$	
$\Delta r_i, \Delta\psi_j$	increments in blade radius, azimuth angle

$\theta_{ij} = \theta_o + \theta_1 \cos\psi_j + \theta_2 \sin\psi_j - \frac{q(r_i - e)}{(R-e)}$	blade geometric pitch angle, radians, positive nose up at radial station i, azimuthal angle ψ_j
$\theta_i = \theta_o - \frac{q(r_i - e)}{(R-e)}$	steady part of θ_{ij}
θ_o	collective geometric pitch angle, radians, positive nose up
θ_1	lateral cyclic pitch angle, radians, positive nose up
θ_2	longitudinal cyclic pitch angle, positive nose up
$\bar{\kappa}_{ij}, \bar{\bar{\kappa}}_{ij}, \bar{\bar{\bar{\kappa}}}_{ij}$	normalization factors for lift, incompressible drag, compressibility drag, at source point ij
ρ	air mass density
σ or σ_{ij}	phase radius, see Eq 2a
$\tau_{ij} = \frac{C_i \cos\theta_{ij}}{r_i \Omega}$	duration of pressure pulse at source point ij, sec
ψ or ψ_j	azimuth angle, see Fig. 1 and 2
$\Psi_{mi}, \Gamma_{mi}, \kappa_{mi}$	phase angles of Fourier cosine series for lift, incompressible drag, compressibility drag, at radius station i
$\phi_{ij} = \arctan\left(\frac{U_p}{U_T}\right)_{ij}$ $= \alpha_{ij} - \theta_{ij}$	non-geometric part of angle of attack at source point ij
ω	frequency of oscillatory pressure, rad/sec

Ω	rotor angular velocity, rad/sec

Subscripts

i	radial station
I	imaginary part
j	azimuthal station
m	harmonic number
o	field point, or steady component
R	real part
x,y,z	direction of force, along positive Cartesian axes
ω	frequency component

SUMMARY

The lifting rotor is considered as a swept surface, area segments of which are subjected to oscillating pressures, expressed as a Fourier series in time, as was done for the propeller in axial flow by Garrick and Watkins.[5] In this case, of course, the theory is extended to include in-plane components of forward speed and azimuthal asymmetry. The sound pressure at any field point is then found by a straightforward numerical integration which uses as inputs (1) lift per unit span as a function of radius and azimuth, (2) forward speed, (3) rate of descent or climb, (4) RPM, (5) rotor geometry, including non-linear compressible airfoil section characteristics, and (6) first harmonic and steady blade root angles of flapping and pitching. This approach has the advantage of calculating either near or far field noise, including all effects other than "thickness pressure"[5] and that due to the "white" components attributable to random turbulence in the boundary layer or the wake. Impulsive changes in load around the azimuth, due either to compressibility or to vortex interactions are therefore easily investigated. Radiation patterns are investigated for the H-34 and HU-1A helicopters, both around the azimuth and in the shaft direction, for several forward speeds, and the sound spectra compared with measurements for selected cases.

CONCLUSIONS AND RECOMMENDATIONS

The theory for calculating propeller rotational noise has been extended to account for (1) asymmetry of inflow, lift, and drag; (2) non-linear section characteristics, compressibility, and reverse flow; (3) first harmonic and steady rigid blade flapping and pitching; (4) rotor shaft tilt; and (5) chordwise distribution of lift and drag forces, such as are found in the operation of lifting rotor-propellers in forward flight. A numerical integration is used to evaluate the sound pressure levels for up to 20 harmonics at a general field point translating with the rotor hub.

By comparison with a closed form solution, it has been shown that the numerical integration is quite accurate for axial flow when azimuthal increments of 1° (or smaller) are used. In addition, the pronounced reduction in first harmonic sound level indicated by the closed form solution at a flight Mach number of two-tenths, two diameters to the side and about three-fourths of a diameter in front of the propellers[5], is shown to be a spurious consequence of a "far field" assumption. Similar nodes at other flight speeds and field points would probably also be severely modified by an "exact" numerical integration using the subject theory.

Application to two helicopters currently in widespread use showed that the first harmonic rotational noise has by far the highest sound pressure levels in hover, but because of the low frequencies is still marginal with respect to the threshold of hearing. The second harmonic frequency falls just above the lowest for which there is experimental data, and there is good correlation with measured sound pressure levels for this component. Successively higher harmonics, however, are predicted to fall off rapidly, whereas the measured values do not. Contaminating influences in the test setup (which were not performed for the present purpose) include the presence of the tail rotor, reciprocating engine exhaust noise, "sounding-board" effect of fuselage and other surfaces, and relatively large uncertainty as to the elevation of the hub with respect to the microphone. Deficiencies in the theory include lack of "thickness" rotational noise, "vortex" noise due to boundary layer turbulence, wake vortex noise, effect of ground plane and downwash field refraction on the radiation pattern, and frequency shifts due to time-varying velocities in the downwash field.

The principal effect of forward speed is to raise the higher harmonic levels. This increase may occur abruptly or gradually, depending on the harmonic content of the aerodynamic section loadings, as would be expected. This increase occurs much more gradually with the four-bladed H-34 than with the two-bladed HU-1. No attempt at generalizations should be

made without more extensive investigation than was possible in this study.

Octave band radiation patterns in the azimuthal sense were close to symmetric, particularly for the HU-1 helicopter, one diameter beneath the hub over a speed range from hover to 115 knots and at radii of two and ten diameters. Some small polar dissymmetry appears in the azimuthal radiation patterns of the H-34 helicopter, for the lower octave band, at the higher speed, and at ten radial diameters.

Variations in octave band sound pressure level were noted with change in vertical distance beneath the rotor. The variations are similar to those for the first harmonic of a propeller in axial flow. For the rotor, a peak occurs between two and five diameters below, depending upon radial distance from the hub.

The reduction of sound pressure level with radius in the first three octave bands, at an azimuth ψ_o=270°, is roughly as one would expect. However, if the onset of spherical spreading is chosen as the criterion for determining "far field", this may be more like one hundred diameters from the hub than three, as is often used. Moreover, a purely mathematical definition of far field may lead to spurious theoretical predictions, as shown by the propeller example mentioned above.

Increasing the number of blades appears to be the most effective means of reducing rotor rotational noise. An example in which the number of blades was increased from two to three for the HU-1 resulted in a significant decrease in sound pressure level. The effects of compressibility, RPM and impulsive downwash were not significant. Increasing blade chord resulted in a small but fairly general decrease in sound pressure level.

The following appear to be promising directions for future work:

1. Perform sound level measurements using existing rotors under conditions specifically designed to isolate rotor noise from all other sources. (Some of this work has undoubtedly already been done in research carried out at Southampton and perhaps United Aircraft, but data have not been generally available.) Correlate the levels so obtained with the results of the present theory as applied to the new test configurations.

2. Using analytical techniques such as proposed in Ref. 10, and perhaps measurements on rotating cylinders and in the boundary layer on full-scale rotors, attempt to predict vortex noise for correlation with Refs. 21 and 22, and ultimately arrive at a method for calculating rotor vortex noise to be added to the rotational noise of the present study.

3. Extend the present digital computer program to allow prediction of the rotational sound fields of tandem rotors and rotors in ground effect.

4. Attempt to predict the effect on rotor noise of both ordered and random velocities in the wake beneath the rotor.

INTRODUCTION

Understanding the lifting rotor-propeller as a noise source has recently become a technical objective of major importance. There are two factors: (1) military use of helicopters in tactical situations imposes the requirements for low external noise levels with a new authority[1]; and (2) the introduction of turbine powerplants in the present generation of rotary-wing and V/STOL aircraft leaves the rotor-propeller as the dominant source of low frequency noise. These components, of course, are precisely those which are attenuated least with distance. Thus, the aircraft's rotor-propeller noise characteristics will, in combination with its approach speed, determine how much time an enemy will have to prepare for the aircraft's arrival.

A second important consideration is the difficulty of attaining a satisfactory sound treatment to reduce rotor noise as experienced inside the aircraft. It is generally accepted (Ref. 2, Figures 9 and 10, for example) that such reductions must be achieved at the source, for frequencies below about 200 cps, since the weight penalty for significant attenuation is usually prohibitive.

From both these viewpoints, as well as consideration of the obvious influences of rotor noise on helicopter ASW operations, commercial applications, and the relatively unexplored operation of VTOL propellers in the transition regime, it is important that greater insight be achieved regarding the mechanism of rotor-propeller noise generation.

Investigations in the field of helicopter rotor noise have the benefit of years of work dealing with airplane propellers.[3,4,5] Differences between measured rotor noise levels and those predicted, however, using the empirical relations for propellers[6] indicate that the applicable range of parameters is too limited, even when used for hover or vertical flight. The profound differences which come about in forward flight are, of course, clear. It is the latter to which this study specifically addressed itself.

The theory of propellers is extended here to allow prediction of the rotational noise generated by lifting rotors in forward flight. It will be assumed that the time-varying pressures experienced at each radial station along a blade are known for a given helicopter configuration and operating condition. From this, the sound radiation amplitude and distribution around the rotor azimuth will be predicted in the fixed, that is, non-rotating system. With these results, it will be possible to treat the rotor like any other noise source on the aircraft in predicting what is experienced in the aircraft or by an observer on the ground.

The effects of the approximately "white" noise which exists in the turbulent boundary layer sheathing the blades, and is modulated for the observer by the blade passage frequencies[7], will be ignored in this study. Also, pressure fluctuations experienced as a result of the passage of the complex wake of distributed shed and trailed vorticity with respect to a non-rotating observer translating with the rotor[8,9] will not be considered. Although some recent analyses[10] promise simplification, the approach of, and in fact the extension suggested in, Ref. 5 is followed rather directly. Effects specifically accounted for in the sections to follow include:

1. Variations in velocity normal to the leading edge, angle of attack, lift and drag with radius and around the azimuth.

2. Non-linear and compressible airfoil section characteristics.

3. The influence of non-uniform induced flow on angle of attack, and (in those instances where steady, two-dimensional section data indicate that the section should be stalled, yet it is not) on velocity normal to the leading edge.

4. Reversed flow.

5. Coning, flapping, and cyclic pitch variations.

The effects of rotor-fuselage or rotor-rotor interference will not be specifically examined except as they may exist in the experimental or theoretical spanwise loadings used as input for the analysis. It is felt, however, that the theoretical investigation reported here is a necessary first step in increasing understanding of lifting rotor-propeller noise.

The underlying philosophy in this approach stems from the impulsive nature of the airloads on a lifting rotor in forward flight. Rabbott and Churchill[11] first showed the very rapid fluctuations which could be expected with azimuthal position; Miller[8], Piziali and DuWaldt[9] and others tied the existence of these very high harmonics theoretically to the proximity of vortex elements trailed from the passage of preceding blades or the same blade in preceding revolutions. Aside from the fact that approximations for other quantities - such as amplitude and phase radius[5] - would probably have to be made for a closed form integration over the propeller-rotor disc, it was felt that analytical representation of the harmonics of airloads associated with non-uniform downwash would be likely to lose components of interest. Since numerical integration would obviate the need for both kinds of approximations, this approach was taken. The problems of

obtaining satisfactory numerical accuracy and limiting digital computer machine time to reasonable amounts were, of course, recognized from the outset, and will be discussed in the Results section of this report.

ANALYSIS

This formulation follows the general procedure developed in Ref. 5 and preserves much of the notation, the exceptions occurring where it conflicts with helicopter terminology.

COORDINATE SYSTEM

The coordinate system is Cartesian, rectangular, right-handed and oriented so that (1) the z-axis is vertical, (2) the positive x-direction points in the direction of flight, and (3) the origin is taken at the center of the rotor hub (see Figure 1), so that the system translates with the flight velocity, V.

Points on the surface area swept out by the rotor blades will be called "source points" and identified as points x, y, z. It will be convenient to use polar coordinates on the area swept by the rotor blades. The azimuth angle, ψ, will be defined in a plane perpendicular to the shaft and taken to be zero on the negative x-axis, as shown in Figure 2.

A general point outside the swept area but translating with the rotor will be called a "field point" and denoted by x_o, y_o, z_o. Defining field point azimuth relative to the pilot, the azimuth angle of a field point, ψ_o, is such that $\psi_o=0$ on the positive x-axis. Since an integration will eventually be performed over the swept area, the "source points" will be specified using a double subscript notation i, j. Here i identifies the radius position and j the azimuthal position.

Equations for determining x, y, z coordinates of the source points are derived geometrically by examining the position of a particular blade of the rotor at any time, t. It is assumed that the blade is inflexible but has a "flapping hinge", offset a distance, e, from the center of rotation. This allows a blade to rotate out of the plane of rotation through an angle β_j, which is assumed to be small. A point on the blade is defined as being a distance r from the hub when $\beta_j=0$. No other motion of the blades with respect to the hub, other than pitch changes (denoted by θ_{ij}), will be accounted for. The rotor shaft, however, is pictured as tilted through an angle α_s in the longitudinal plane. Blade point coordinates are then given (see, for example, Ref. 12), when small angle assumptions are made for sin β and cos β, by

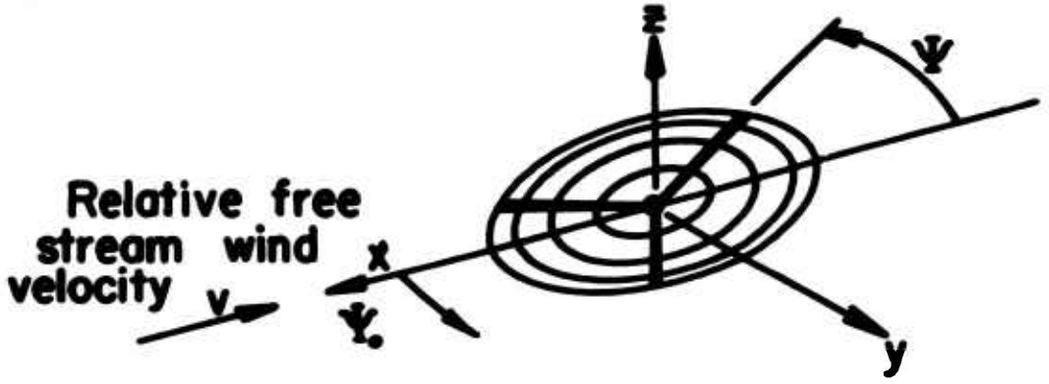

Fig.1. COORDINATE SYSTEM.

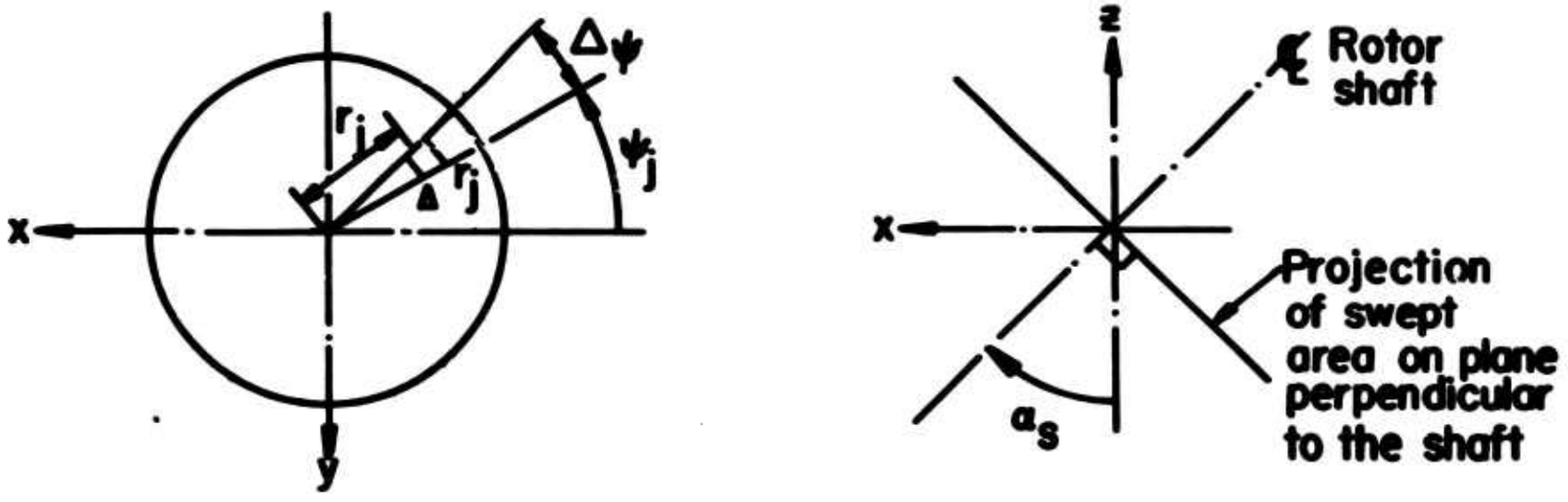

Fig. 2. COORDINATE SYSTEM.

$$x_{ij} = -r_i\cos\psi_j\cos\alpha_s - \beta_j[r_i - e]\sin\alpha_s$$

$$y_{ij} = -r_i\sin\psi_j$$

$$z_{ij} = [r_i - e]\beta_j\cos\alpha_s - r_i\cos\psi_j\sin\alpha_s \qquad (1)$$

THE ACOUSTIC EQUATION

As in Ref. 5, we define

$$P(x_o, y_o, z_o, t) \triangleq R_e[P_\omega(x_o, y_o, z_o)e^{i\omega t}]$$

$$= R_e[P_m(x_o, y_o, z_o)e^{imB\Omega t}]$$

as the sinusoidally varying pressure at a field point (x_o, y_o, z_o) with the frequency $\omega = mB\Omega$.

Here Ω is the rotational frequency of the rotor, and R_e, of course, signifies taking the real part of a complex number. Steady conditions will be assumed; i.e., what happens in one revolution happens in every other, and in fact, what happens to one blade at a particular azimuth is repeated on every other blade when it is at that azimuth. It follows that all phenomena will be periodic with the fundamental period $T = \frac{2\pi}{B\Omega}$; thus m is the harmonic number. If we can determine the harmonic components of the forces acting on the fluid at a source point in the directions of the coordinate axes, namely $F_{m_{x_{ij}}}$, $F_{m_{y_{ij}}}$, and $F_{m_{z_{ij}}}$, then we can calculate the sound pressure at a field point from the expression

$$R_e[P_m(x_o, y_o, z_o)e^{imB\Omega t}]$$

$$= R_e\left[\frac{1}{4\pi}\left\{F_{m_x}\frac{\partial}{\partial x_o} + F_{m_y}\frac{\partial}{\partial y_o} + F_{m_z}\frac{\partial}{\partial z_o}\right\}\frac{e^{-ik\sigma}}{S}e^{imB\Omega t}\right] \qquad (2)$$

which is given, in slightly different form, as Eq. (6) in Ref. 5. Here,

$$k = \frac{mB\Omega}{C}$$

$$S = \sqrt{(x_o - x)^2 + \gamma^2[(y_o - y)^2 + (z_o - z)^2]}$$

$$\sigma = \frac{M(x_o - x) + S}{\gamma^2}$$

$$M = \frac{V}{C}$$

C = velocity of sound

$$\gamma = \sqrt{1-M^2} \qquad (2a)$$

REPRESENTATION OF FLUID FORCES IN TERMS OF FORCES ON THE BLADES

The forces on the fluid are those which cause the rotor to experience, as reactions, lift and drag. An area element of the swept surface may be thought of as having such forces on it as arise from calculating a force per unit of projected blade area and then multiplying by the differential of swept area. This step may be obvious, but if it is kept in mind, it will emphasize that we are dealing with "effective areas" and "effective pressures." Losing sight of this might make it appear that we are calculating fluid pressures in the x-direction different from those in the y-direction, or, as another example, that we are thinking of viscous drag forces as arising from fluid pressures just as normal forces do; in fact, neither of these statements is true.

Let us examine the force per unit blade area, irrespective of its source or direction, which is experienced by an element of the swept surface at some azimuthal and radial station. It will have a time history such that as each rotor blade sweeps through, pulses are experienced. The duration of these pulses is τ_{ij}, and they recur after a period T, as shown in Figure 3. Note that if the blade chord length is C_i and the blade geometric pitch angle θ_{ij}, then the projection of the chord length on the swept surface is $C_i\cos\theta_{ij}$ and $\tau_{ij} = \frac{C_i\cos\theta_{ij}}{r_i\Omega}$. To avoid the complications which otherwise arise, it will be assumed from this point that

$$C_i\cos\theta_{ij} \approx C_i\cos\theta_i \Delta C_i' \text{ and } \tau_{ij} \approx \tau_i \Delta \frac{C_i'}{r_i\Omega}$$

where θ_i is the mean pitch angle at a given radius. Since

$$\theta_{ij}^n = \theta_o + \theta_1\cos(\psi_j) + \theta_2\sin(\psi_j) - \frac{q(r_i - e)}{R-e}$$

where q is the twist built into the blade in degrees per

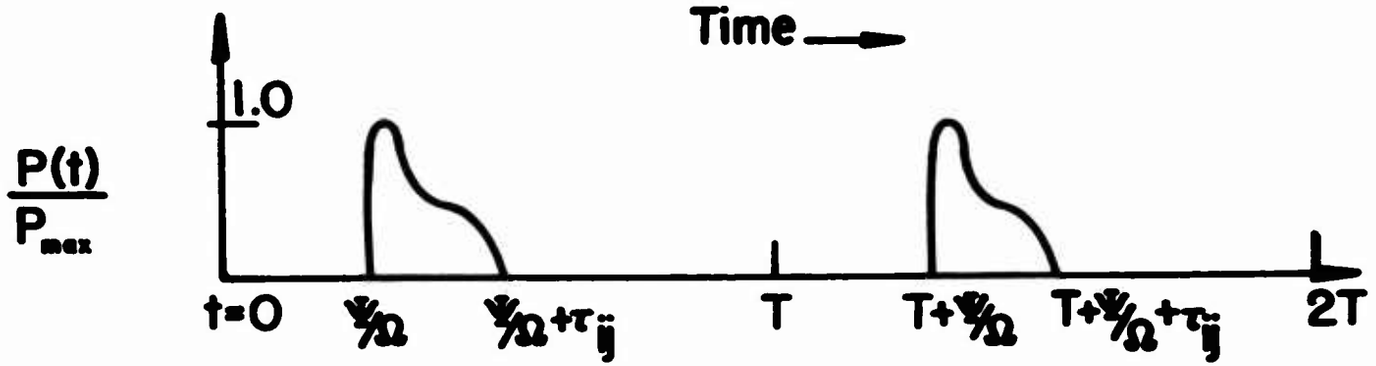

Fig. 3. PULSE PERIOD.

fraction of blade radius, approximating θ_{ij} by θ_i is tantamount to neglecting θ_1 and θ_2, which are rarely higher than about 10°, and the total angle θ_{ij} will almost always be less than 25°.

The shape of the pulses will, of course, depend on the distribution of force over the chord. Now suppose we limit ourselves to operating regimes where the rotor blade is unstalled and reverse flow can be ignored. If we handle lift, incompressible drag and wave drag separately, then we can assume with little error that only the magnitude of the pulses in Figure 3 will vary with azimuth, and that their shapes will be constant, except for the variation of τ_i with radius. In Ref. 5, the effect of chordwise force distribution is discussed at some length as having appreciable effects only on the higher harmonics. On the other hand, the rotor "bang" or "slap" noise reported in Refs. 7 and 13 is a relatively high frequency phenomenon, and is such an important aspect of rotor noise that chordwise distribution differences have been purposely retained in this analysis. Putting aside for the moment the question of the magnitude of the pressure pulses, their shapes can be expressed as a real Fourier series:

$$f_i = a_{o_i} + \sum_{m=1}^{\infty} a_{m_i} \cos m B\Omega t + b_{m_i} \sin m B\Omega t)$$

Note that the shape function, f_i, can be thought of as a function either of chord length projection on the swept surface, C_i' or of time, t. This function lacks the index j, identifying azimuth, since it is thought of as "normalized," and, also for the moment, as beginning at t=0, which coincides with ψ_j=0. For convenience the coefficients a_{o_i}, a_{m_i}, and b_{m_i} are normalized so that $f_{i_{max}}$ =1.0. Thus, to account for the variation in lift and drag around the azimuth, we must establish normalization factors for these Fourier coefficients.

Since we have specified that the shape represented by the normalized coefficients will always have a maximum ordinate equal to unity, then the aerodynamic lift acting on a span length Δr_i is

$$L_{ij}(t) = C_{L_{ij}} \frac{1}{2} \rho (U_{ij})^2 C_i \Delta r_i \bar{\Delta\kappa}_{ij} \int_{chord} \bar{f}_i \, dC_i' \Delta r_i$$

where

$\bar{\kappa}_{ij}$ = normalization factor for lift

U_{ij} = resultant relative wind velocity normal to blade leading edge

ρ = air mass density

$C_{L_{ij}}$ = lift coefficient

Similarly, for incompressible profile drag

$$D_{v_{ij}}(t) = C_{D_{v_{ij}}} \frac{1}{2}\rho(U_{ij})^2 C_i \Delta r_i \bar{\Delta\kappa}_{ij} \int_{\text{chord}} \bar{f}_i \, dC_i' \Delta r_i$$

and for compressible (wave) drag

$$D_{w_{ij}}(t) = C_{D_{w_{ij}}} \frac{1}{2}\rho(U_{ij})^2 C_i \Delta r_i \bar{\bar{\Delta\kappa}}_{ij} \int_{\text{chord}} \bar{\bar{f}}_i \, dC_i' \Delta r_i$$

Since sound is an oscillatory phenomenon, we may drop the steady term in the Fourier series. Furthermore, since we have expressed the amplitudes of the force components $F_{m_{x_{ij}}}$, $F_{m_{y_{ij}}}$, and $F_{m_{z_{ij}}}$ as the complex multiplier of the time function

$$e^{imB\Omega t}$$

we will prefer to rewrite the real Fourier series in the form

$$\bar{f}_i = \sum_{m=1}^{\infty} \bar{a}_{m_i} \cos mB\Omega t + \bar{b}_{m_i} \sin mB\Omega t) = \sum_{m=1}^{\infty} c_{m_i} \cos(mB\Omega t - \psi_{m_i})$$

$$= R_e\left[\sum_{m=1}^{\infty} c_{m_i} e^{i(mB\Omega t - \psi_{mi})}\right]$$

Therefore, the normalized coefficient $c_{m_i} e^{-i\psi_{mi}}$ is associated with the blade lift, by the equation directly above; then we can define two more sets of similar quantities associated with (1) incompressible drag, say d_{m_i} and Γ_{mi}, and (2) compressi-

bility drag, namely e_{m_i} and κ_{mi}.

Analytical expressions for such Fourier constants are derived by the usual means (see, for example, Ref. 14), for the three chordwise shapes shown in Figures 4(a) through (c). The selection of these shapes as approximations for lift, incompressible drag and wave drag was based on a perusal of two-dimensional section data below stall, and computational convenience.

The corresponding formulae are as follows:

$$\frac{c_{m_i}}{\int_{\text{chord}} \bar{f}_i dC_i'} = \frac{r_i}{C_i' Bm^2 \pi}\left\{\left[d\left(1-\cos\frac{BmC_i'}{r_i}\right)+\frac{\ell}{a}\left(1-\cos\frac{BmaC_i'}{r_i}\right)\right]^2 + \left[\frac{mBC_i'}{r_i}-\left(d\sin\frac{BmC_i'}{r_i}+\frac{\ell}{a}\sin\frac{BmaC_i'}{r_i}\right)\right]^2\right\}^{1/2}$$

$$\psi_{mi} = \arctan\left\{\frac{\left[\frac{mBC_i'}{r_i}-\left(d\sin\frac{BmC_i'}{r_i}+\frac{\ell}{a}\sin\frac{BmaC_i'}{r_i}\right)\right]}{d\left(1-\cos\frac{BmC_i'}{r_i}\right)+\frac{\ell}{a}\left(1-\cos\frac{BmaC_i'}{r_i}\right)}\right\}$$

$$\frac{d_{m_i}}{\int_{\text{chord}} \bar{f}_i dC_i'} = \frac{2}{\pi m}\sin\frac{BmC_i'}{2r_i}$$

$$\Gamma_{mi} = \frac{BmC_i'}{2r_i}$$

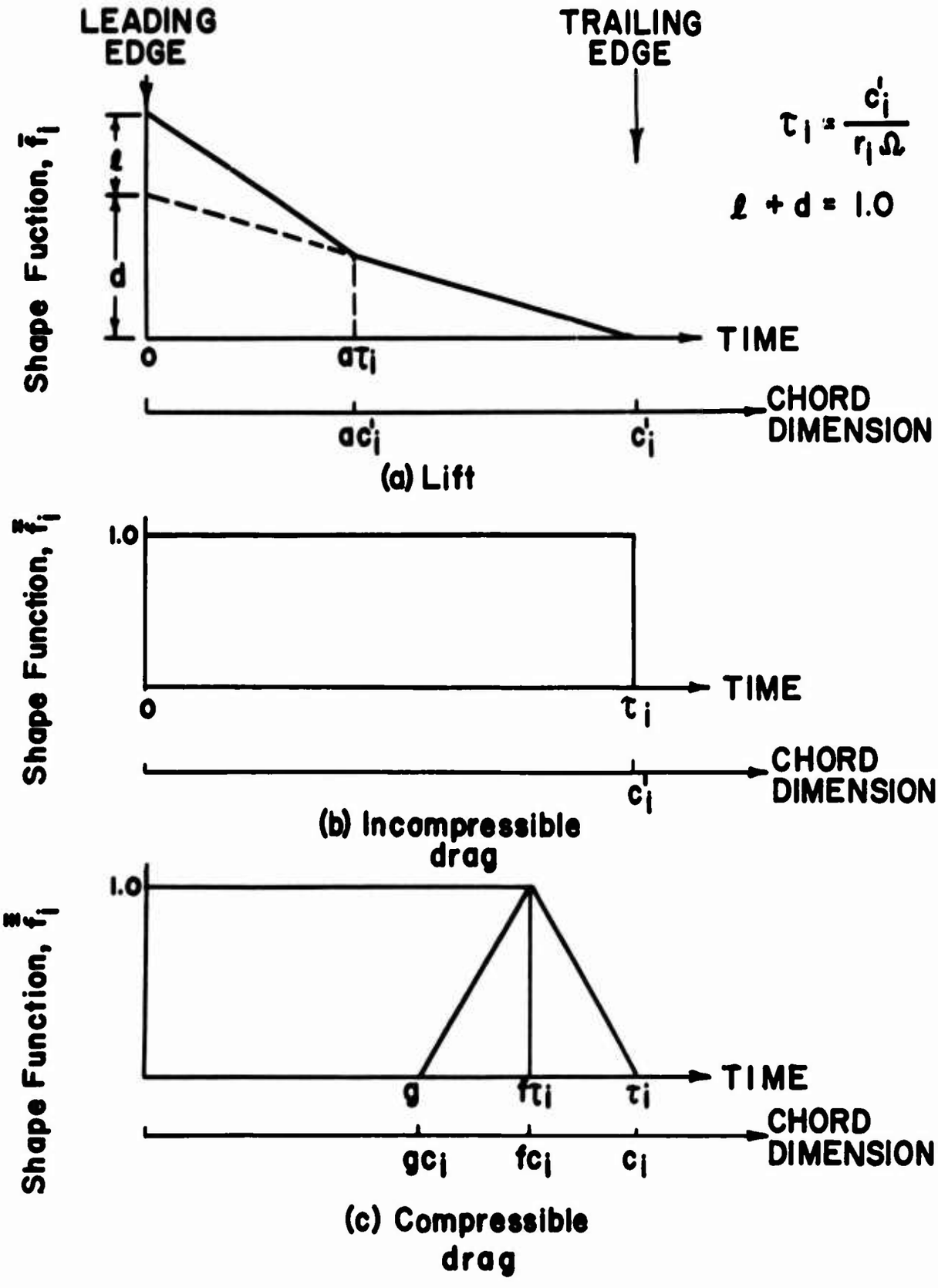

Fig. 4. IDEALIZED FORCE DISTRIBUTION VERSUS CHORD.

$$\frac{e_{m_i}}{\int_{chord} \bar{\bar{f}}_i dC_i'} = \frac{r_i}{C_i' Bm^2 \pi (1-f)(f-g)} \{ [(1-g)\cos\frac{BmfC_i'}{r_i} - (1-f)\cos\frac{BmgC_i'}{r_i} -$$

$$(f-g)\cos\frac{BmC_i'}{r_i}]^2 + [(1-g)\sin\frac{BmfC_i'}{r_i} - (1-f)\sin\frac{BmgC_i'}{r_i} - (f-g)\sin\frac{BmC_i'}{r_i}]^2 \}^{1/2}$$

$$\kappa_{mi} = \arctan\left\{ \frac{(1-g)\sin\frac{BmfC_i'}{r_i} - (1-f)\sin\frac{BmgC_i'}{r_i} - (f-g)\sin\frac{BmC_i'}{r_i}}{(1-g)\cos\frac{BmfC_i'}{r_i} - (1-f)\cos\frac{BmgC_i'}{r_i} - (f-g)\cos\frac{BmC_i'}{r_i}} \right\} \quad (3)$$

Note that the lift, incompressible drag and wave drag coefficients are all functions of (1) local "free stream" Mach number, M_{ij}, perpendicular to the blade leading edge and (2) aerodynamic angle of attack α_{ij}.

To allow for the fact that these pulses do not always start at t=0, but at time $t+\psi_j/\Omega$, we need merely multiply by

$$e^{-imB\Omega(\psi_j/\Omega)} = e^{-imB\psi_j}$$

where

$\psi_j \triangleq (j-1)\Delta\psi$

$\Delta\psi$ = increment in azimuth angle from one station on the swept area to another.

$j = 1, 2, 3 \ldots n$

n = total number of azimuthal sections into which the swept area is divided

From these definitions it follows that the m^{th} harmonic component of the forces experienced by the fluid due to blade lift and drag may be expressed as minus the following:

$$R_e[L_{m_{ij}} e^{imB\Omega t}]$$

$$= R_e\left\{\frac{\frac{1}{2}\rho C_{L_{ij}} [U_{ij}]^2 C_i}{\int_{\text{chord}} \bar{f}_i dC_i'} c_{m_i} e^{-i\Psi_{mi}} e^{-imB\psi_j} e^{imB\Omega t}\right\} r_i \Delta\psi \Delta r_i$$

$$R_e[D_{m_{ij}} e^{imB\Omega t}] = R_e\left\{\frac{1}{2}\rho C_i [U_{ij}]^2 \left[\frac{C_{D_{v_{ij}}} d_{m_i}}{\int_{\text{chord}} \bar{f}_i dC_i'} e^{-i\Gamma_{mi}} + \right.\right.$$

$$\left.\left. \frac{C_{D_{w_{ij}}} e_{m_i}}{\int_{\text{chord}} \bar{\bar{f}}_i dC_i'} e^{-i\kappa_{mi}}\right] e^{-imB\psi_j} e^{imB\Omega t}\right\} r_i \Delta\psi \Delta r_i \qquad (4)$$

Before these sinusoidally varying forces can be evaluated or expressed in terms of components along the coordinate axes, it is necessary to establish (1) the direction and magnitude of the resultant velocities U_{ij} (since lift and drag forces are defined as perpendicular and parallel to them, respectively), and (2) the blade orientation.

RESULTANT VELOCITY AT A BLADE SECTION

Rotor aerodynamics derivations (see, for example, Ref. 12) usually start by defining two velocity components in a plane normal to the blade leading edge. These are U_p and U_T, components parallel and perpendicular to the shaft axis, respectively. The convention for U_p is positive up; U_T, of course, is always taken positive when directed toward the airfoil leading edge.

Accounting for components of forward speed, rotational speed, an average induced velocity component v (assumed positive down) and an effective component normal to the chord as a result of flapping velocity $\dot{\beta}$, yields

$$U_T = V\cos\alpha_s \sin\psi + \Omega r$$

$$U_p = V(\sin\alpha_s - \beta\cos\alpha_s\cos\psi) - v - \dot{\beta}(r-e)$$

This neglects the radial component of velocity, assumes that each strip of airfoil perpendicular to the leading edge acts as an airfoil in two-dimensional flow with the same resultant velocity normal to the leading edge and the same angle of attack, and makes the usual small angle assumptions. The actual induced velocity is a quantity, which, in general, varies both over the blade radius and azimuth, and its calculation has been the subject of extensive research. Its effect on angle of attack may be quite significant, especially where U_p might otherwise be small. It is usually assumed, however, that induced velocities in the plane of the rotor are small compared to U_T, except where that velocity is small, in which case the resulting forces are unimportant. For this reason, the resulting velocity U_{ij} will be calculated using an induced velocity v assumed to be uniform over the disc, and calculated from the momentum theory expression (Ref. 15).

$$v = \frac{\text{thrust}}{2\pi R^2 \rho [(V\sin\alpha_s - v)^2 + (V\cos\alpha_s)^2]^{1/2}}$$

The approach used to account for the actual variations in induced velocity over the disc, both normal and in the plane of the rotor, will be explained in the following section.

DETERMINATION OF BLADE ELEMENT ANGLE OF ATTACK, LIFT AND DRAG

As shown in Figure 5, the blade angle of attack, α_{ij}, is a function of the velocity components U_p and U_T and the local geometric blade pitch angle, θ_{ij}.

In this study, it will be assumed that the lift, or more exactly, the loading per unit span normal to the blade chord, the "aerodynamic section loading," is known from experiments or previous calculations. Actually, measurements reported in Ref. 16 and 17 are to be used as inputs to this analysis. This eliminates the need for an accurate knowledge of v as a function of r and ψ, which is acknowledged as a necessity if anything but the lowest harmonics of blade airloads is needed.

The procedure is as follows. Normal force coefficients $C_N(M, \alpha)$ will be tabulated for the airfoil section of interest, as will the aerodynamic section loading (ASL) for a given flight con-

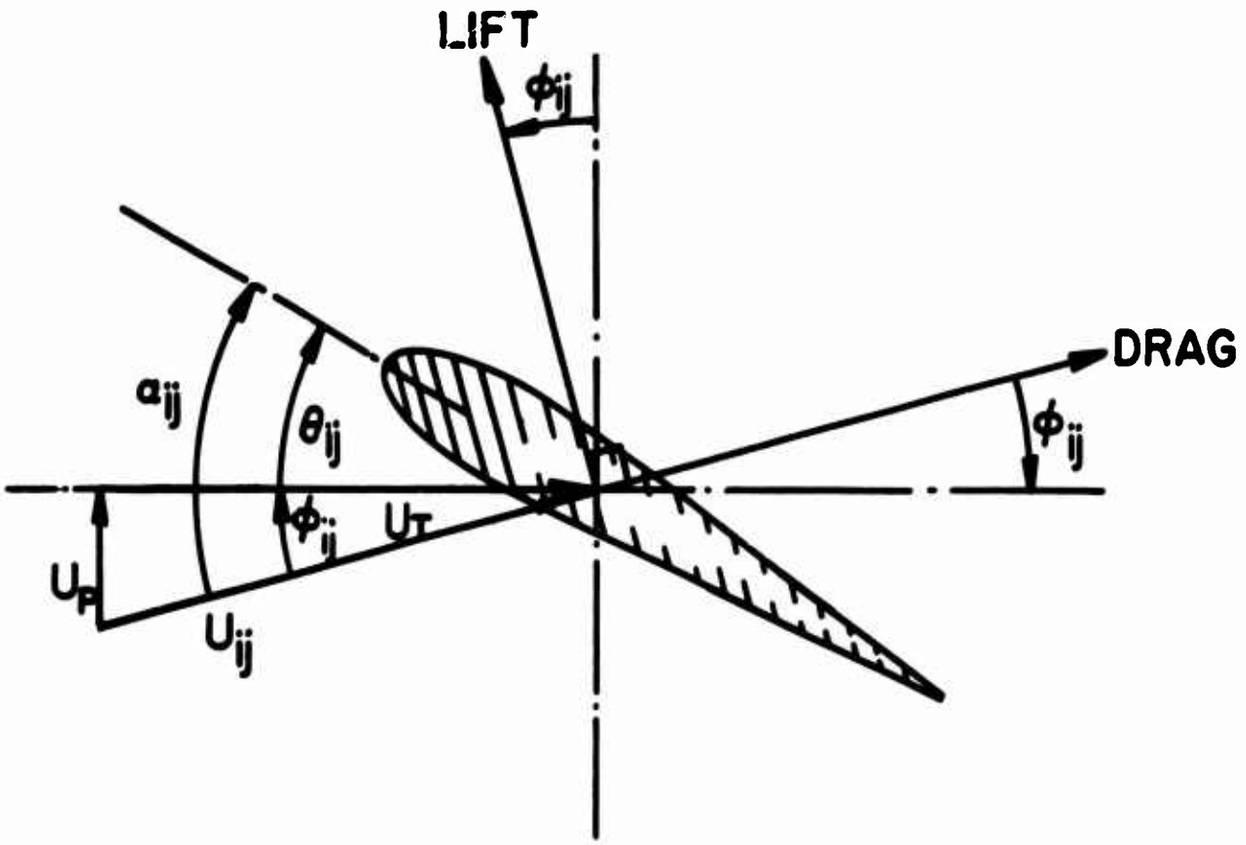

Fig. 5. BLADE SECTION QUANTITIES.

dition as a function of r and ψ. For each element of swept area corresponding to a source point, the resultant velocity will be calculated from

$$U_{ij} = \sqrt{U_p^2+U_T^2}$$

$$= \sqrt{(V\cos\alpha_s\sin\psi_j+\Omega r_i)^2+(V[\sin\alpha_s-\beta_j\cos\alpha_s\cos\psi_j]-v-\dot{\beta}_j[r-e])^2}$$

the Mach number from $M_{ij} = \frac{U_{ij}}{C}$

and the normal force coefficient from

$$C_{N_{ij}} = \frac{(ASL)_{ij}}{1/2\rho(U_{ij})^2 C_i \Delta r_i} . \qquad (5)$$

The table of airfoil coefficients then will be entered with the known values of $C_{N_{ij}}$ and M_{ij}, and the corresponding value of α_{ij} read out, interpolating when necessary. With M_{ij} and α_{ij} thus known, similar airfoil coefficient tables for $C_{L_{ij}}$ and $C_{D_{ij}}$ as functions of these same variables will be entered and the lift and drag coefficients read. A simultaneous "look-up" for $C_{D_{ij}}$ at the corresponding α_{ij} but with $M_{ij}=0$ will be made to determine $C_{D_{v_{ij}}}$. This subtracted from $C_{D_{ij}}$ will yield $C_{D_{w_{ij}}}$. This information is all that is needed in addition to Eq. (3) and Eq. (5) to completely determine $L_{m_{ij}}$ and $D_{m_{ij}}$ as written in Eq. (4).

It is important to note that the value of C_N given by Eq. (5) may exceed any that can be found in the tables of two-dimensional coefficients, as pointed out in Ref. 18. This can be explained in several ways: (1) the in-plane components induced by the vortex wake may be significantly increasing the resultant velocity U_{ij}, (2) the effects of radial flow may be sufficiently energizing the boundary layer to delay stall, (3) unsteady effects may be sufficient to delay stall. In view of the paucity of airfoil section data either in the presence of spanwise flow or under unsteady conditions, the approach taken

here was to have the machine program evaluate the minimum increment required in U_{ij} to make $C_{N_{ij}}$ fall within the steady, two-dimensional data. For that radius and azimuthal station, the adjusted value of U_{ij} will thereafter be used.

Certain details of the "table look-up" operation involving C_N, C_L, C_D, and α are worth noting. The present program is set up for symmetric airfoils; all values, therefore, are tabulated as positive. The extension to cambered sections would not be difficult. In any case the sign of the quantities U_T and U_p do not appear explicitly, so care must be taken to differentiate between regions of positive and negative angle of attack, and between normal and reversed flow. The signs of U_T and (ASL) are tested and the procedures listed in Table I are followed.

Considerations leading to Eq. (6) in the section to follow will show that these special procedures represent the aerodynamic forces as vectors in the appropriate direction. This is a straightforward transformation of coordinates operation; again, using the approximations $\cos\beta \approx 1$ and $\sin\beta \approx \beta$, it follows that

$$F_x = [(L\sin\phi - D\cos\phi)\cos\alpha_s \sin\psi + (L\cos\phi + D\sin\phi)(\beta\cos\alpha_s\cos\psi - \sin\alpha_s)]$$

$$F_y = [(L\cos\phi + D\sin\phi)\beta\sin\psi - (L\sin\phi - D\cos\phi)\cos\psi]$$

$$F_z = [(L\sin\phi - D\cos\phi)\sin\psi\sin\alpha_s + (L\cos\phi + D\sin\phi)(\beta\sin\alpha_s\cos\psi + \cos\alpha_s)] \quad (6)$$

where, for convenience, the subscripts m, i and j are omitted and considered to be understood.

APPLICATION OF THE ACOUSTIC EQUATION

Now to use Eq. (2) to calculate the m^{th} harmonic of sound pressure at a field point (x_o, y_o, z_o) due to the m^{th} harmonic oscillatory pressure at a source point identified by the indices (i,j), we need only (a) to note that

TABLE I
SPECIAL "TABLE-LOOK-UP" INSTRUCTIONS
FOR NEGATIVE LIFT AND REVERSE FLOW

Steps \ Case	ASL Negative U_T Positive	ASL Positive U_T Negative	ASL Negative U_T Negative
1 Enter C_N vs α in region	$0 \leq \alpha \leq 15°$	$165° \leq \alpha \leq 180°$	$165° \leq \alpha \leq 180°$
2 Use for C_L	Minus C_L obtained	C_L obtained	Minus C_L obtained
3 Use for C_D	C_D obtained	Minus C_D obtained	Minus C_D obtained
4 Use for α	Minus α obtained	α obtained minus 180°	180° minus α obtained

$$\frac{\partial}{\partial x_o}\left(\frac{e^{-ik_m\sigma_{ij}}}{S_{ij}}\right) = \frac{-e^{-ik_m\sigma_{ij}}}{S_{ij}}\left[\frac{ik_m M}{\gamma^2}+\left(\frac{ik_m}{\gamma^2}+\frac{1}{S_{ij}}\right)\frac{(x_o-x)}{S_{ij}}\right]$$

$$\frac{\partial}{\partial y_o}\left(\frac{e^{-ik_m\sigma_{ij}}}{S_{ij}}\right) = \frac{-e^{-ik_m\sigma_{ij}}}{(S_{ij})^2}\left[ik_m+\frac{\gamma^2}{S_{ij}}\right](y_o-y)$$

$$\frac{\partial}{\partial z_o}\left(\frac{e^{-ik_m\sigma_{ij}}}{S_{ij}}\right) = \frac{-e^{-ik_m\sigma_{ij}}}{(S_{ij})^2}\left[ik_m+\frac{\gamma^2}{S_{ij}}\right](z_o-z) \qquad (7)$$

(b) to substitute $L_{m_{ij}}$ and $D_{m_{ij}}$ from Eq. (4) for L and D, respectively, in Eq. (6), and (c) to substitute the resulting force components and the Eq. (7) expressions into Eq. (2). The resulting equation can be broken into real and imaginary parts and, after algebraic manipulation, cast in the following form:

$$P_m(x_o,y_o,z_o)_{ij_R} = \frac{1}{4\pi}\frac{K_{ij}}{(S_{ij})^2}\{\bar{A}_{ij}[\bar{K}_{m_{ij}}\sin\phi_{ij}-\bar{L}_{m_{ij}}\cos\phi_{ij}] -$$

$$\bar{B}_{ij}[\bar{K}_{m_{ij}}\cos\phi_{ij}+\bar{L}_{m_{ij}}\sin\phi_{ij}]+\frac{S_{ij}M}{\gamma^2}k_m[\bar{G}_{m_{ij}}(\bar{I}_{ij}\cos\phi_{ij}-\bar{J}_{ij}\sin\phi_{ij}) -$$

$$\bar{E}_{m_{ij}}(\bar{I}_{ij}\sin\phi_{ij}+\bar{J}_{ij}\cos\phi_{ij})]\}$$

$$P_m(x_o,y_o,z_o)_{ij_I} = \frac{1}{4\pi}\frac{K_{ij}}{(S_{ij})^2}\{\bar{A}_{ij}[\bar{D}_{m_{ij}}\sin\phi_{ij}+\bar{C}_{m_{ij}}\cos\phi_{ij}] -$$

$$\bar{B}[\bar{D}_{m_{ij}}\cos\phi_{ij}-\bar{C}_{m_{ij}}\sin\phi_{ij}]+\frac{S_{ij}M}{\gamma^2}k_m[\bar{H}_{m_{ij}}(\bar{I}_{ij}\cos\phi_{ij}-\bar{J}_{ij}\sin\phi_{ij}) -$$

$$\bar{F}_{m_{ij}}(\bar{I}_{ij}\sin\phi_{ij}+\bar{J}_{ij}\cos\phi_{ij})]\} \qquad (8)$$

where

$$\bar{A}_{ij} = \{\gamma^2(y_o-y_{ij})\cos\psi_j - [(x_o-x_{ij})\cos\alpha_s + \gamma^2(z_o-z_{ij})\sin\alpha_s]\sin\psi_j\}$$

$$\bar{B}_{ij} = \{(x_o-x_{ij})\bar{J}_j + \gamma^2[(y_o-y_{ij})\beta_j\sin\psi_j + (z_o-z_{ij})\beta_j\cos\psi_j\sin\alpha_s+\cos\alpha_s)]\}$$

$$\bar{C}_{m_{ij}} = \{\frac{1}{S_{ij}}\bar{G}_{m_{ij}} - \frac{k_m}{\gamma^2}\bar{H}_{m_{ij}}\}$$

$$\bar{D}_{m_{ij}} = \{-\frac{1}{S_{ij}}\bar{E}_{m_{ij}} + \frac{k_m}{\gamma^2}\bar{F}_{m_{ij}}\}$$

$$\bar{E}_{m_{ij}} = \frac{C_{L_{ij}}c_{m_i}}{\int\bar{f}_i dC_i}\sin(k_m\sigma_{ij}+\Psi_{m_i}+mB\psi_j)$$

$$\bar{F}_{m_{ij}} = \frac{C_{L_{ij}}c_{m_i}}{\int\bar{f}_i dC_i}\cos(k_m\sigma_{ij}+\Psi_{m_i}+mB\psi_j)$$

$$\bar{G}_{m_{ij}} = \frac{C_{D_{v_{ij}}}d_{m_i}}{\int\bar{f}_i dC_i}\sin(k_m\sigma_{ij}+\Gamma'_{m_i}+mB\psi_j) + \frac{C_{D_{w_{ij}}}e_{m_i}}{\int\bar{\bar{f}}_i dC_i}\sin(k_m\sigma_{ij}+\kappa_{m_i}+mB\psi_j)$$

$$\bar{H}_{m_{ij}} = \frac{C_{D_{v_{ij}}} d_{m_i}}{\int \bar{f}_i dC_i} \cos(k_m \sigma_{ij} + \Gamma_{m_i} + mB\psi_j) +$$

$$\frac{C_{D_{w_{ij}}} e_{m_i}}{\int \bar{f}_i dC_i} \cos(k_m \sigma_{ij} + \kappa_{m_i} + mB\psi_j)$$

$$\bar{I}_{ij} = \cos\alpha_s \sin\psi_j$$

$$\bar{J}_{ij} = (\beta_{ij}\cos\alpha_s \cos\psi_j - \sin\alpha_s)$$

$$\bar{K}_{ij} = \{\frac{1}{S_{ij}} \bar{F}_{m_{ij}} + \frac{k_m}{\gamma^2} \bar{E}_{m_{ij}}\}$$

$$\bar{L}_{ij} = \{\frac{1}{S_{ij}} \bar{H}_{m_{ij}} + \frac{k_m}{\gamma^2} \bar{G}_{m_{ij}}\}$$

and

$$K_{ij} = 1/2\rho C_i (U_{ij})^2 r_i \Delta\psi \Delta r_i$$

$$S_{ij} = \sqrt{(x_o - x_{ij})^2 + \gamma^2[(y_o - y_{ij})^2 + (z_o - z_{ij})^2]}$$

$$\sigma_{ij} = \frac{M(x_o - x_{ij}) + S_{ij}}{\gamma^2} .$$

The integration proceeds by summing all the real parts of the oscillatory pressure of harmonic m, contributed by all the combinations of i and j; this also applies to the imaginary parts of the sound pressure components. If P_{m_R} and P_{m_I} are in psi, then the sound pressure level in decibels is

$$db_m = 10 \log_{10} \frac{5.5\left[\left(\sum\sum_{ij} P_{m_{ij_R}}\right)^2 + \left(\sum\sum_{ij} P_{m_{ij_I}}\right)^2\right]}{0.0002}.$$

RESULTS

The dangers inherent in a numerical integration of an expression of the sort given in Eq. (8) lie in the alternating nature of the trigonometric functions in the expressions for $\bar{E}_{m_{ij}}$, $\bar{F}_{m_{ij}}$, $\bar{G}_{m_{ij}}$, and $\bar{H}_{m_{ij}}$. The arguments of these functions vary around the swept area of the rotor-propeller as the sum $(mB\psi_j+k_m\sigma_{ij})$. The quantity k_m will be recognized as the inverse of the wave length of the m^{th} component of sound, and thus $k_m\sigma_{ij}$ is the number of waves of this component between the source point at ij and the field point. This fact is embodied in the definition of σ_{ij} as the "phase radius." Clearly, as $(mB\psi_j+k_m\sigma_{ij})$ becomes a larger and larger number, more and more significant figures must be carried to obtain a meaningful answer, since only that part left after subtracting 2π times the largest integer leaving a positive quantity is pertinent. The term $mB\psi_j$, of course, may be thoughtof as "good" to an infinite number of places, and since $k_m=mB\Omega/C$ this can also be thought of as infinitely "good", any error being dismissed as making exact some other case with a slightly different rotational speed, Ω. The phase radius σ_{ij}, therefore, is critical. The digital program is arranged, accordingly, to iterate on the value of S_{ij}, using a recurrence scheme where

$$S_{ijk} = S_o+\Delta S_k$$

where

$$\Delta S_{k+1} = \frac{[S_{ijk}]^2-S_o^2+[\Delta S_k]^2}{2(S_o+\Delta S_k)}.$$

The computer continues to iterate until

$$\Delta S_{ijk+1} < 10^{-5}\text{feet}.$$

This, for example, is within about $1/3\text{x}10^{-4}$ wave lengths for the 20th harmonic of a six-bladed rotor turning at 300 RPM.

As a test both of the program itself and of the accuracy of the numerical integration, a calculation was performed for the sound pressure level at the fundamental frequency generated by a two-bladed, 10-foot-diameter propeller, producing 1600 pounds of thrust at 1582 RPM and a forward speed corresponding to

M=0.2, and drawing 2680 foot-pounds of torque.

Results for this case are given in Figure 5 of Ref. 5 as a function of x_o when y_o=20 feet, z_o=0. The present program is, of course, capable of the same calculation, merely by setting α_s=90°, $\theta_{ij}=\theta_o$, β_j=0, and the remaining input appropriately. If only this is done, however, a one-to-one correspondence would not exist between the Garrick and Watkins results and those obtained here. The following approximations, made in the earlier work, must also be introduced in the subject analysis, at least for this one check case:

$$r_i = r_{effective} = 0.8R \quad \Big\} \text{ effective ring}$$

$$B\sum_i 1/2\rho C_i (U_{ij})^2 [C_{L_{ij}} \cos\phi_{ij} + C_{D_{ij}} \sin\phi_{ij}] \Delta r_i = \text{thrust} = 1600 \text{ pounds}$$

$$B\sum_i 1/2\rho C_i (U_{ij})^2 [C_{D_{ij}} \cos\phi_{ij} - C_{L_{ij}} \sin\phi_{ij}] \Delta r_i = \text{torque} = 2680 \text{ foot-pounds}$$

} uniform lift and drag

$$c_{m_i} = e_{m_i} = d_{m_i} \simeq \frac{mBC}{4r}$$

$$\Psi_{mi} = \kappa_{mi} = \Gamma_{mi} \simeq 0$$

} approximate square wave

$$S \simeq S_o - \frac{\gamma^2 y_o y}{S_o} \text{ in exponentials}$$

$$\simeq S_o \text{ in denominator of fractions}$$

$$(\tfrac{1}{S})^2 \text{ neglected compared to } \tfrac{1}{S}$$

} "far field" approximation

The case described above was run both with and without the "far field" and square wave approximations, using an interval of 1°. The results are compared with those of Ref. 5 in Figure 6. It is interesting to note that (1) the numerical integration duplicates the closed form analysis, (2) the sharp reduction in sound level predicted roughly one diameter ahead of the

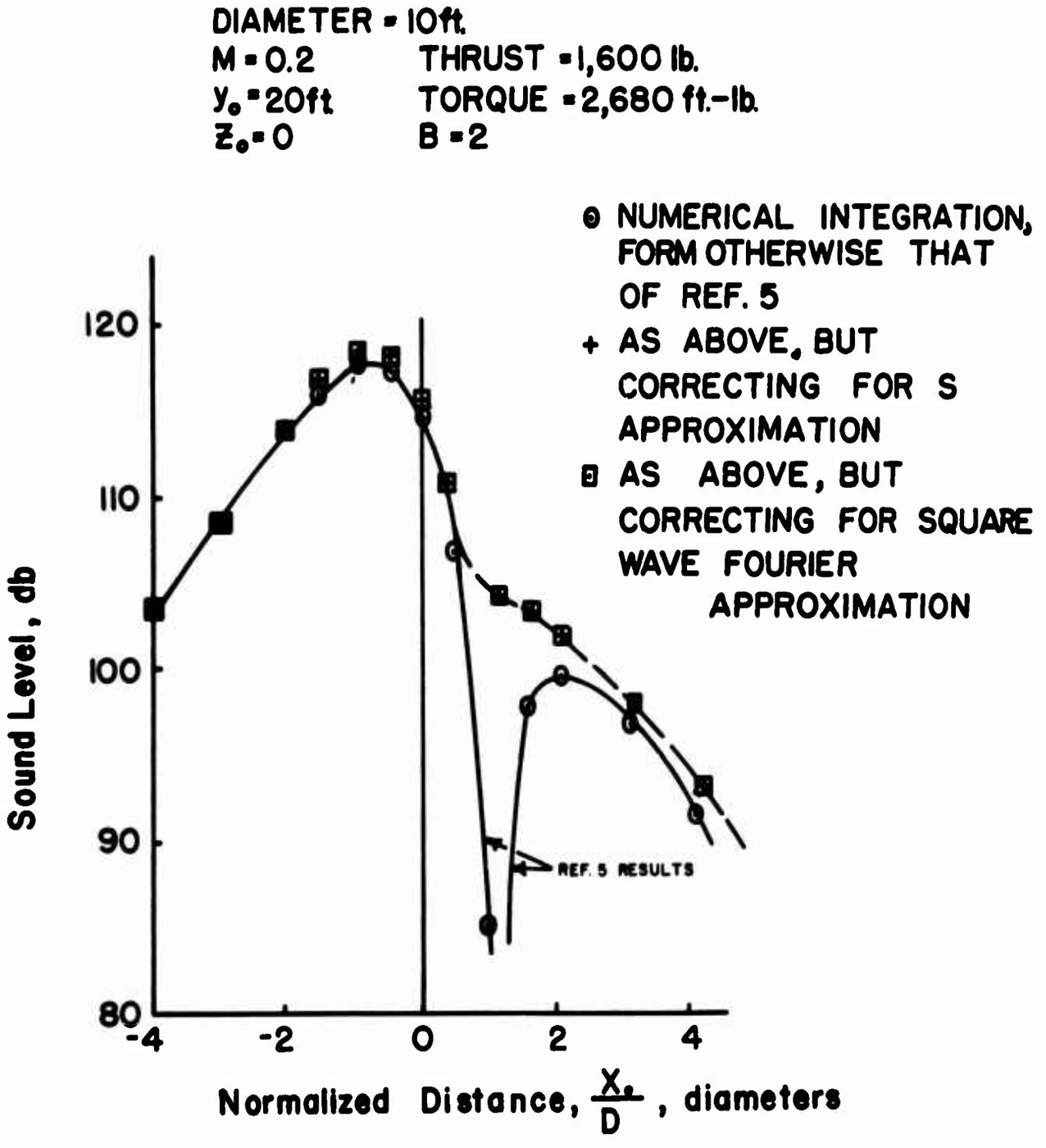

Fig. 6. FIRST HARMONIC PROPELLER NOISE COMPARISON.

propeller appears to be spurious, and a result of the "far field" approximation, and (3) for this harmonic, the square wave approximation leads to no significant errors.

COMPARISON WITH HELICOPTER NOISE MEASUREMENTS

Although this correlation with earlier computations is encouraging, the crucial test for any prediction method is a comparison with experimental results. Simultaneous aerodynamic section loadings and sound pressure measurements for an isolated rotor were not available; however, such measurements are contained individually in Refs. 16 and 19, respectively, for the complete H-34 helicopter in a hover. The gross weights, moreover, were roughly the same in the two tests. Accordingly the sound pressure levels were calculated for the H-34 helicopter in hover for 220 main rotor RPM at a radial distance 200 feet from the rotor hub, and at a field point azimuth angle of 150°. The radial and azimuthal coordinates of the field point correspond closely to "Position 23" in Ref. 19, and these horizontal distances could be well controlled in the referenced tests. Vertical distances were subject to a greater percentage of uncertainty, since the pilot was attempting to hover the aircraft with the wheels 5 feet off the ground, and the microphones were hand-held. It will be shown later that from hub height to two rotor diameters beneath the rotor, sound levels in an octave band can vary as much as 25 decibels. Accordingly, the z_o distance was chosen as -10 feet and -16 feet to indicate the sensitivity of this parameter. These dimensions were chosen as, roughly, engine height and wheel height, respectively.

The results of the calculation are shown in Figure 7 as vertical bars. To approximate measurements made over a reflective surface, all the levels indicated as "calculated" have actually had 3 decibels added to them.

The comparison with the measured values is notable more in the lack of correlation than in the agreement obtained. The first harmonic frequency is below the response range of the instrumentation used, so no check can be made for this component. The second harmonic falls very close to a cluster of the measured peaks, but for the third and higher harmonics calculated levels are substantially low.

The source of discrepancy can be sought in both the theory and the test results. Consider first the latter. The tail rotor and the reciprocating engine frequencies are indicated on the same figure; note that the tail rotor fundamental is exactly 6 times that of the main rotor. With a view toward more refined test data as well as to substantiate the data presented in Ref. 19, a second narrow-band analysis, not presented in

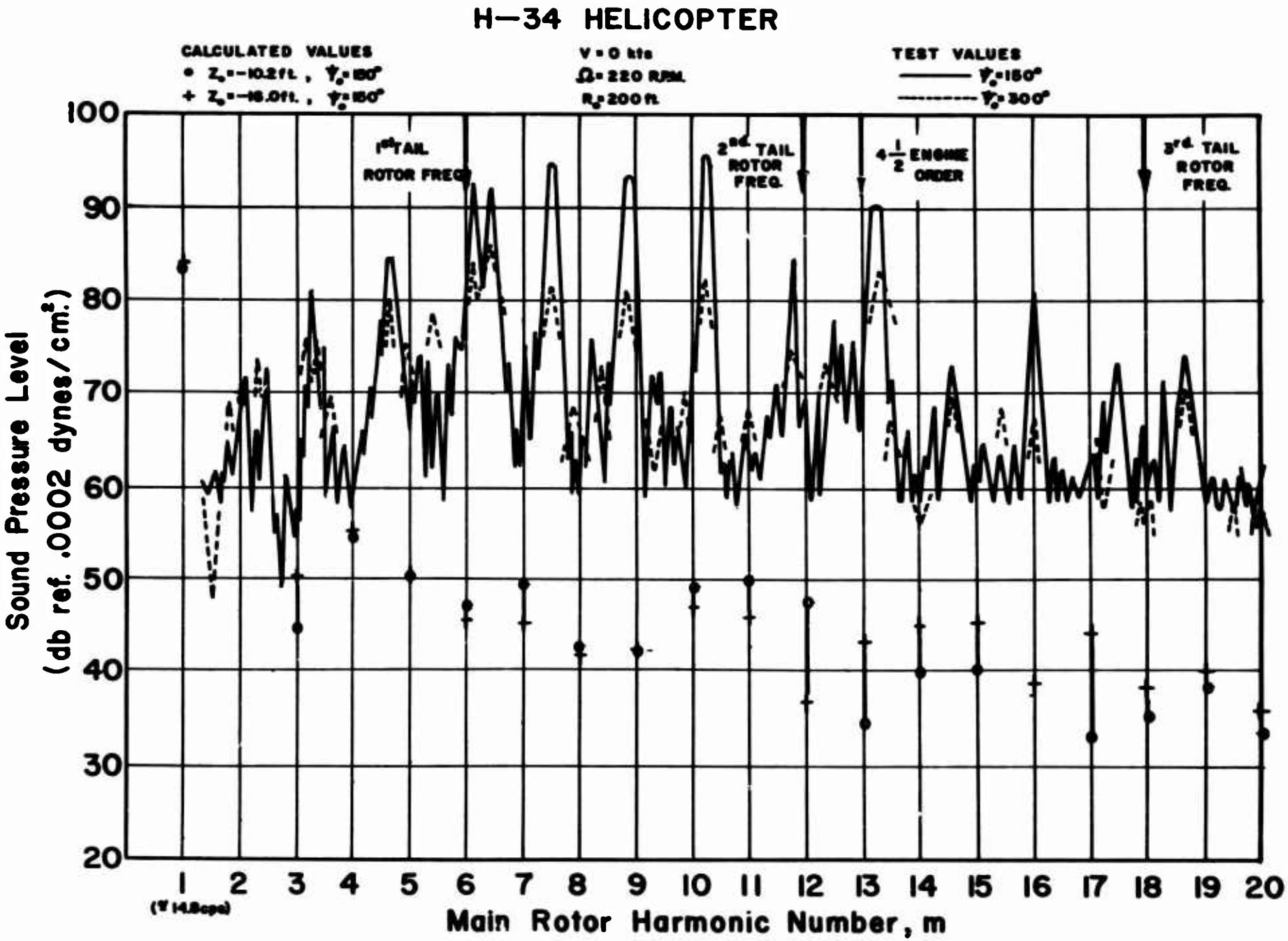

Fig.7. COMPARATIVE SOUND LEVELS, CALCULATED versus TEST.

Ref. 19, was obtained. This second sound spectrum is for the same aircraft under the same operating conditions, but with the field point azimuth shifted to ψ_o=300°; at this field point, maximum masking of the tail rotor and engine exhaust noise would be expected. Some idea as to the contribution of sources other than the main rotor is given by comparing the test curves for ψ_o=300° and ψ_o=150° in Figure 7. Since the masking certainly does not eliminate the effect of the unwanted noise sources, "corrected" test data would be still lower than that for ψ_o=300°.

It is reasonable to question the number of azimuthal stations needed to properly represent harmonics as high as the twentieth. This case was, therefore, run with various numbers of azimuthal increments. These are listed in Table II. It was found that the breakdown shown as "Trial 1" resulted in accurate calculation of harmonics up to the 7th. The limiting harmonic was raised to the 13th when the size of the azimuthal steps was decreased as indicated by "Trial 2" in Table II. Finally, for hover, it was established that harmonics up to the 20th will be substantially unaffected if the azimuthal increments are reduced to smaller values than those associated with "Trial 3". The values shown as "calculated" in Figure 7 were obtained using the "Trial 3" breakdown.

In considering shortcomings of the theory, it must be noted that the prediction method has been concerned from the outset with only the sound resulting from resultant lift and drag forces. Pressure fields due to blade thickness, boundary layer turbulance and wake effects have all been neglected, and, thus, one would expect underestimation of the actual sound field. Another effect, not accounted for here, is suggested by the fact that some of the measured peaks in the low harmonic range are shifted appreciably from integer multiples of the fundamental. Since the rotational noise "sources" are viewed as fixed on the swept area in this analysis, such an effect cannot be associated with doppler shifts due to source motion. On the other hand, much of the sound is received after passing through the non-uniform and time-varying vertical flow field just beneath the rotor. This could cause frequency shifts and changes in the radiation pattern due to refraction. It is likely, however, that for radiation pattern changes the presence of the ground reflecting plane has a more pronounced influence. A very curious aspect of the experimental spectrum in Figure 7 is the fact that the 6th, 9th and 12th harmonic peaks do not appear to have been shifted.

In spite of all the uncertainties in the comparison between test and calculation discussed above, it seems that for harmonics higher than the 3rd, rotational noise is probably not the major source in hover. It is worth noting, however, that

TABLE II
SWEPT AREA BREAKDOWN FOR NUMERICAL INTEGRATION:
H-34 HELICOPTER

Radial Station r_i (ft)	Width of Ring Δr_i (ft)	Number of Azimuthal Stations Trial 1	Trial 2	Trial 3	Trial 4	Trial 5
4.8	1.6	12	24	48	48	96
8.4	5.6	12	24	48	96	192
14.0	5.6	12	24	48	192	384
18.2	2.8	24	48	96	192	384
21.0	2.8	24	48	96	192	384
23.8	2.8	48	96	192	192	384
26.6	2.8	48	96	192	96	192

because of the high 1st harmonic, the calculated overall noise levels would check reasonably well with measured overall levels even in hover.

ROTOR NOISE IN FORWARD FLIGHT

In the machine computation of rotor noise, basic input data were obtained from Ref. 16 and Ref. 17, i.e., the data for ASL, α_s, β, θ versus helicopter and flight velocity. Table III provides specific cross-reference information. Tables V, VI, and VII are exact print-outs of the airfoil input data used, i.e., C_L, C_D, C_N versus α and M for 12 percent, 15 percent and 18 percent symmetric airfoils, respectively. In view of their length, these three tables are located immediately preceding the list of References at the end of this report.

The effect of forward speed is shown in Figures 8 through 15 for the H-34 and HU-1 helicopters. The major influence of forward flight is clearly in the higher harmonics, as would be expected. Since the prediction method is limited to the harmonics contained in the representation chosen for the chordwise pressure distributions shown in Figure 3, it is appropriate to examine the values of the Fourier amplitude coefficients, c_{m_i}, d_{m_i} and e_{m_i}. These are shown as functions of harmonic number for seven radial stations in Figures 16 through 21. The "flat" character of these curves at the more outboard stations indicates that the pressure distributions shown as a function of time in Figure 3 are well approximated by impulses for these and higher values of r_i/c_i.

The Fourier amplitude coefficients of an impulse are, of course, constant for all harmonics (Ref. 5, Figure 3). Deviations from impulse-type harmonic content occur in the inboard stations; it follows that before eliminating Eq. (3) in favor of a constant, the relative importance of inboard versus outboard stations as noise sources must be established. The greater variations in velocity over the inboard blade sections at high forward speed would be expected to emphasize the contributions of these inboard sections. Accordingly, sound pressure levels were calculated for the H-34 helicopter, flying at 115 knots and a rotor speed of 231 RPM at a field point where R_o=200 feet, ψ_o=150°, and z_o=-10.2 feet. It had been found that in hover, the contribution of the outboard-most 10 percent of radius could be more than 50 percent of the sound in almost all harmonics. But at V=115 knots, the important contributions come from the more inboard rings. Accordingly, revised integration breakdowns, Trials 4 and 5 in Table II, were defined. The percentage contribution from the concentric rings of swept

TABLE III
CROSS REFERENCES FOR INPUT DATA FOR ASL, α_s, β, θ

Helicopter	Velocity	Ref.	Page		
			ASL	β, θ	α_s
	0		19	19	10
H-34	23	16	29	29	10
	79		64	64	10
	115		109	109	10
	0		152-153	317	5,35,319
HU-1	34	17	110-111	269	5,35,271
	88		124-125	285	5,35,287
	113		138-139	301	5,35,303

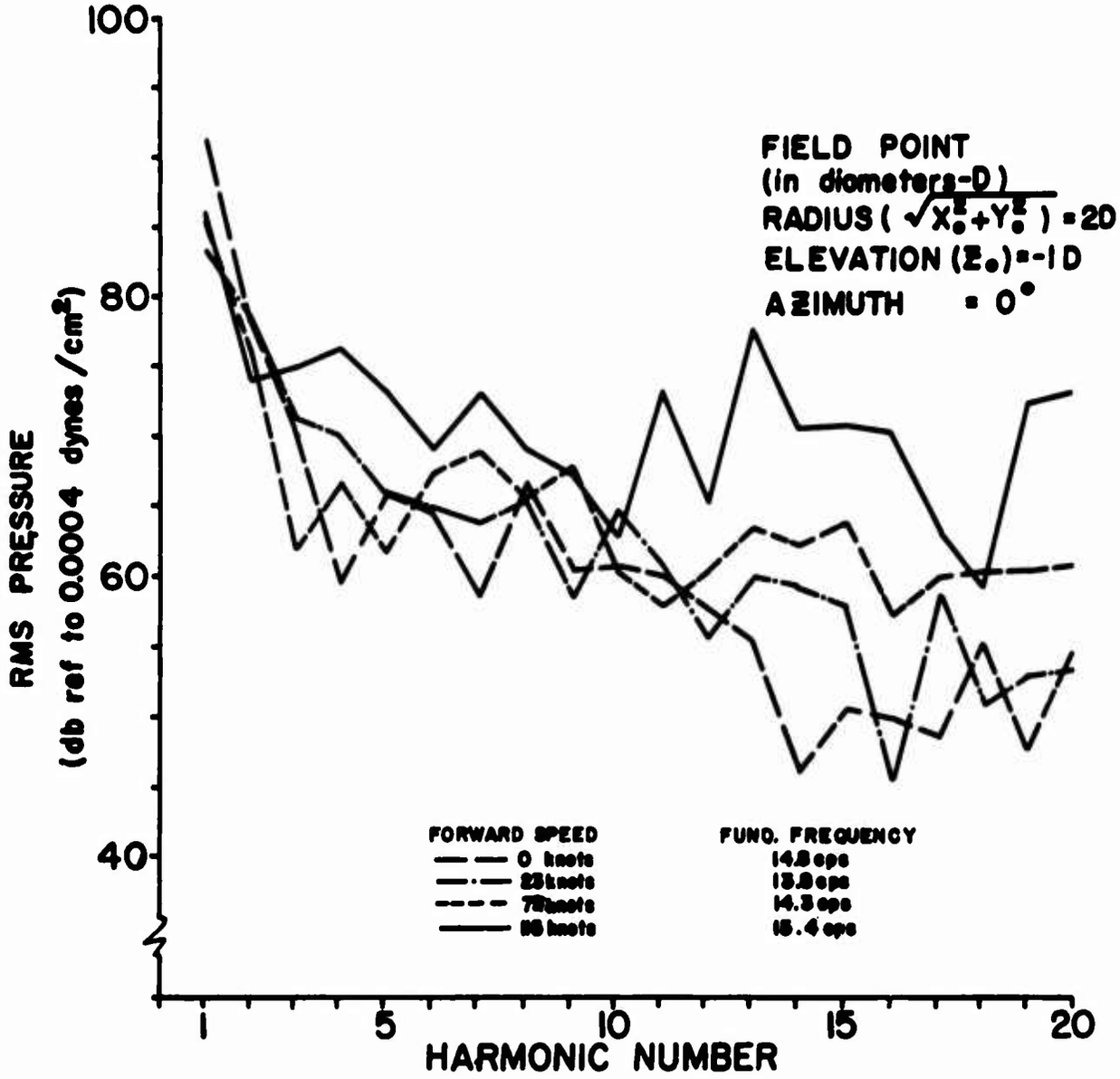

Fig.8. MAIN ROTOR ROTATIONAL NOISE FOR H-34 HELICOPTER.

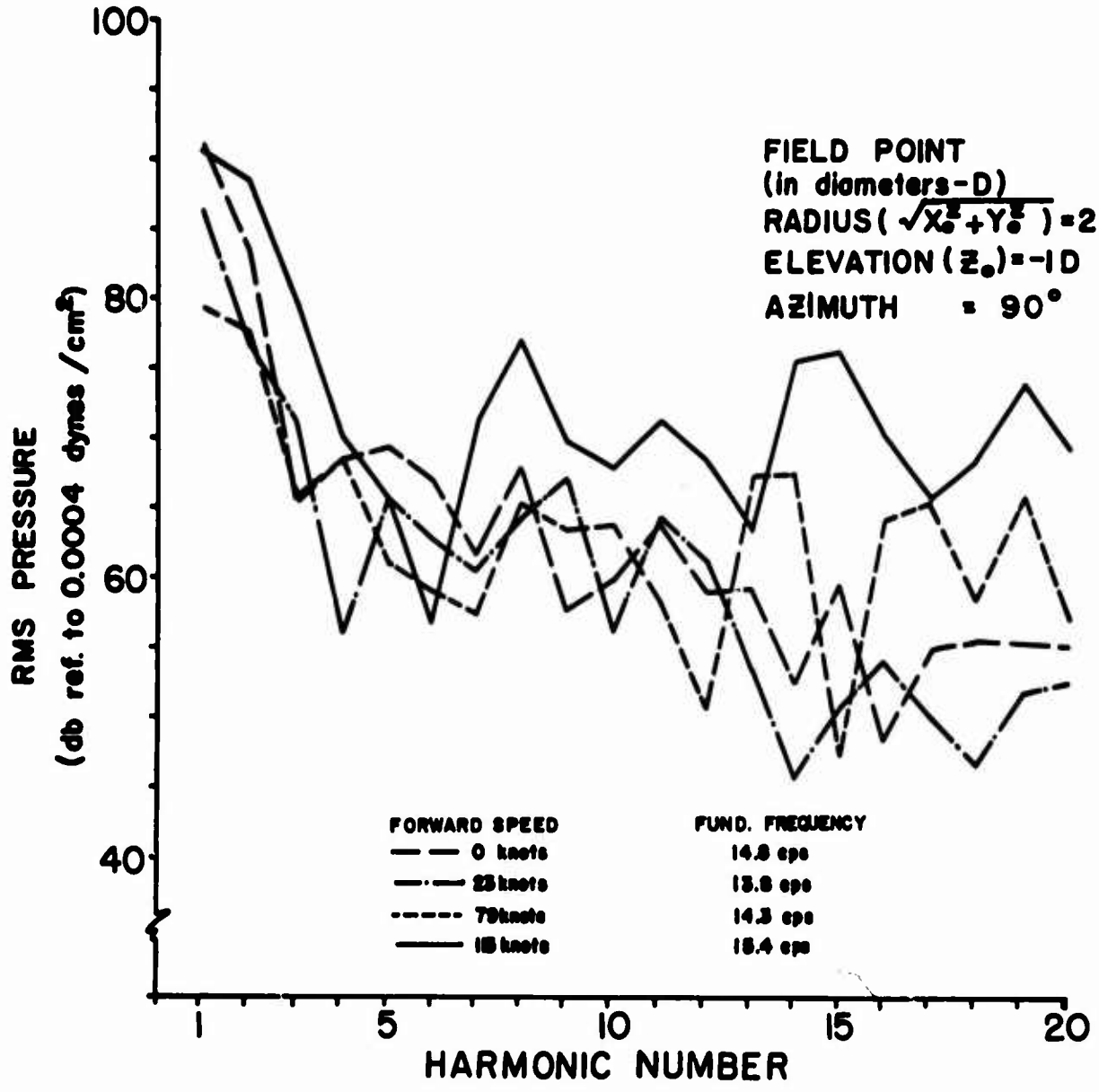

Fig. 9 MAIN ROTOR ROTATIONAL NOISE FOR H-34 HELICOPTER.

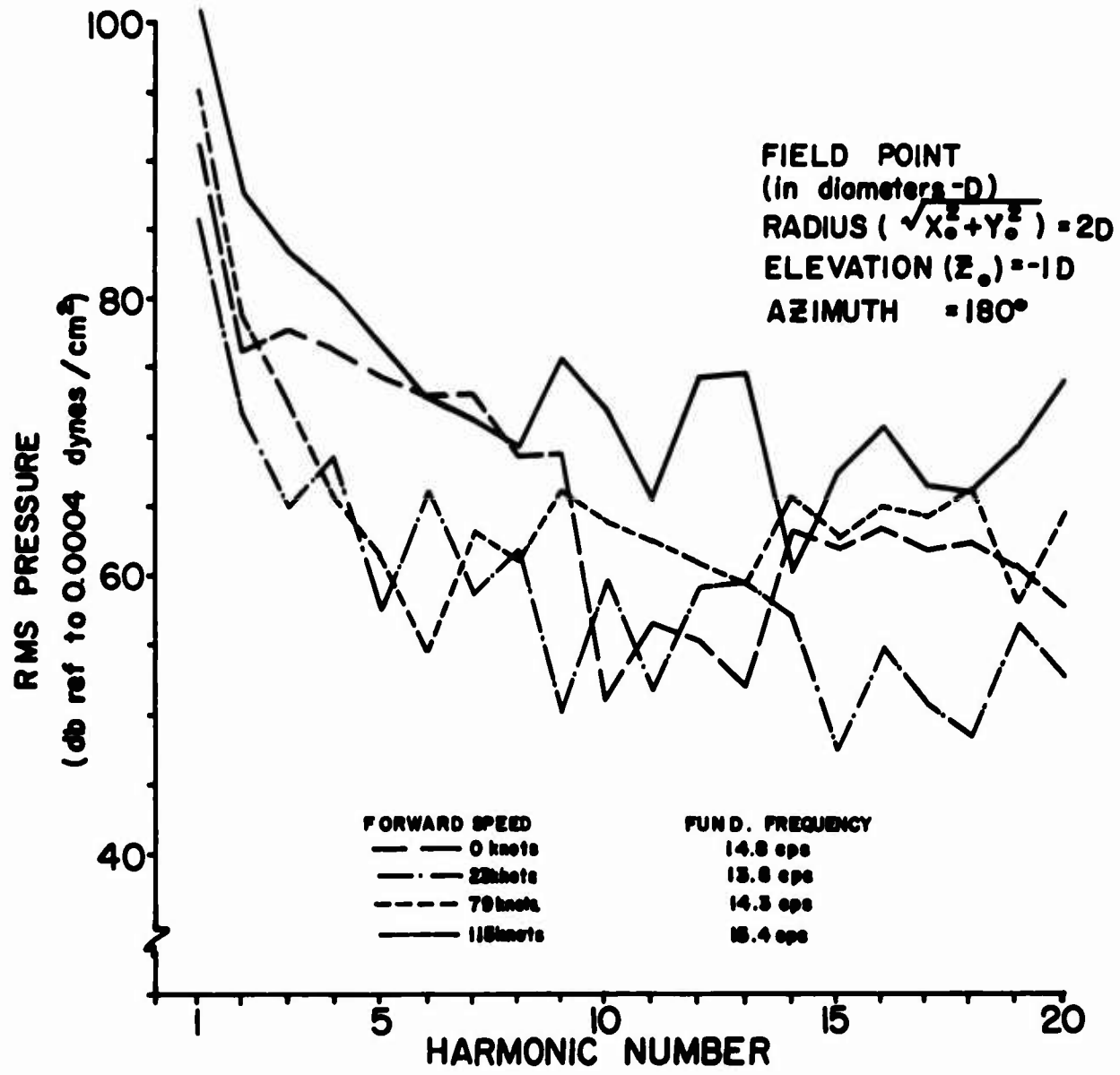

Fig.10 MAIN ROTOR ROTATIONAL NOISE FOR H-34 HELICOPTER.

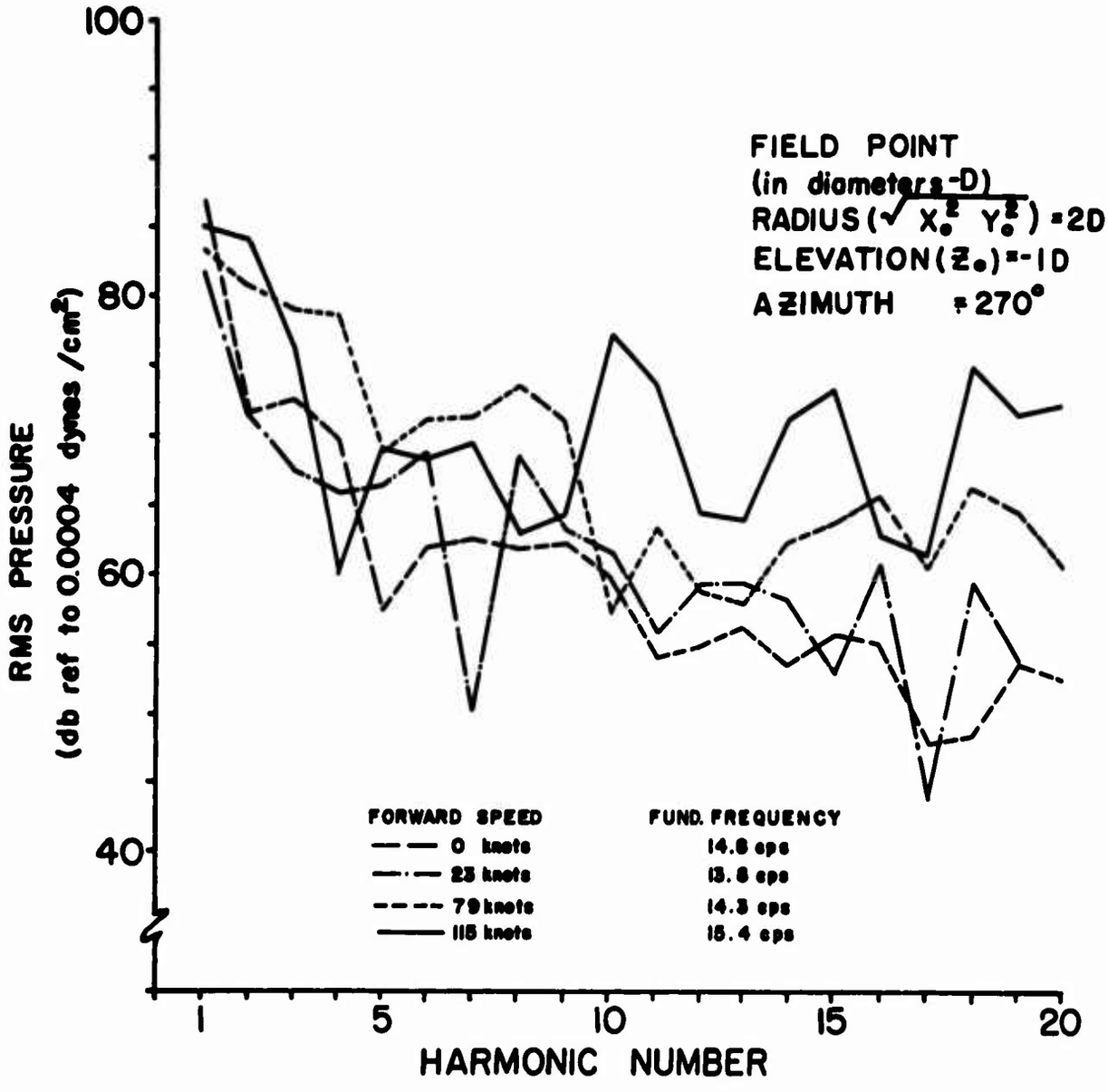

Fig.11. MAIN ROTOR ROTATIONAL NOISE FOR H-34 HELICOPTER.

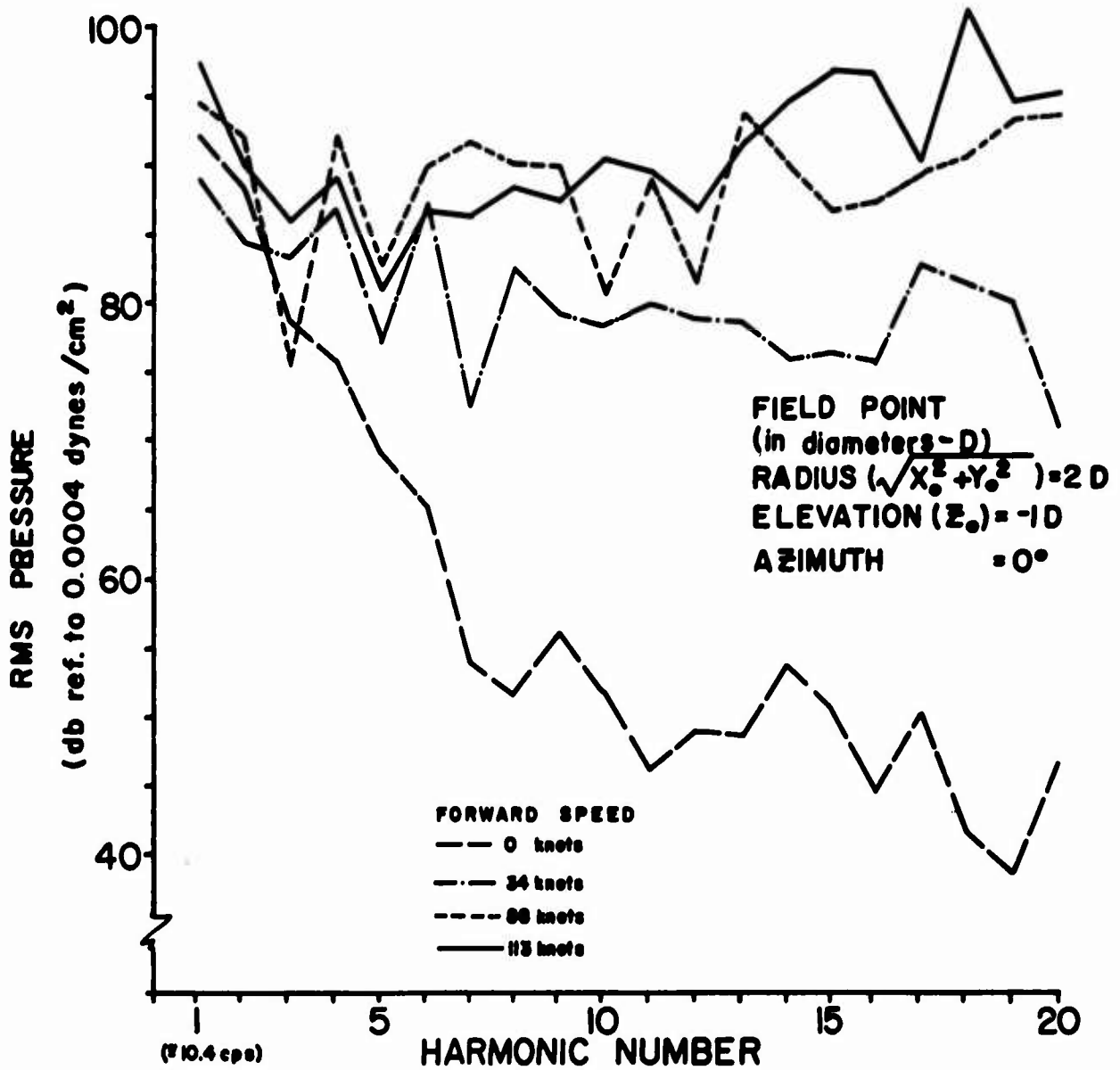

Fig.12. MAIN ROTOR ROTATIONAL NOISE FOR HU—1 HELICOPTER.

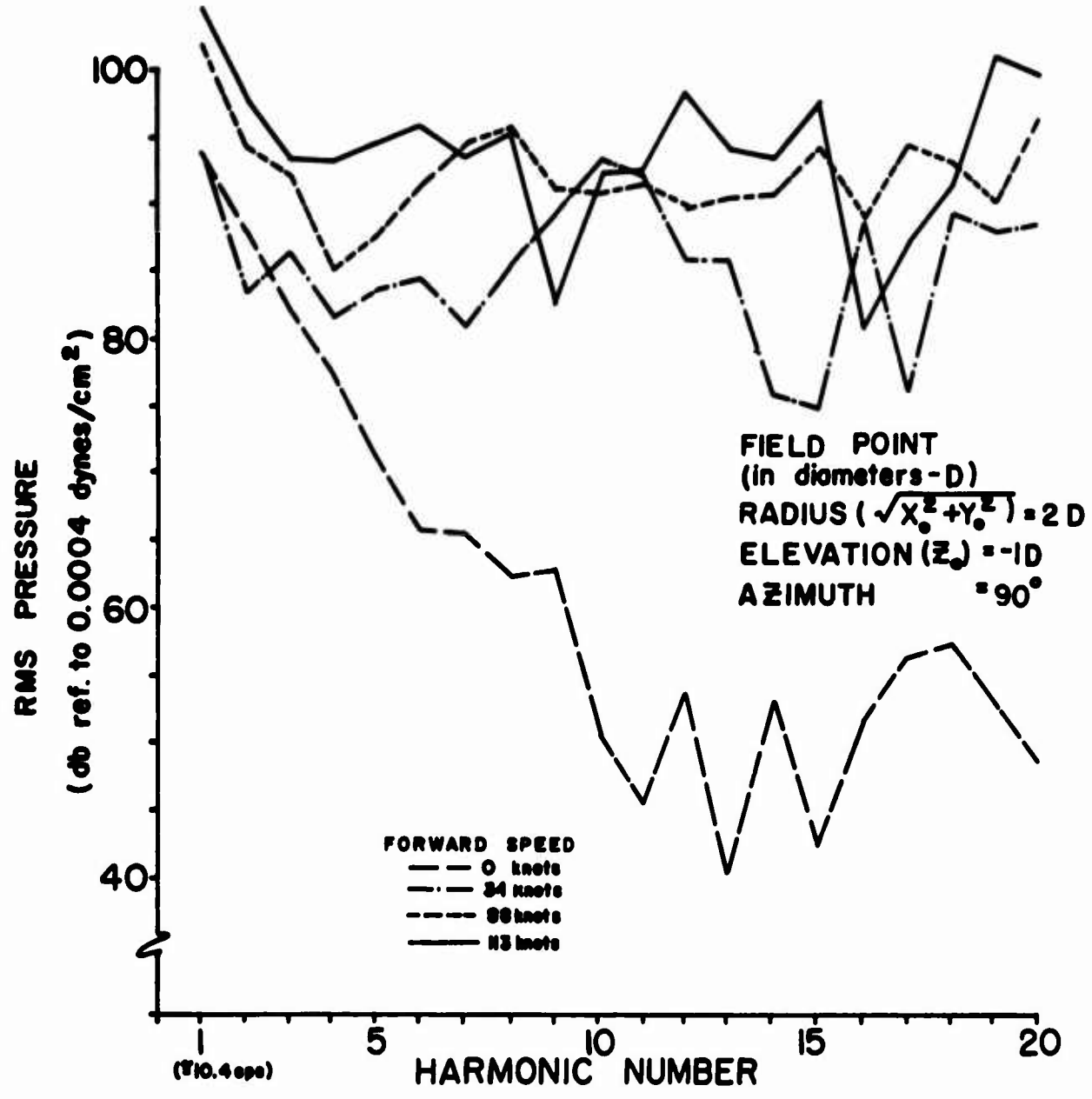

Fig.13. MAIN ROTOR ROTATIONAL NOISE FOR HU—1 HELICOPTER.

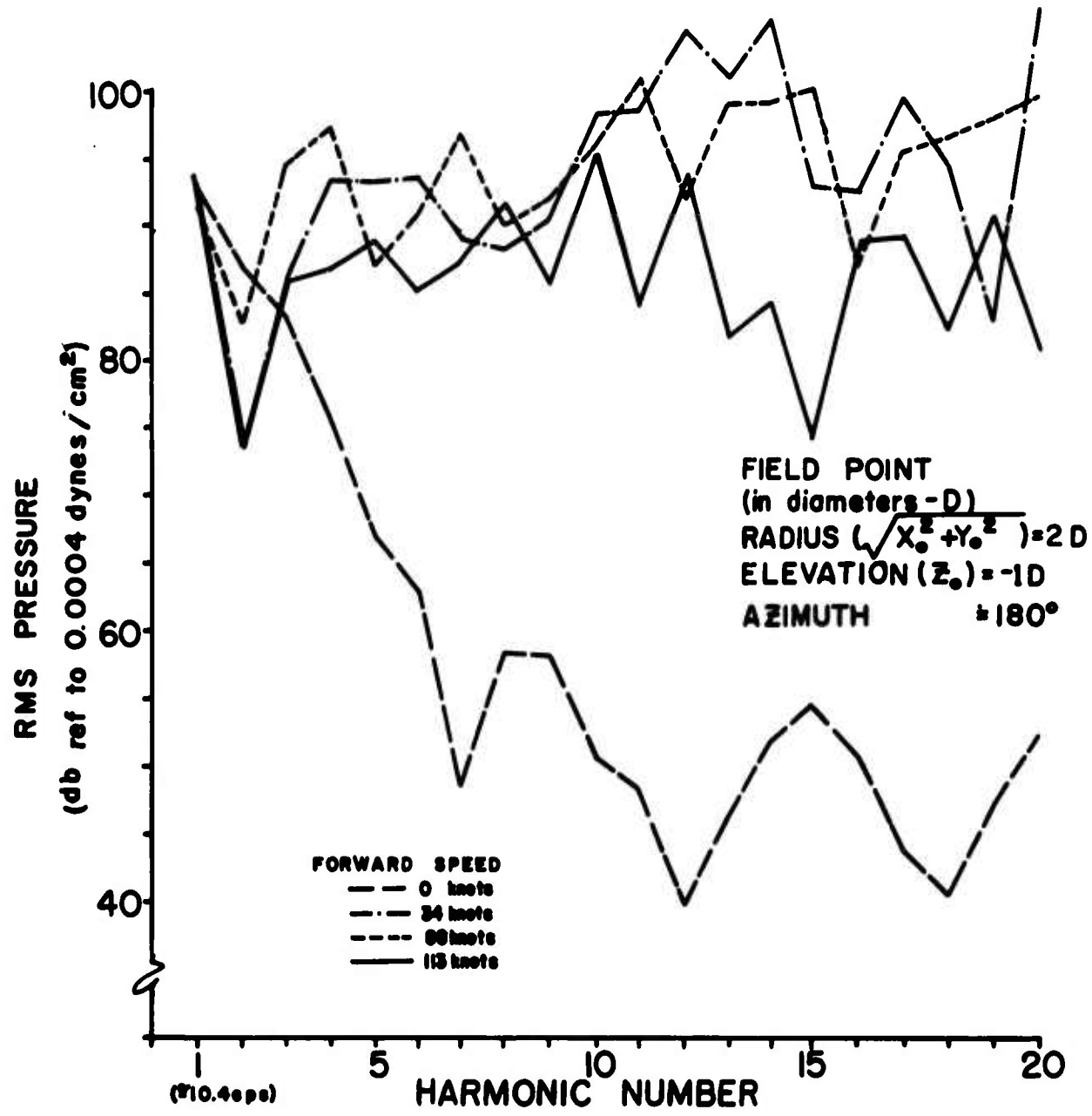

Fig.14. MAIN ROTOR ROTATIONAL NOISE FOR HU-1 HELICOPTER.

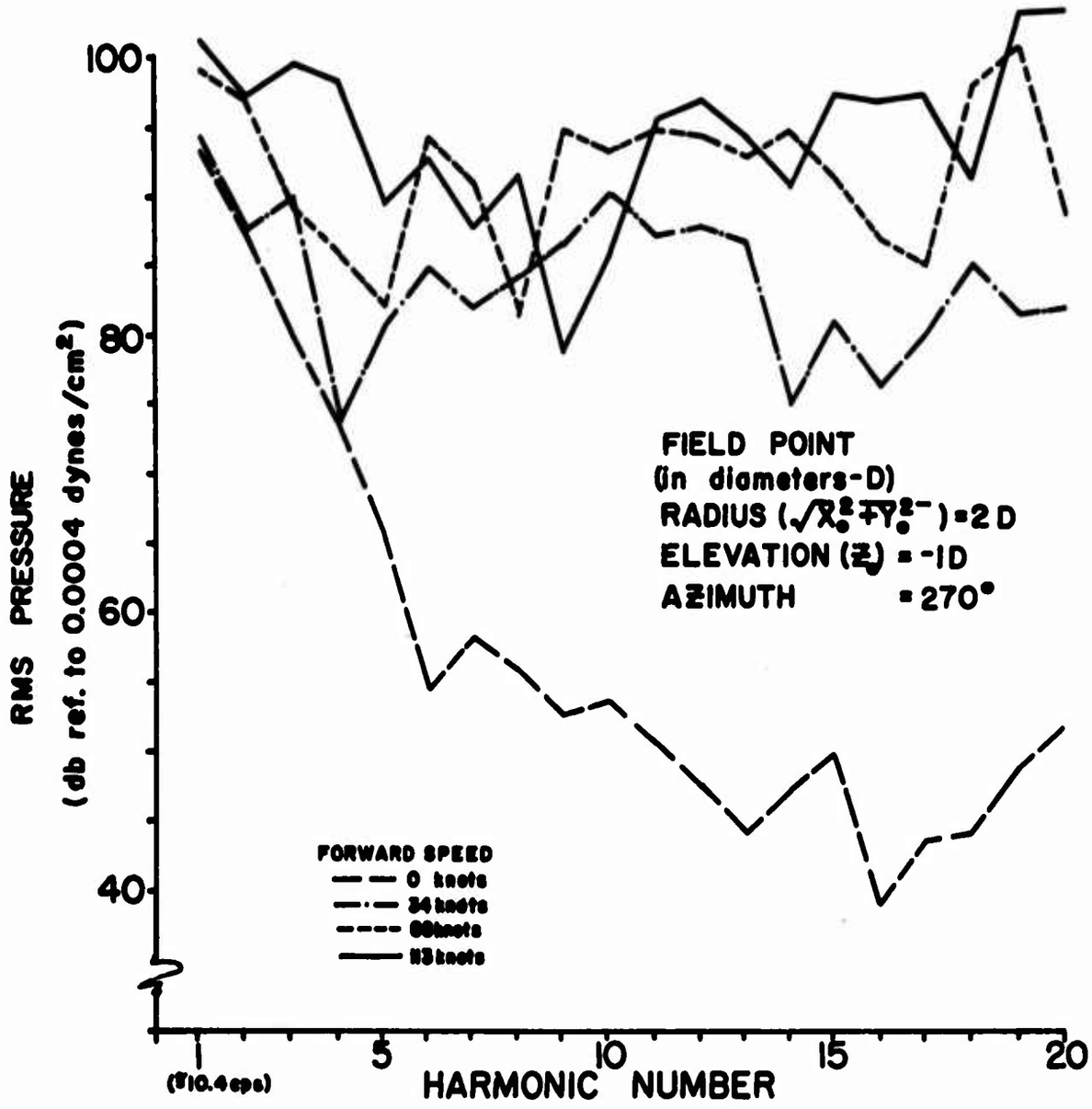

Fig.15. MAIN ROTOR ROTATIONAL NOISE FOR HU—1 HELICOPTER.

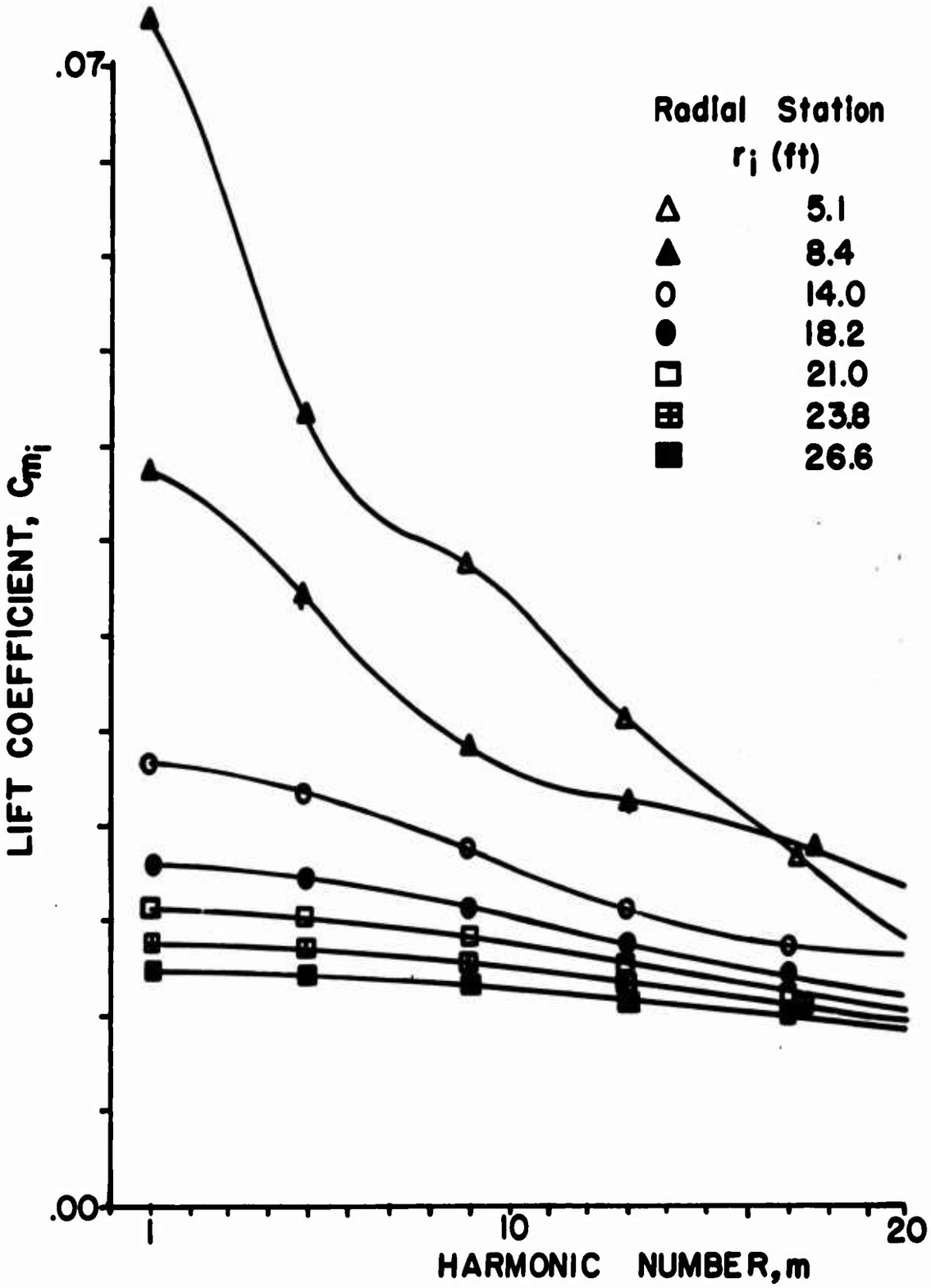

Fig. 16. FOURIER AMPLITUDE COEFFICIENTS FOR H-34 HELICOPTER.

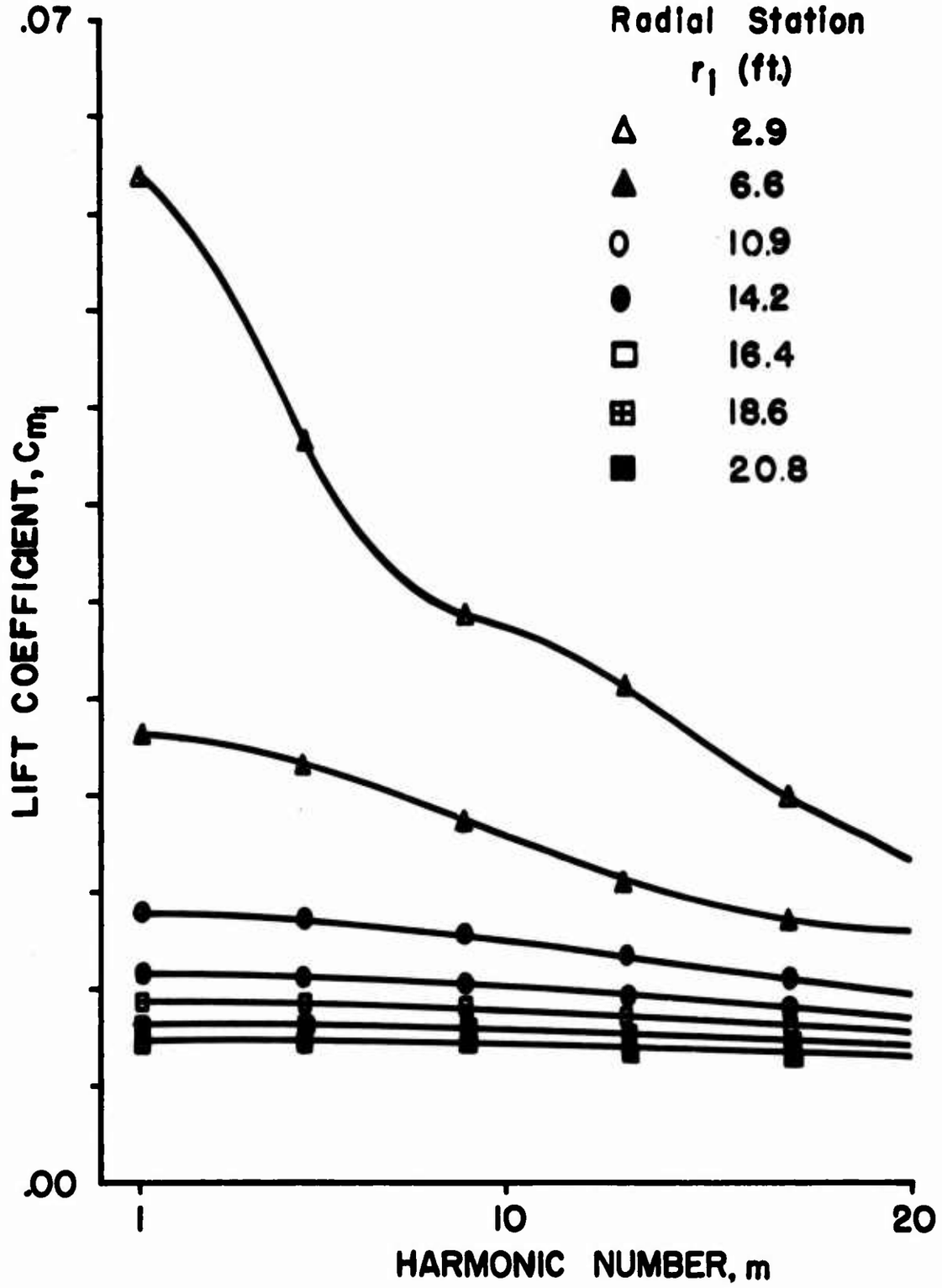

Fig.17. FOURIER AMPLITUDE COEFFICIENTS FOR HU—1 HELICOPTER.

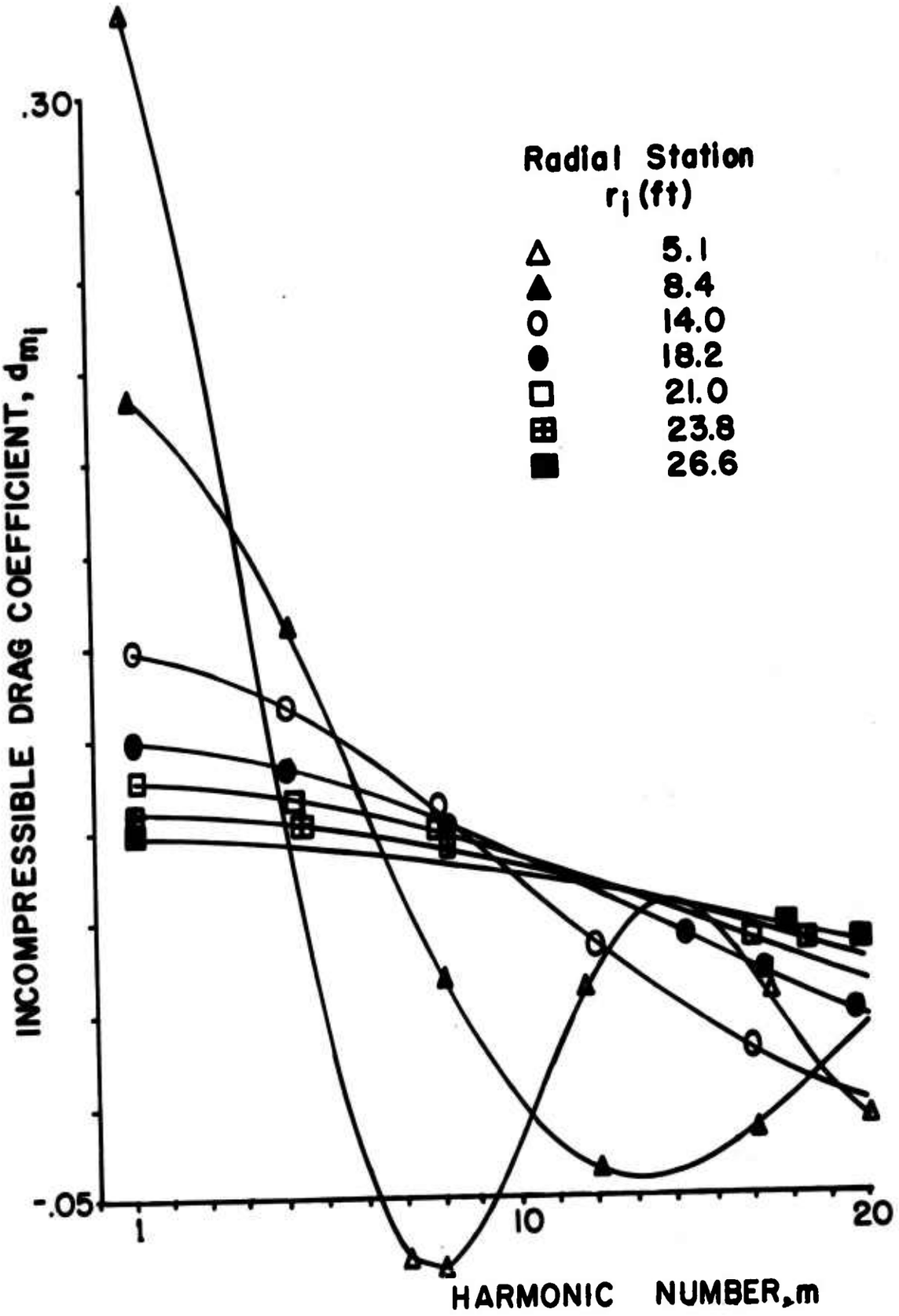

Fig.18. FOURIER AMPLITUDE COEFFICIENTS FOR H—34 HELICOPTER.

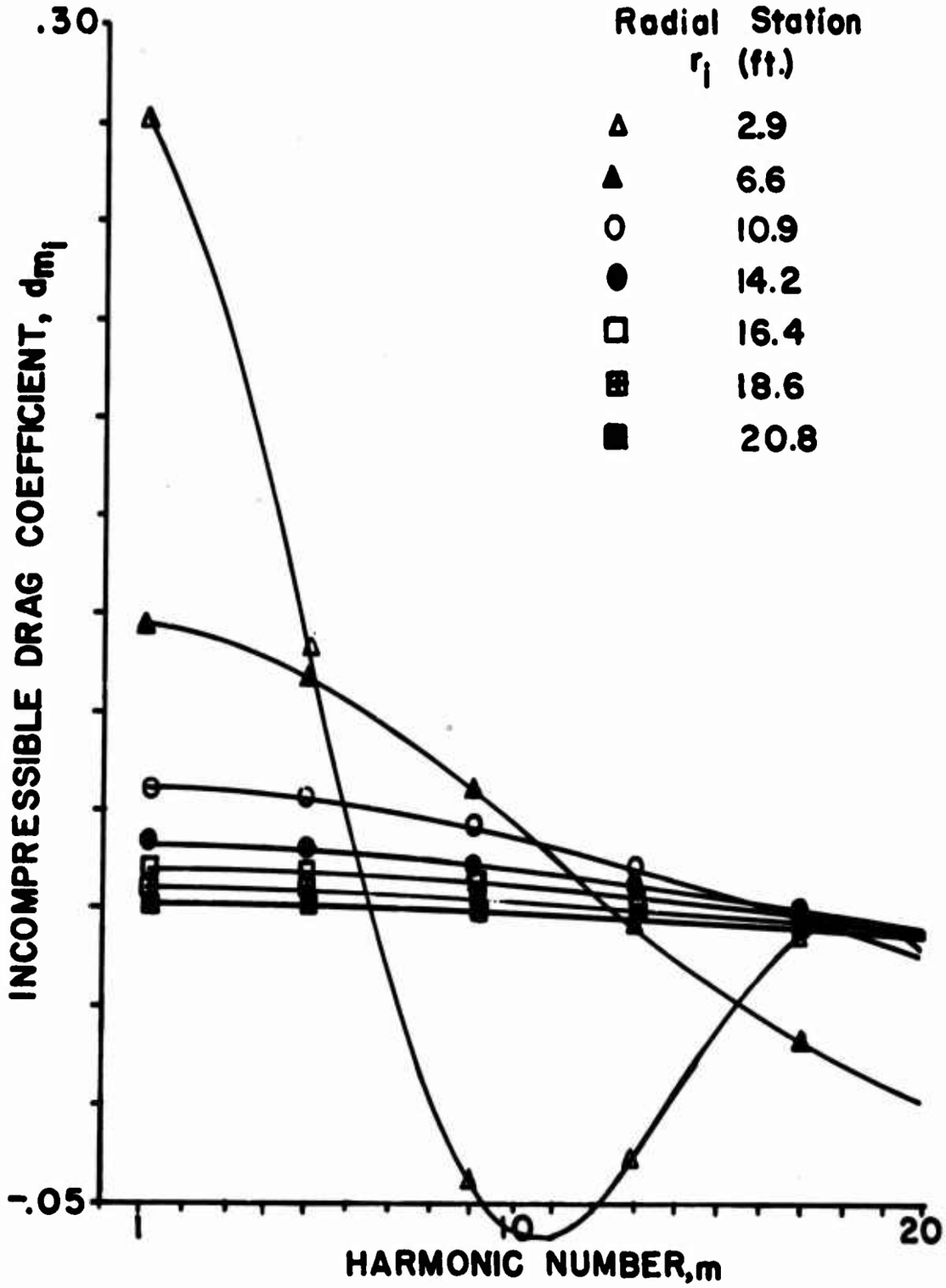

Fig. 19. FOURIER AMPLITUDE COEFFICIENTS FOR HU-1 HELICOPTER.

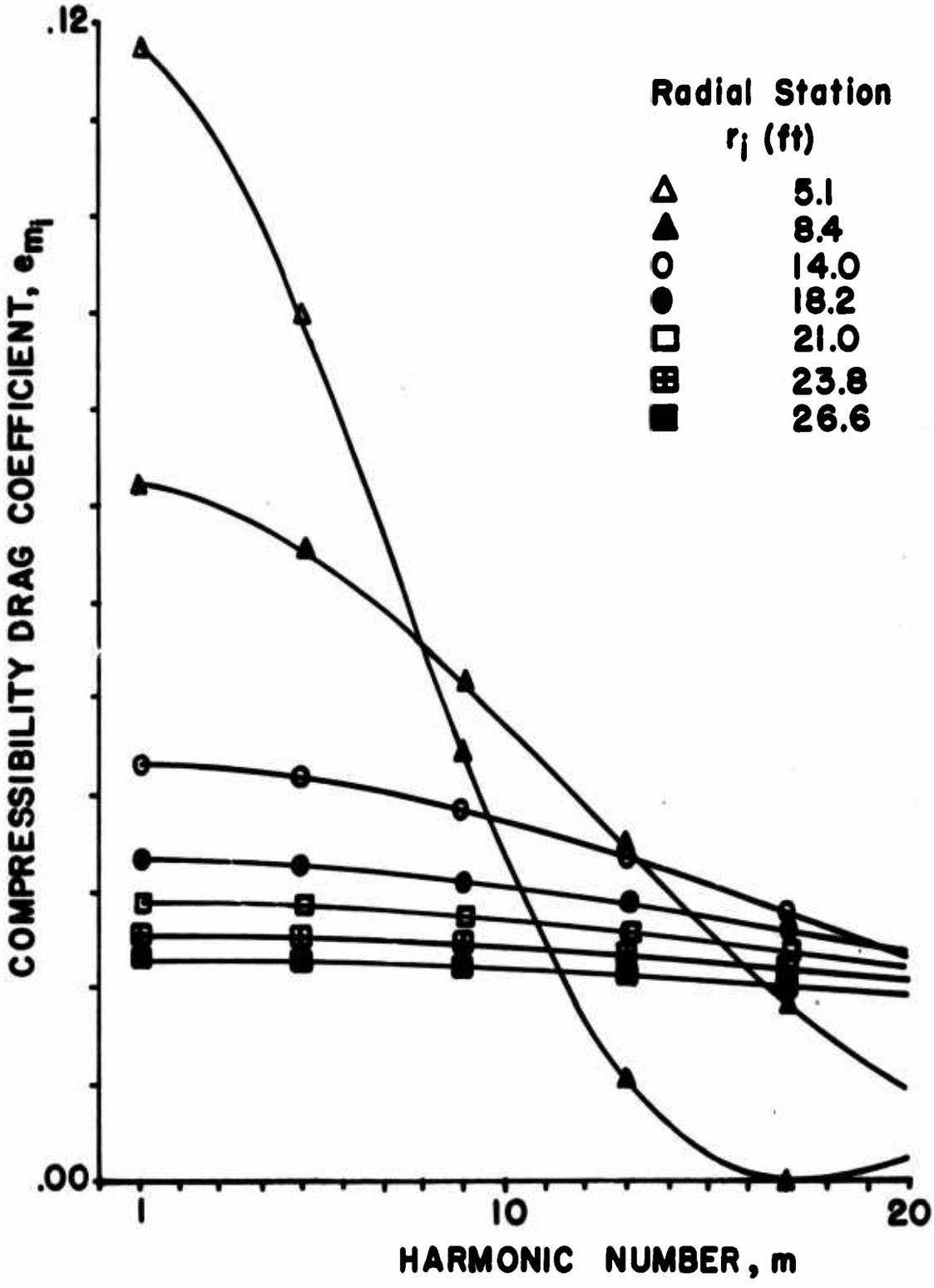

Fig.20. FOURIER AMPLITUDE COEFFICIENTS FOR H-34 HELICOPTER.

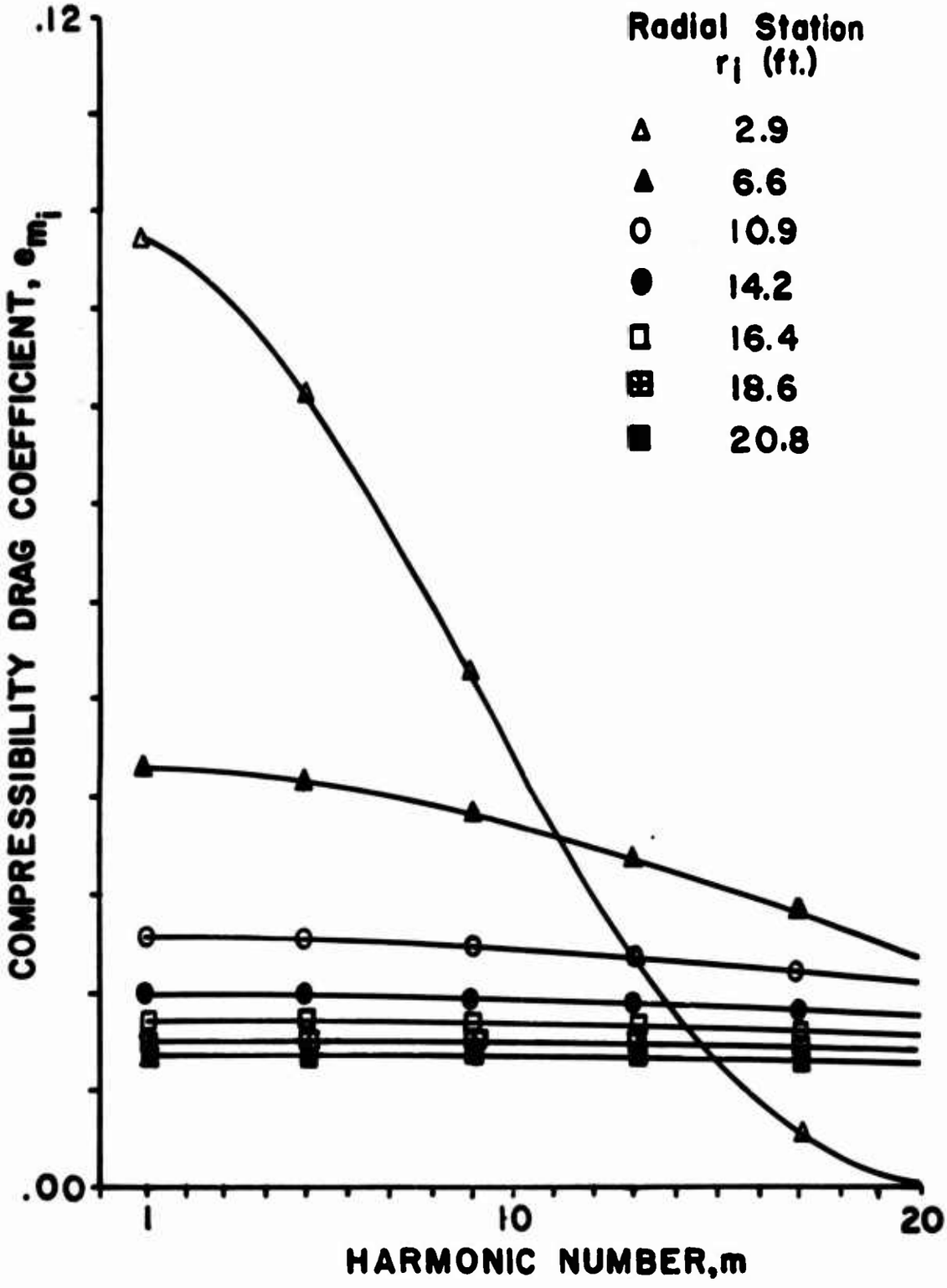

Fig. 21. FOURIER AMPLITUDE COEFFICIENTS FOR HU—1 HELICOPTER.

area are indicated in Table IV based on a Trial 4 breakdown. Note that a percentage greater than 100 means that the outboard rings had a canceling rather than a reinforcing effect. It would be expected that the higher the harmonic content of the aerodynamic section loading, the more azimuthal stations might be required to properly predict the higher harmonics. In spite of this, no important differences were noted between Trials 3 and 4, so the Trial 3 breakdown was used for all calculations from hover to maximum forward speed.

It is interesting that the increase in higher harmonic noise level with forward speed, as shown in Figures 8 through 11 (i.e., for the H-34 helicopter), is rather gradual. The same increase for the HU-1 helicopter, as shown in Figures 12 through 15, however, appears to take place almost entirely between hover and the "transitional" forward speed of 34 knots. The cause of this is most likely to be in the aerodynamic section loading; a comparison of this basic information is, therefore, shown in Figures 22 and 23 for the H-34 and HU-1, respectively. The oscillatory nature of these curves can be seen to increase markedly for the HU-1 between V=0 and V=34 knots, while there is a gradual increase in the number of "wiggles" with speed for the H-34.

RADIATION PATTERNS

Enough calculations have been performed to allow sound radiation patterns to be examined for individual harmonics. Such a presentation, however, would entail a very large number of figures. Since field measurements are often made using octave band filters, it was decided to present the calculated data in that form, in spite of harmonics falling on frequencies which are borderline between one octave band and another. Figures 24 through 27 show azimuthal patterns for the H-34 in hover and at three forward speeds in the first three octave bands at a radius of two rotor diameters. Figures 28 through 30 show similar data at a distance of ten diameters.

Although dissymmetries begin to become appreciable for the H-34 at higher forward speeds, there is nearly polar symmetry. Only at ten diameters and in the first octave band radiation pattern of the H-34 at high forward speed, does the pattern tend to be lobe-like on either side of the longitudinal center line of the helicopter and facing roughly aft. The existence of azimuthal asymmetry apparently depends on both field point radius and speed. These changes with field point radius are shown by comparison of Figures 25 and 28, Figures 26 and 29, and Figures 27 and 30, for field points located in a plane one diameter below the helicopter. The patterns might show greater changes at other values of observer elevation; these were not investigated.

TABLE IV
PERCENT OF TOTAL SOUND PRESSURE*
PRODUCED BY FRACTIONS OF THE SWEPT AREA

Harmonic Number	% Radius Included						
	100%	90%	80%	70%	57.5%	40%	23.5%
1	100	89.1	72.2	54.0	33.4	16.9	3.70
2	100	95.0	51.9	25.1	17.9	9.8	1.30
3	100	90.3	80.9	14.3	78.1	49.4	7.00
4	100	101.6	113.0	43.2	20.5	6.7	3.00
5	100	98.7	46.3	33.2	21.2	5.4	0.51
6	100	101.8	189.5	392.0	200.8	13.7	3.74
7	100	100.0	77.3	60.3	54.8	12.2	1.80
8	100	96.8	122.6	21.0	73.4	14.8	1.50
9	100	106.2	172.6	22.1	91.6	33.8	2.50
10	100	101.0	85.0	0.5	25.3	9.1	0.60
11	100	98.5	86.8	152.4	76.8	10.4	2.00
12	100	99.6	31.5	22.3	22.1	3.8	0.20
13	100	100.0	120.9	43.1	21.3	6.7	0.40
14	100	101.2	27.2	151.6	31.3	7.6	0.80
15	100	99.4	56.4	37.8	23.9	3.5	0.20
16	100	100.8	79.7	60.8	36.9	5.6	0.20
17	100	100.2	87.9	55.4	19.6	4.5	0.80
18	100	100.1	72.4	42.3	15.4	2.6	0.07
19	100	100.5	44.3	10.5	35.4	5.9	0.40
20	100	100.2	42.0	67.0	37.3	9.0	0.80

*Percent of $\sqrt{P_R^2+P_I^2}$ for H-34, V=115 knots, x_o=161.366 feet, y_o=100 feet, z_o=10.2feet using Trial 4 (see Table II) source point grid.

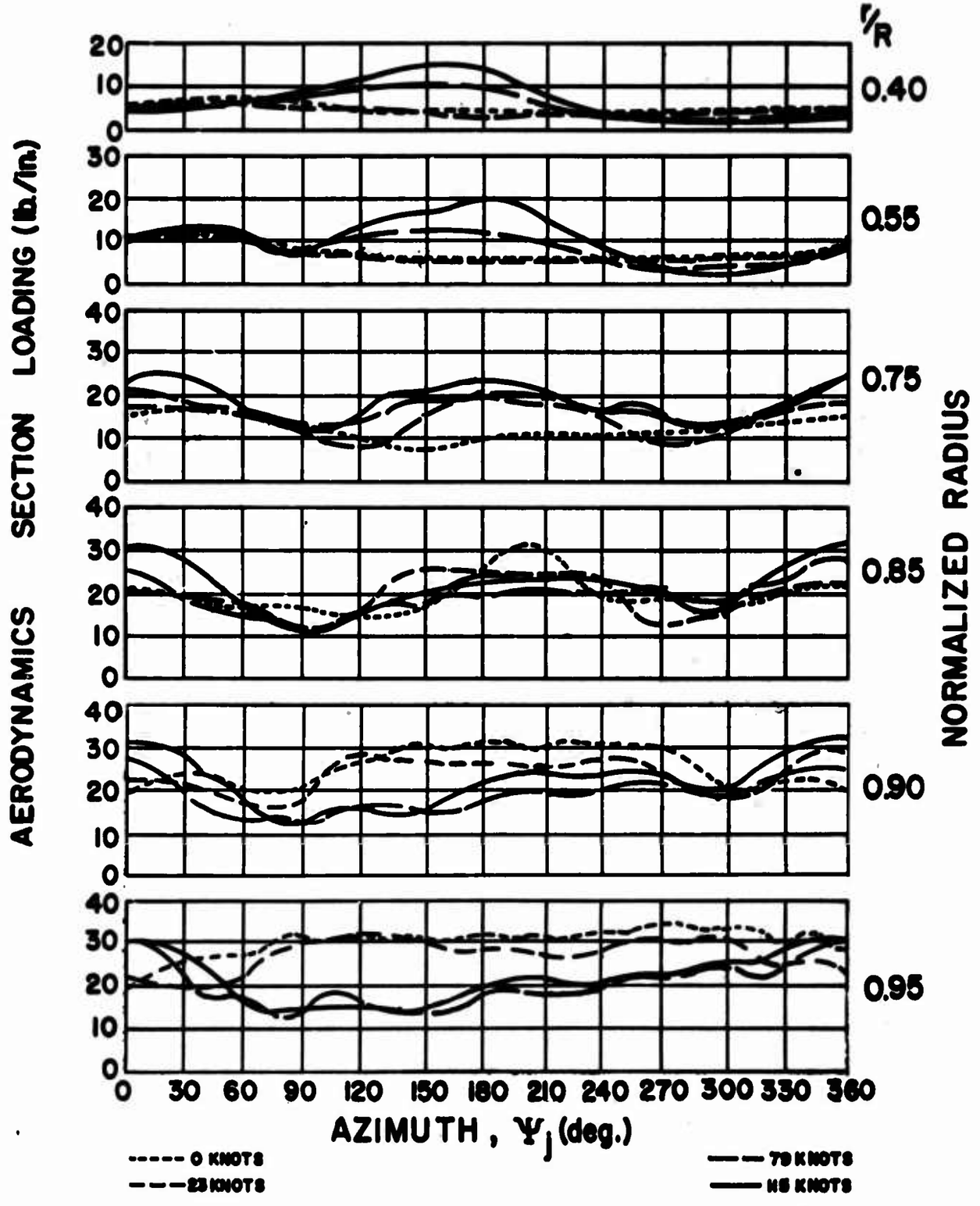

Fig. 22. AERODYNAMIC SECTION LOADING, H-34 HELICOPTER.

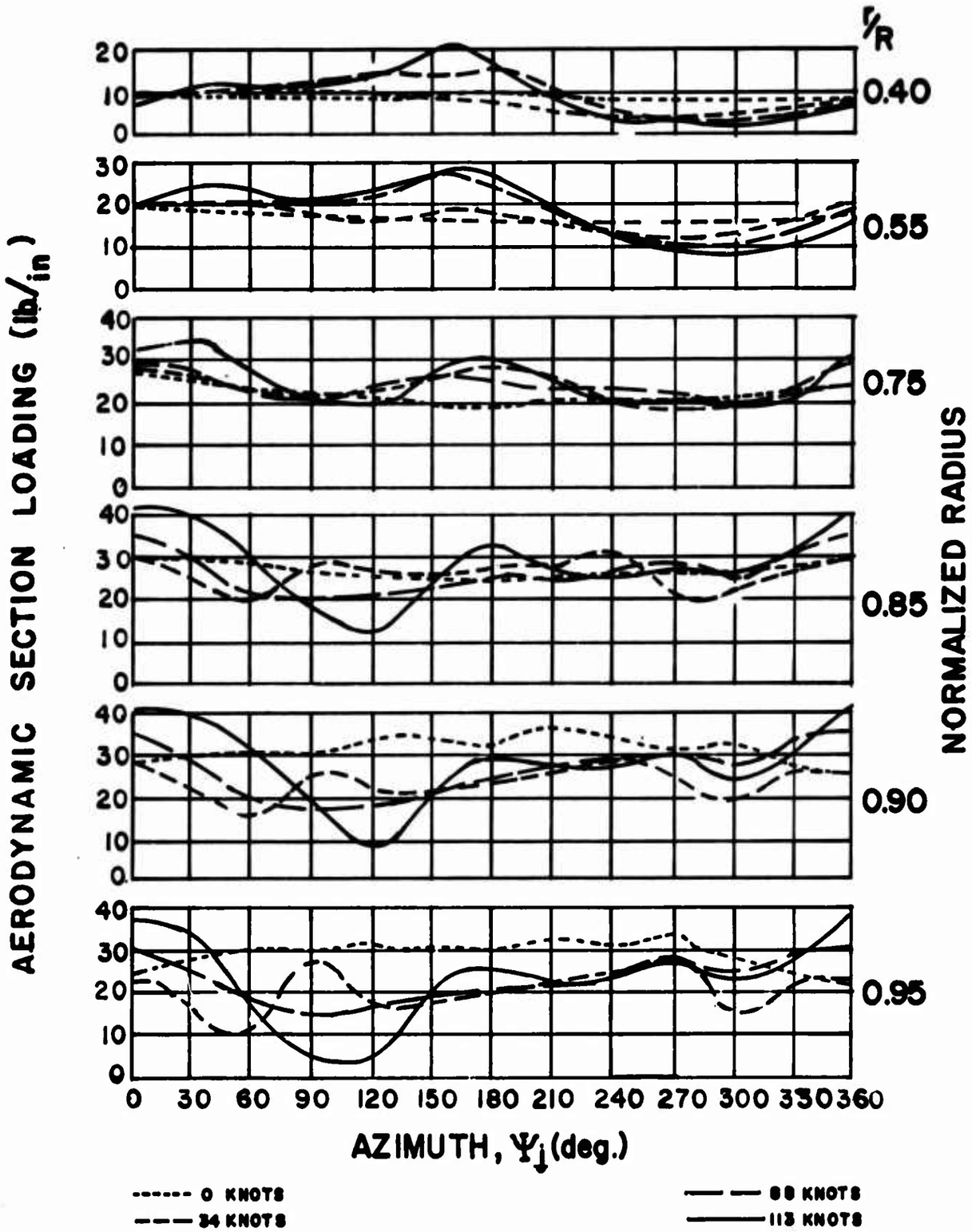

Fig. 23. AERODYNAMIC SECTION LOADING, HU—1 HELICOPTER.

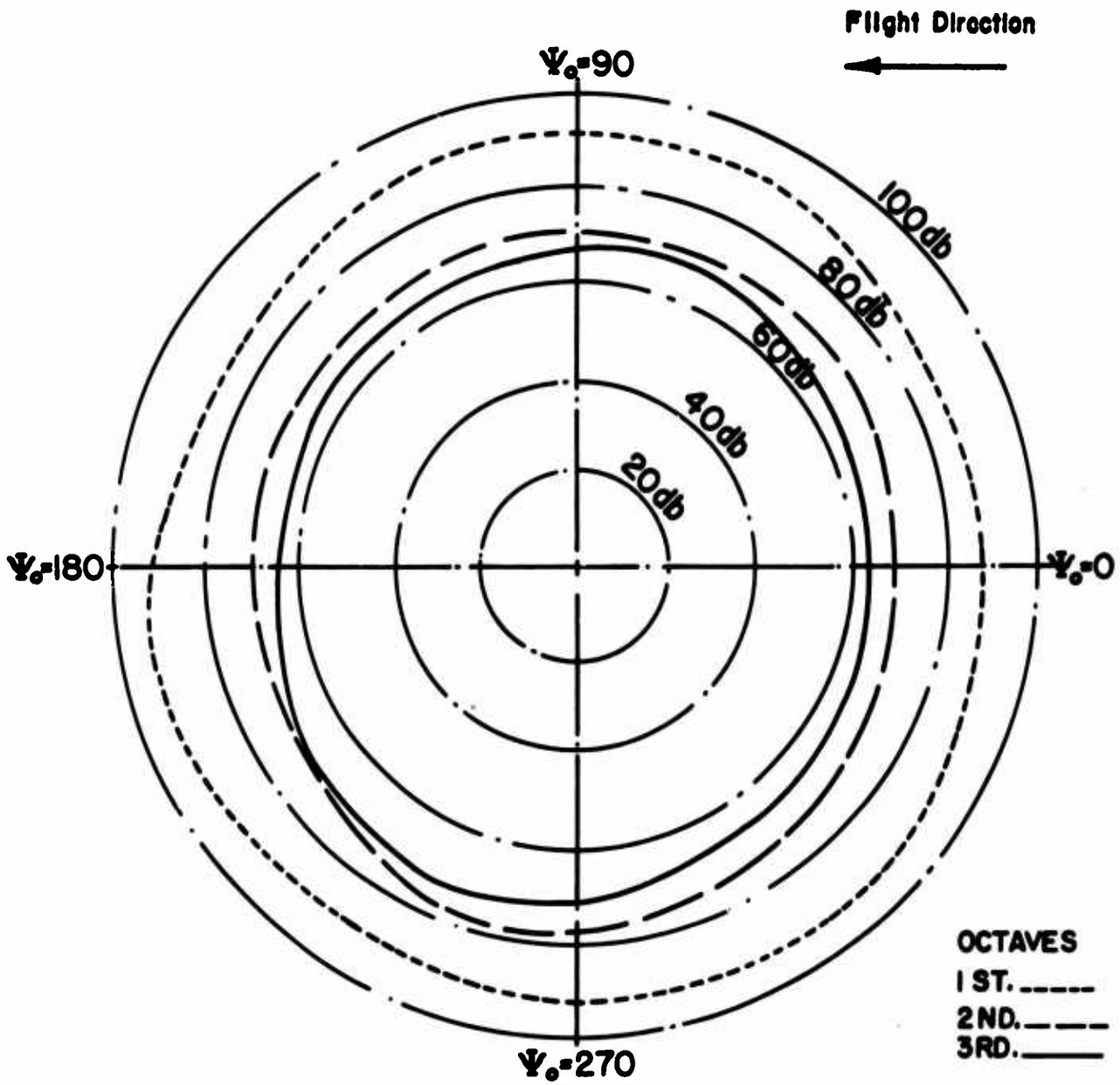

V= 0 KTS

$$\frac{R_o}{D} = 2 \quad , \quad \frac{Z_o}{D} = -1$$

Fig.24. RADIATION PATTERN IN OCTAVE BANDS, H—34 HELICOPTER.

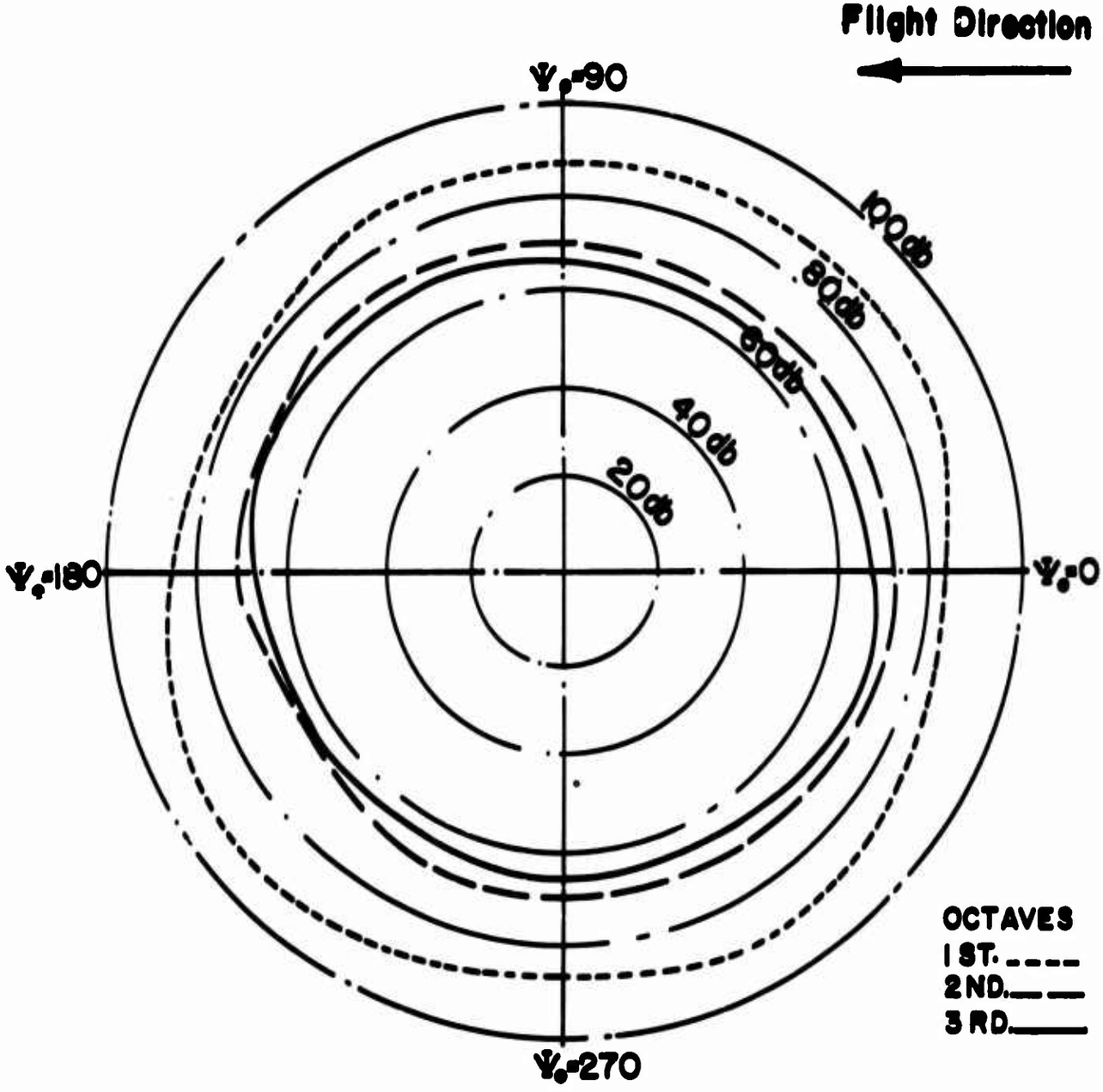

V=23 KTS

$$\frac{R_0}{D} = 2 \quad , \quad \frac{Z_0}{D} = -1$$

Fig.25. RADIATION PATTERN IN OCTAVE BANDS, H—34 HELICOPTER.

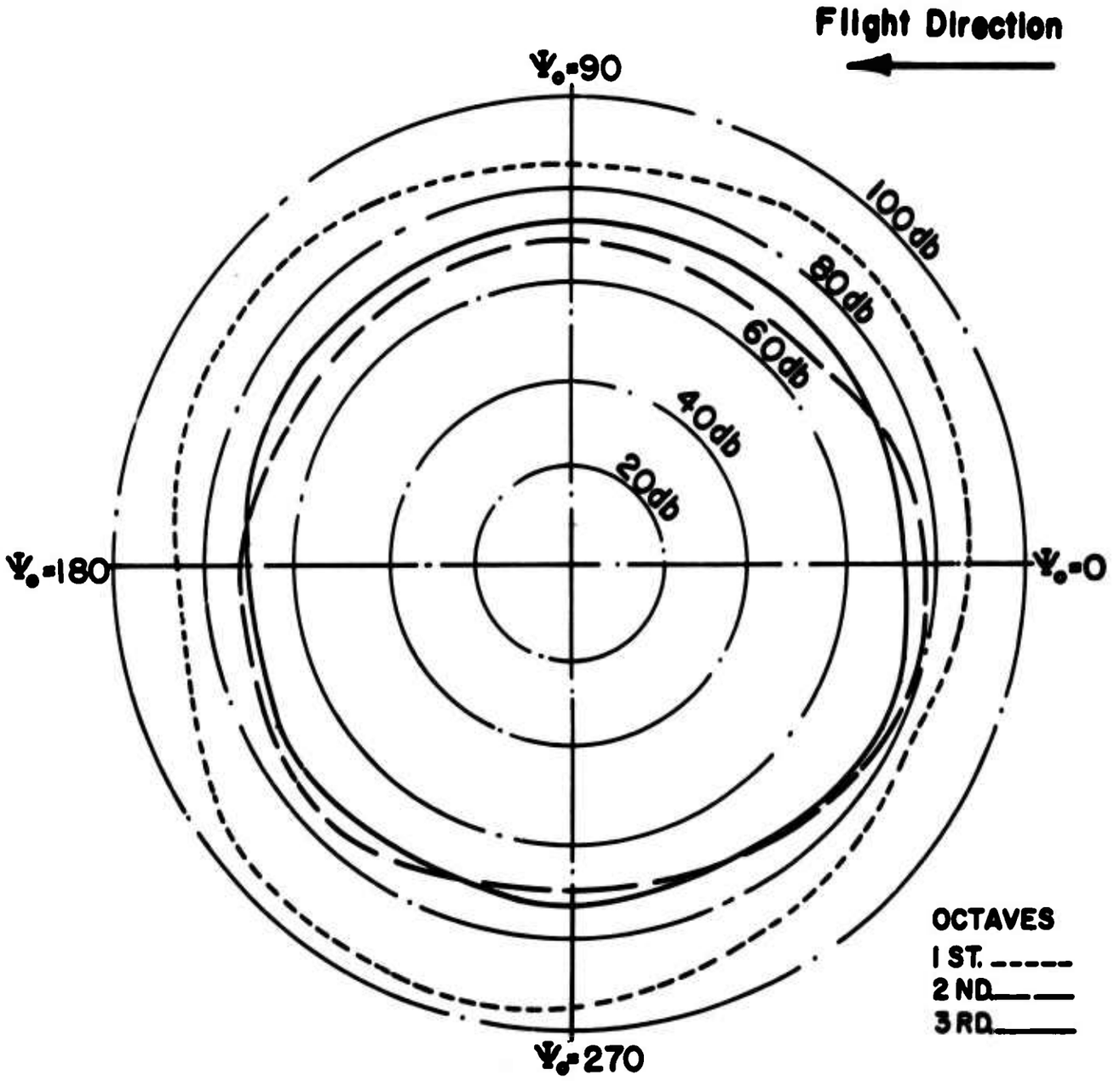

V=79 KTS

$$\frac{R_0}{D} = 2 \quad , \quad \frac{Z_0}{D} = -1$$

Fig.26. RADIATION PATTERN IN OCTAVE BANDS, H—34 HELICOPTER.

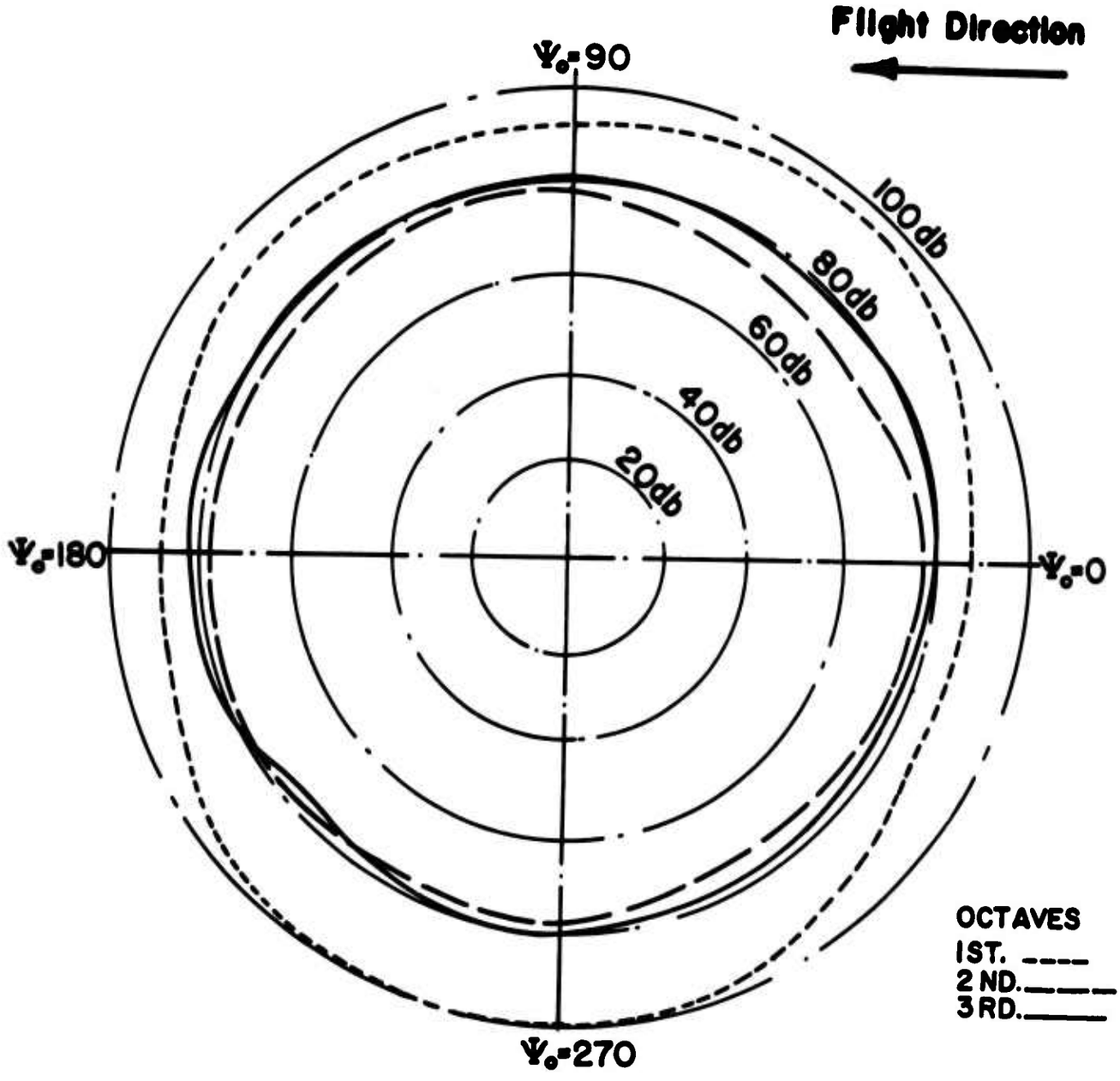

V=115 KTS

$$\frac{R_0}{D} = 2 \quad , \quad \frac{Z_0}{D} = -1$$

Fig.27. RADIATION PATTERN IN OCTAVE BANDS, H—34 HELICOPTER.

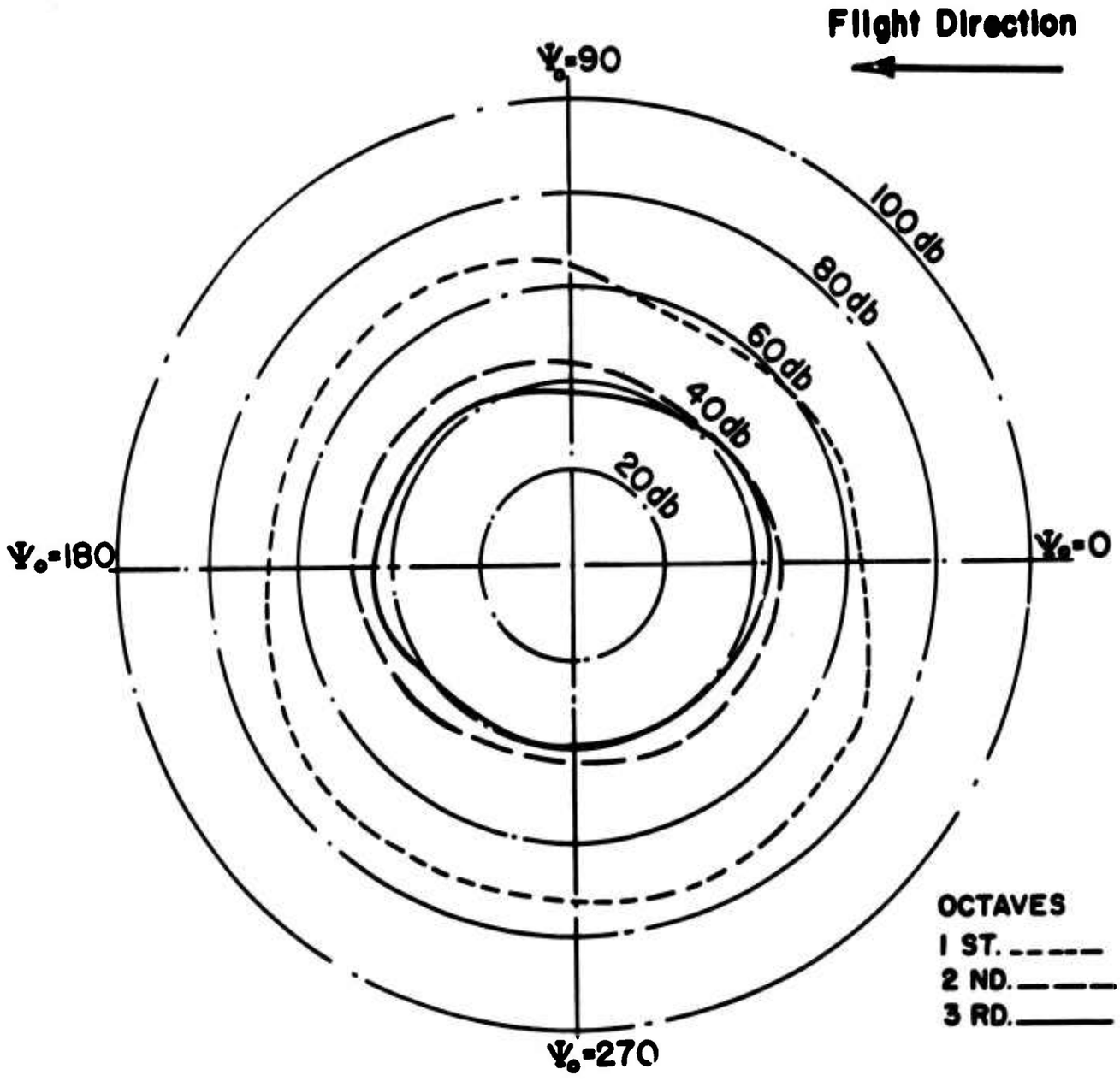

V= 23 KTS

$$\frac{R_0}{D} = 10 \quad , \quad \frac{Z_0}{D} = -1$$

Fig. 28. RADIATION PATTERN IN OCTAVE BANDS, H—34 HELICOPTER.

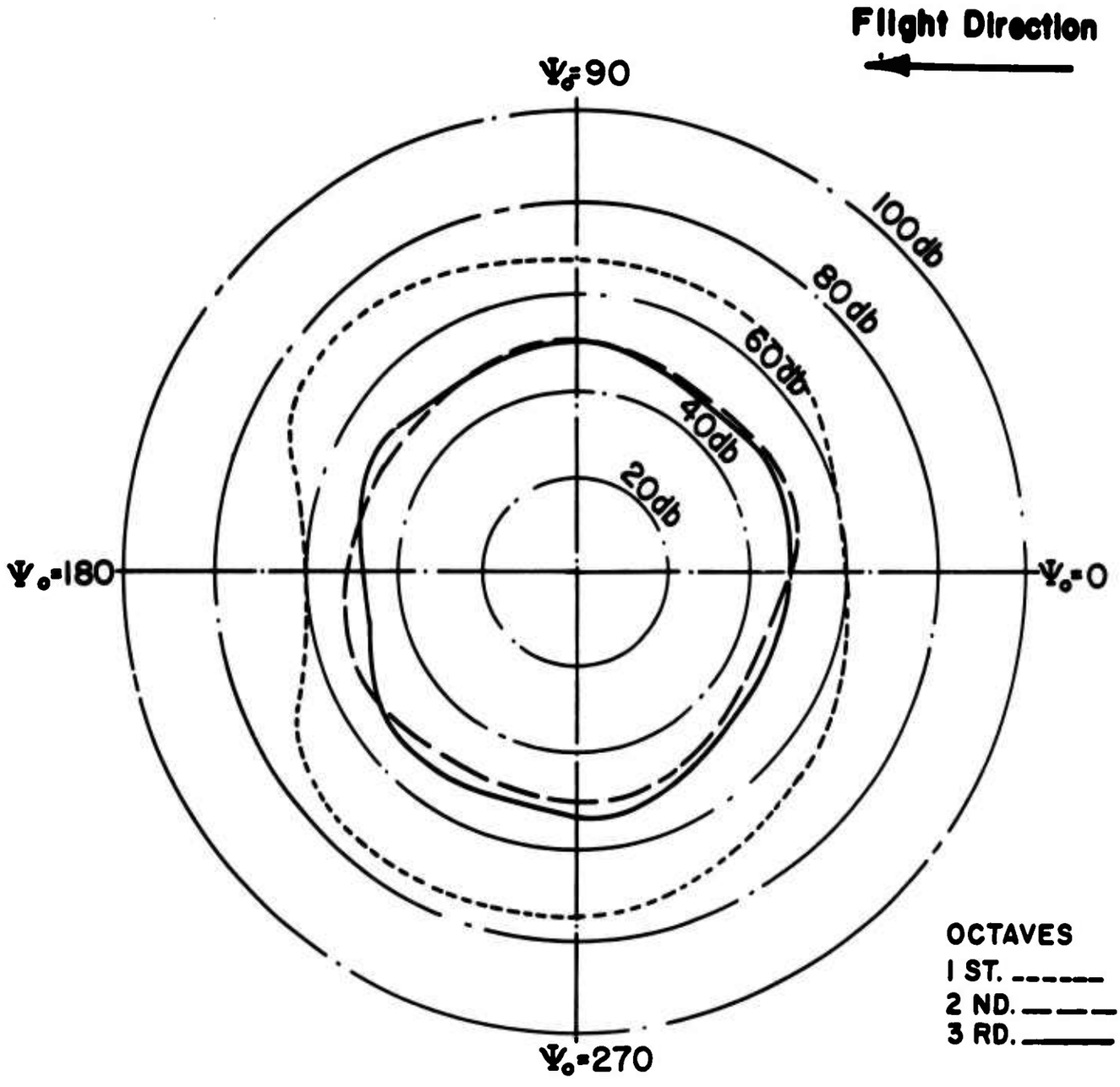

V=79 KTS

$$\frac{R_o}{D} = 10 \quad , \quad \frac{Z_o}{D} = -1$$

Fig.29 RADIATION PATTERN IN OCTAVE BANDS, H—34 HELICOPTER.

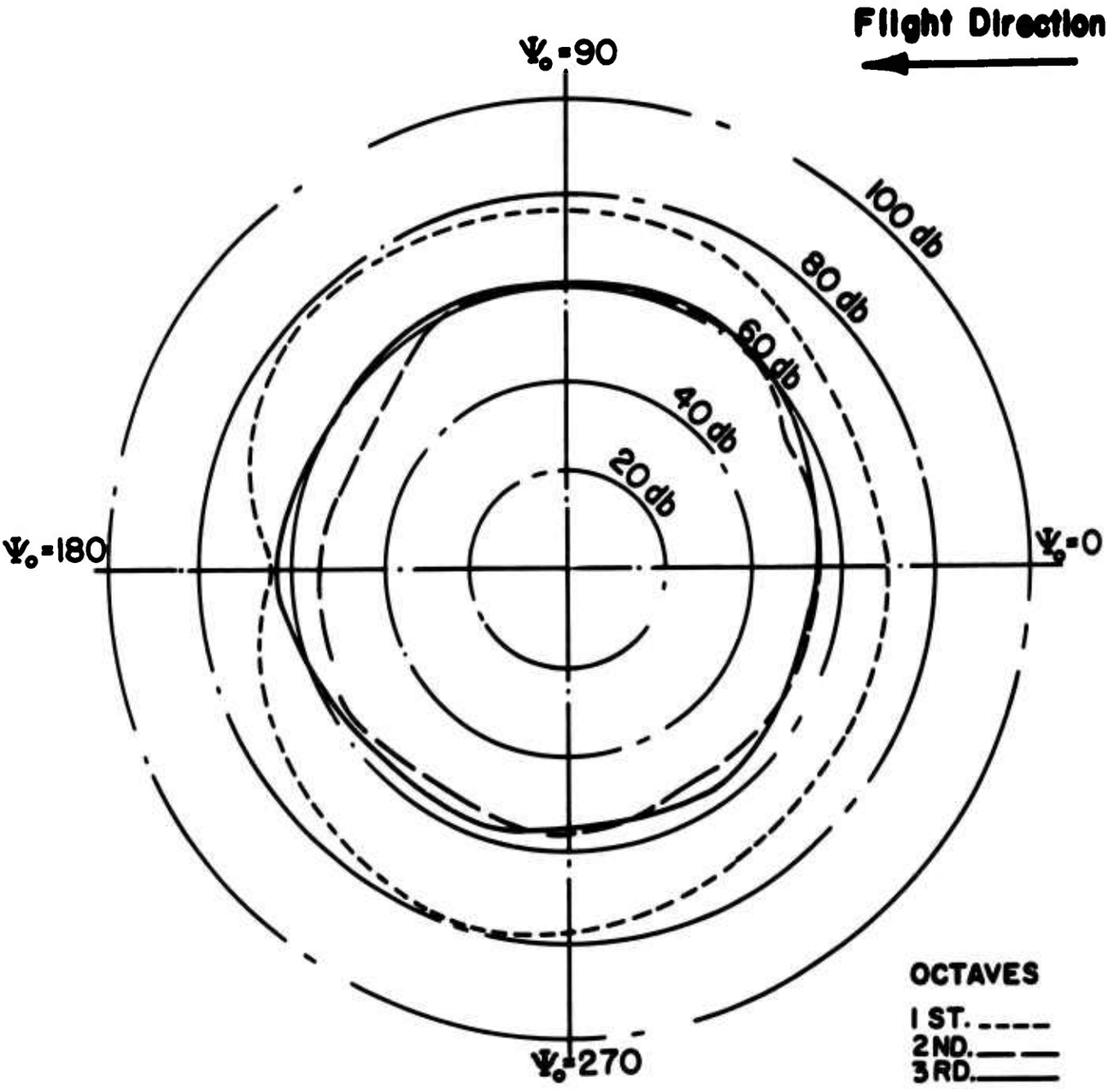

V=115 KTS

$$\frac{R_o}{D} = 10 \quad , \quad \frac{Z_o}{D} = -1$$

Fig.30 RADIATION PATTERN IN OCTAVE BANDS, H—34 HELICOPTER.

Radiation patterns for the HU-1 are available but, since the data indicate more symmetry than the patterns for the H-34, these are not presented.

The results of Garrick and Watkins[5] would lead one to predict that rotor radiation patterns in the z_o direction would show greater variations. Figures 31 and 32 for the H-34 helicopter show that this is indeed so for the first three octaves at $R_o/D=2,10$ and $\psi_o=270$. In fact, the general character of the variation beneath a lifting rotor is roughly the same as that of the fundamental behind a propeller in axisymmetric flow, regardless of forward speed. Sound pressure levels increase, rapidly in most cases, for hub height downward and then fall off slowly as the z_o distance is increased negatively. At two radial diameters (Figure 31), the maxima occur at about two diameters of negative elevation; at ten radial diameters (Figure 32), the maxima occur at about five diameters of negative elevation.

Variations with radial distance are of great interest for the problem of aural detection. In this instance the individual frequency components are most pertinent, since attenuation due to atmospheric or terrain absorption[1] is dependent on frequency. However, to reduce the data presented, the calculated results are again given by octave band. The radial trends are shown on Figures 33 and 34 for the H-34 at V=0 and V=115 knots, respectively. In both cases $\psi_o=270°$ and $z_o/D=-1$.

The particular point of interest is the distance beyond which "spherical spreading"[20] can be assumed to take place. Figures 33 and 34, therefore, have, in addition to the calculated sound levels, a line which represents "spherical spreading" extrapolated inward from a point 100 diameters from the rotor center. Since the correction for spherical spreading is

$$\Delta db = 20 \log_{10}\left(\frac{R_1}{R_2}\right)$$

where

R_1 = distance from source point where sound pressure level is known

R_2 = distance from source to point where one wishes to know the sound pressure level,

and since the abscissa of Figures 33 and 34 is a log scale, the curves of spherical spreading are straight lines with slopes of -20 decibels per decade. Where the calculated curve becomes tangent to and henceforth follows this line, then the total

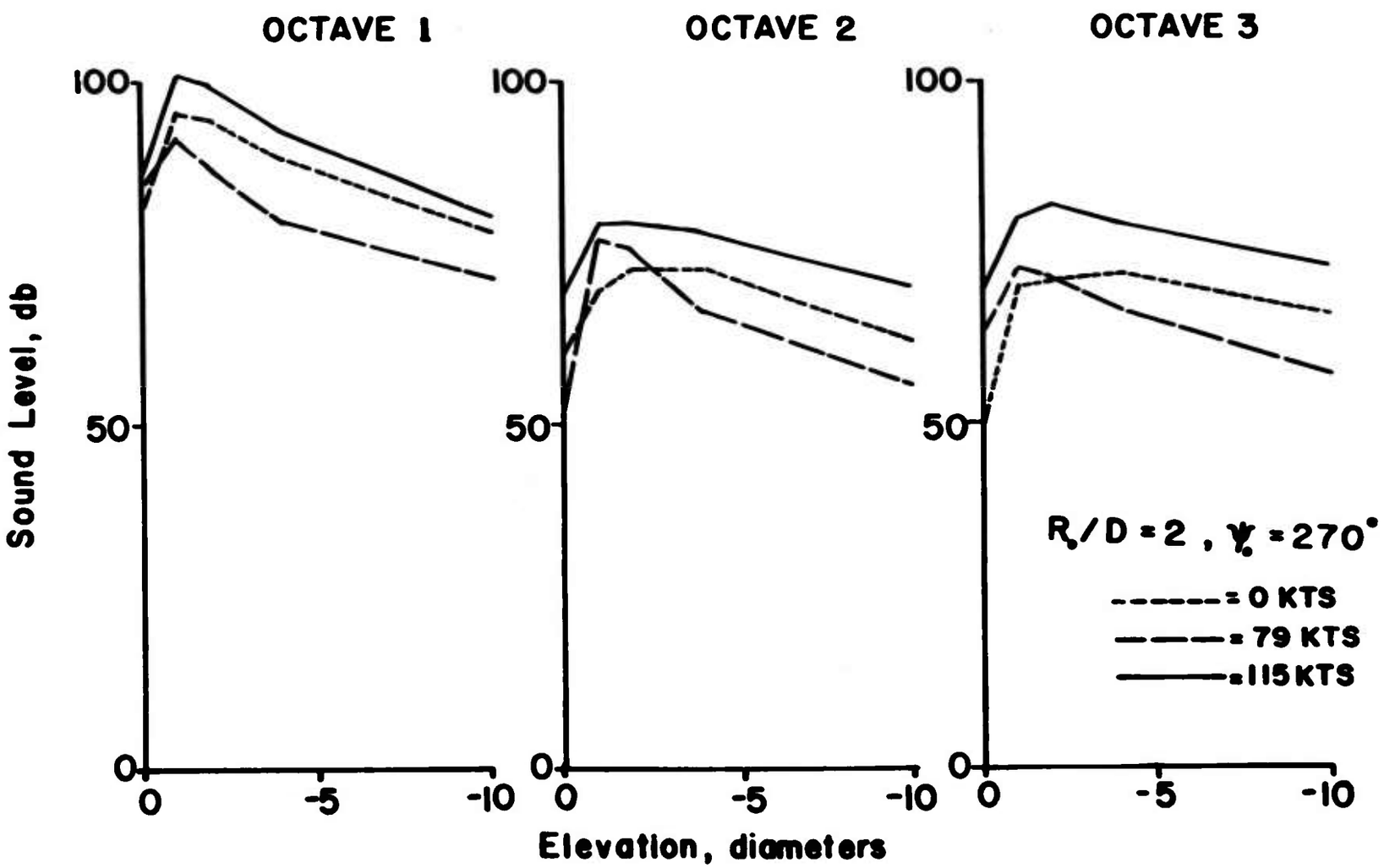

Fig. 31. VERTICAL RADIATION PATTERN, H-34 HELICOPTER.

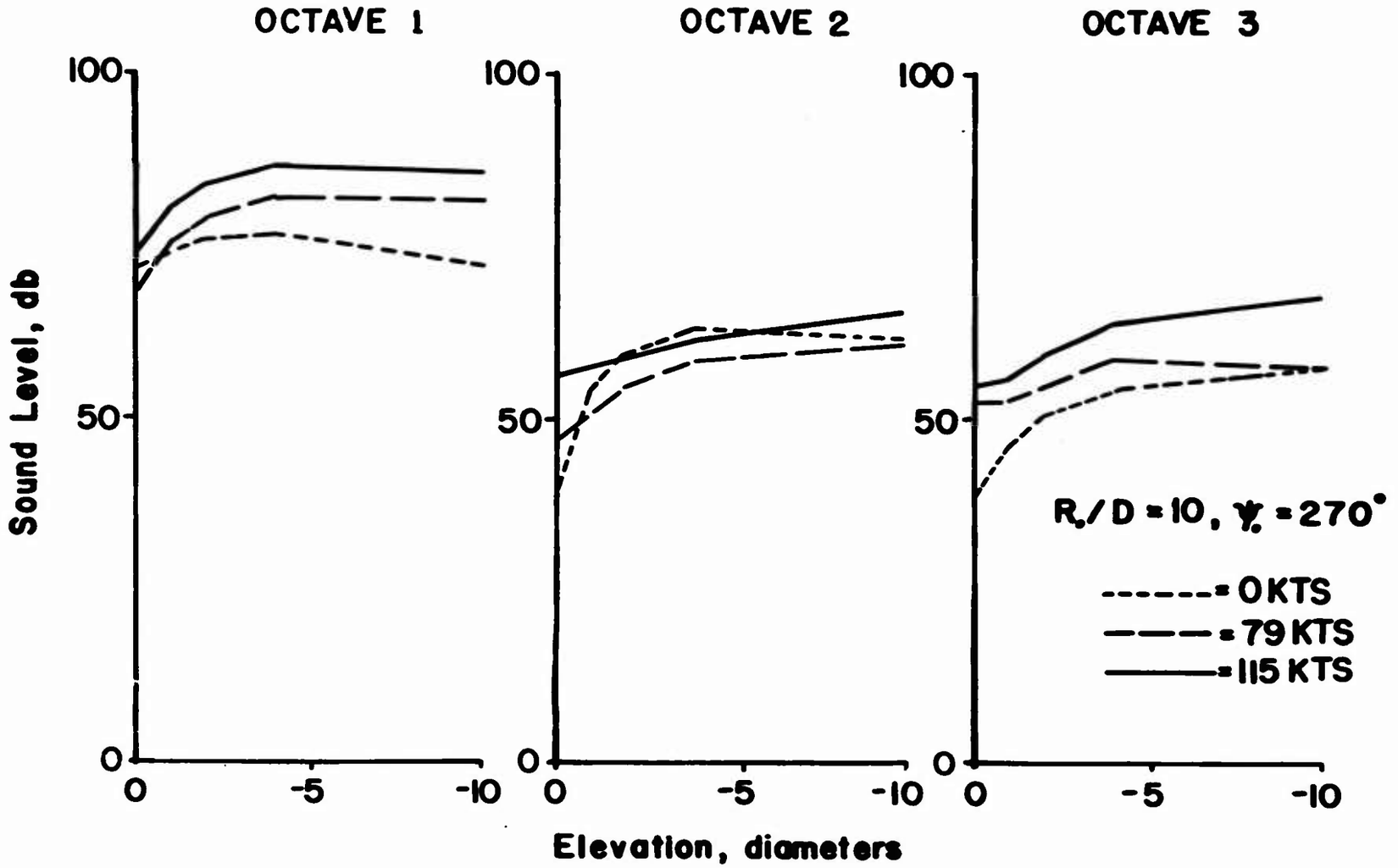

Fig. 32. VERTICAL RADIATION PATTERN, H-34 HELICOPTER.

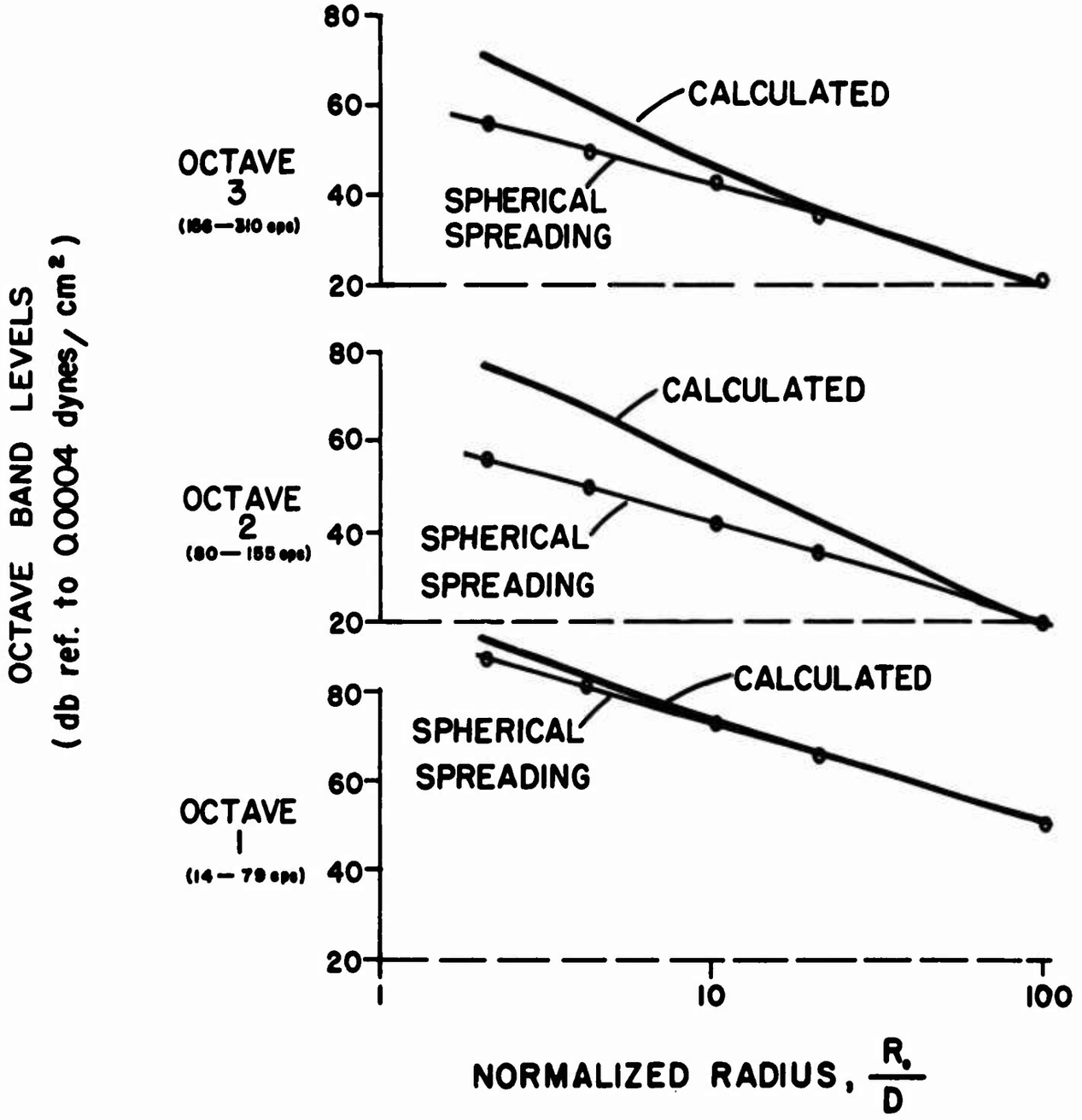

$V = 0$ KTS, $\psi_o = 270°$, $Z_o/D = -1$

Fig. 33. CALCULATED & SPHERICAL SPREADING FOR H-34 HELICOPTER.

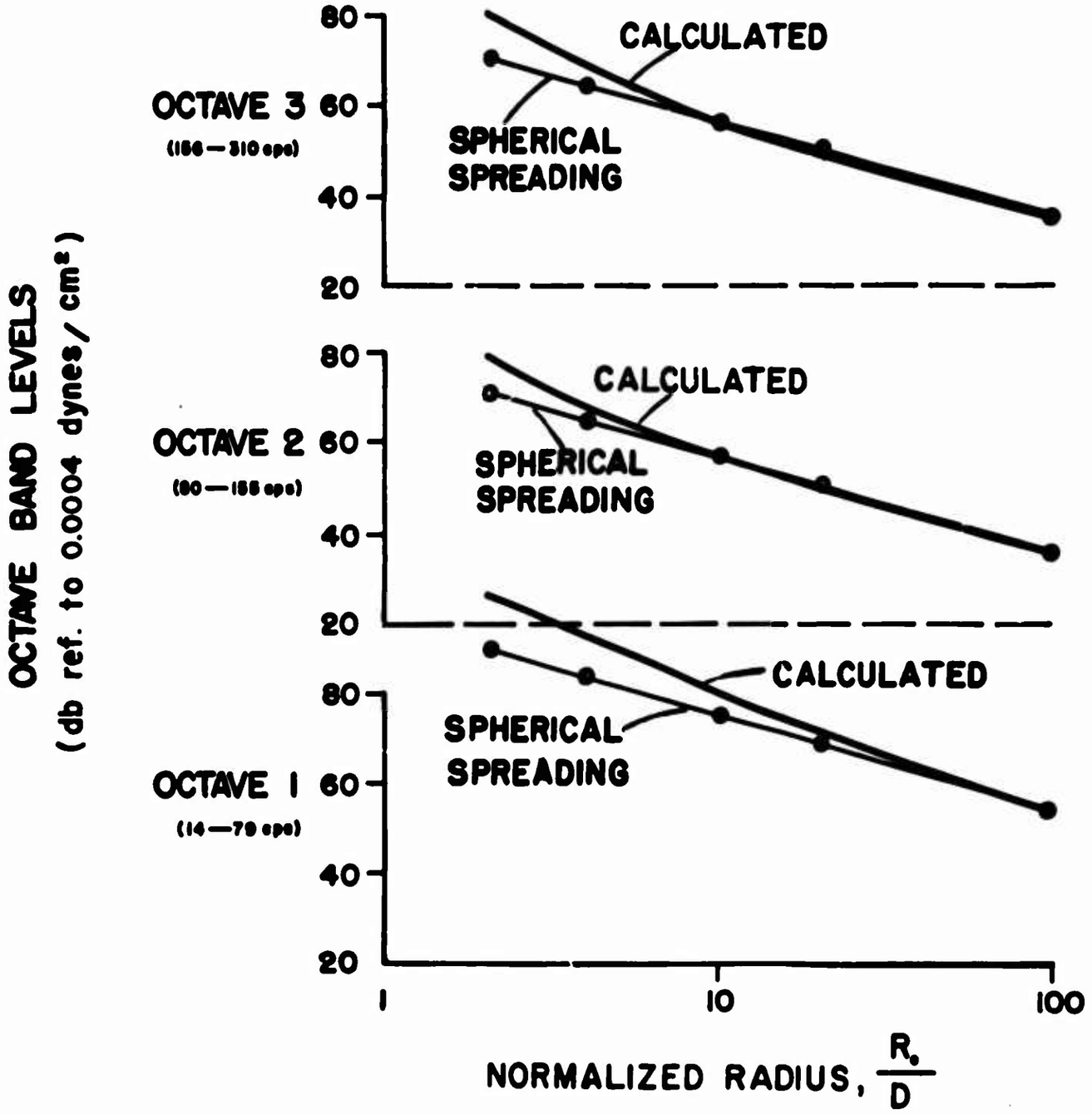

$V = 115$ KTS , $\psi_o = 270°$, $Z_o/D = -1$

Fig.34. CALCULATED & SPHERICAL SPREADING FOR H-34 HELICOPTER.

variation with radius can be said to be due to spherical spreading alone. If this is the criterion for the "far field," then Figure 34 shows that the "far field" could be one hundred diameters from the source. Note in Figure 34 that if a distance of three diameters were used as the base for extrapolating the sound pressure level in the first octave band to a distance of one hundred diameters, as is often suggested, an error of 10 decibels could result.

TREND STUDIES

Compressibility effects were examined by comparing sound pressure levels associated with 12-percent and 18-percent airfoils. Since one would expect larger compressibility effects at higher velocity, the trend is examined for the H-34 in the 115-knot case. The results are presented on Figure 35. For the field point chosen, there is not much change in sound level between the 12-percent and 18-percent airfoils.

The effect of RPM was investigated with the H-34 flying at 79 knots. One notes that, in reality, there would be a change in $\mu=V/\Omega R$; this implies a change in ASL variation with azimuth. However, in order to isolate the RPM effect, such changes in ASL are neglected. Airfoil section characteristics are the same for both cases; appropriate changes in β and θ are made, however. The results are given for RPM=214 and 245 on Figure 36. For the field point chosen, the only significant adverse effect of increasing RPM appears to be in the fifth harmonic.

The effect of increasing blade chord was also investigated, again using data from the H-34 at 79 knots. The comparison is made of normal chord and one 1.5 times normal. Appropriate changes are made in β and θ, assuming that blade weight and pitch mass moment of inertia increase linearly with chord. Again, constant airfoil section characteristics are assumed. The results are presented on Figure 37, where a small but fairly general decrease in sound level is noted for the larger chord.

The effect of changing the number of blades from two to three was investigated for the HU-1 in the 88-knot case. The chord and ASL are adjusted to preserve constant total lift. No adjustment is required in β and θ, again assuming a linear decrease in blade weight with chord (which provides the proper balance of lift and centrifugal moments to preserve β). The results are presented on Figure 38; for the field point chosen, there is a very significant decrease in sound level for all harmonics due to increasing the number of blades from two to three.

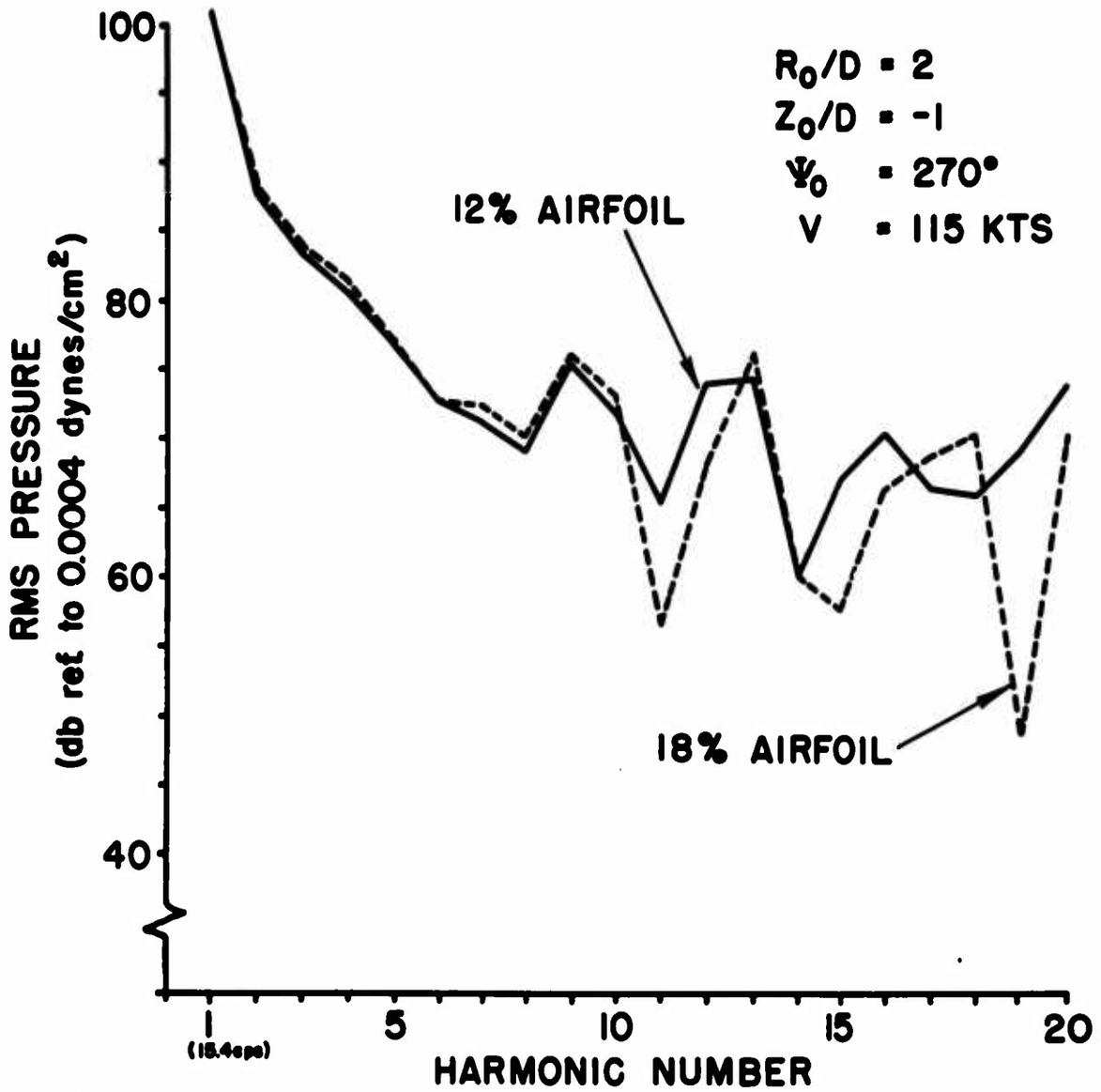

Fig. 35. COMPRESSIBILITY EFFECTS FOR H-34 HELICOPTER.

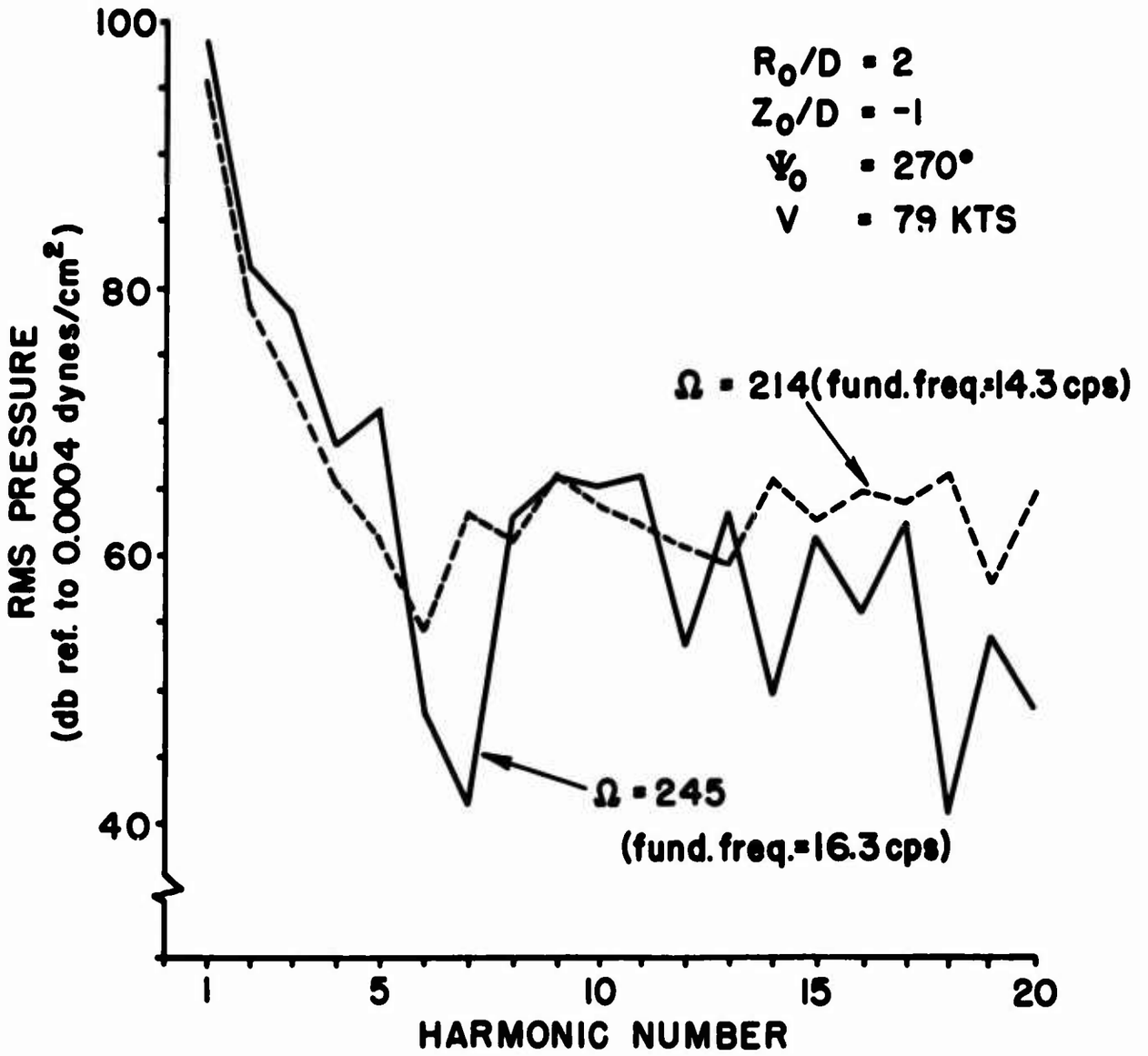

Fig. 36. EFFECT OF R.P.M.
FOR H-34 HELICOPTER.

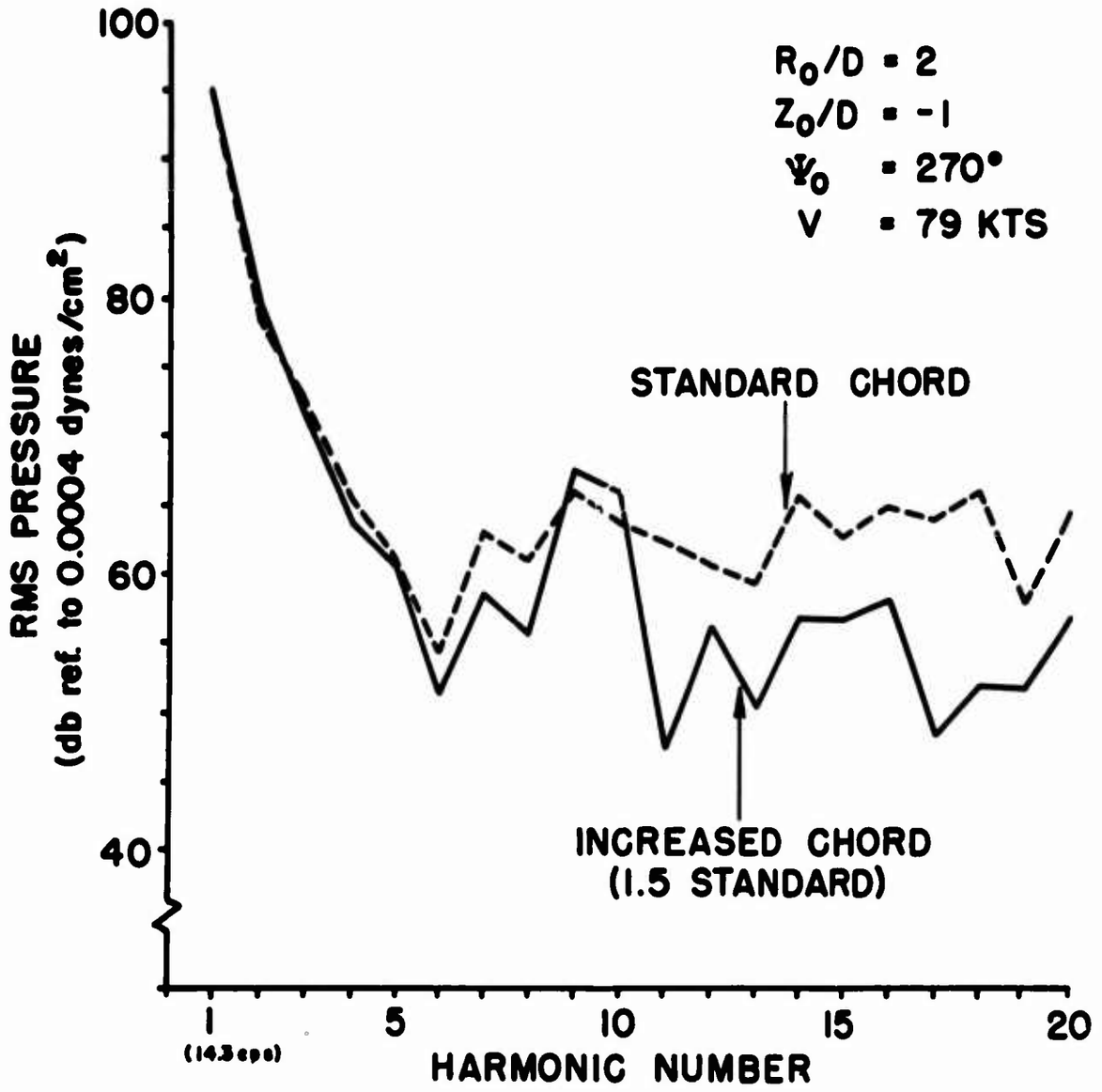

Fig. 37. EFFECT OF INCREASED CHORD FOR H-34 HELICOPTER.

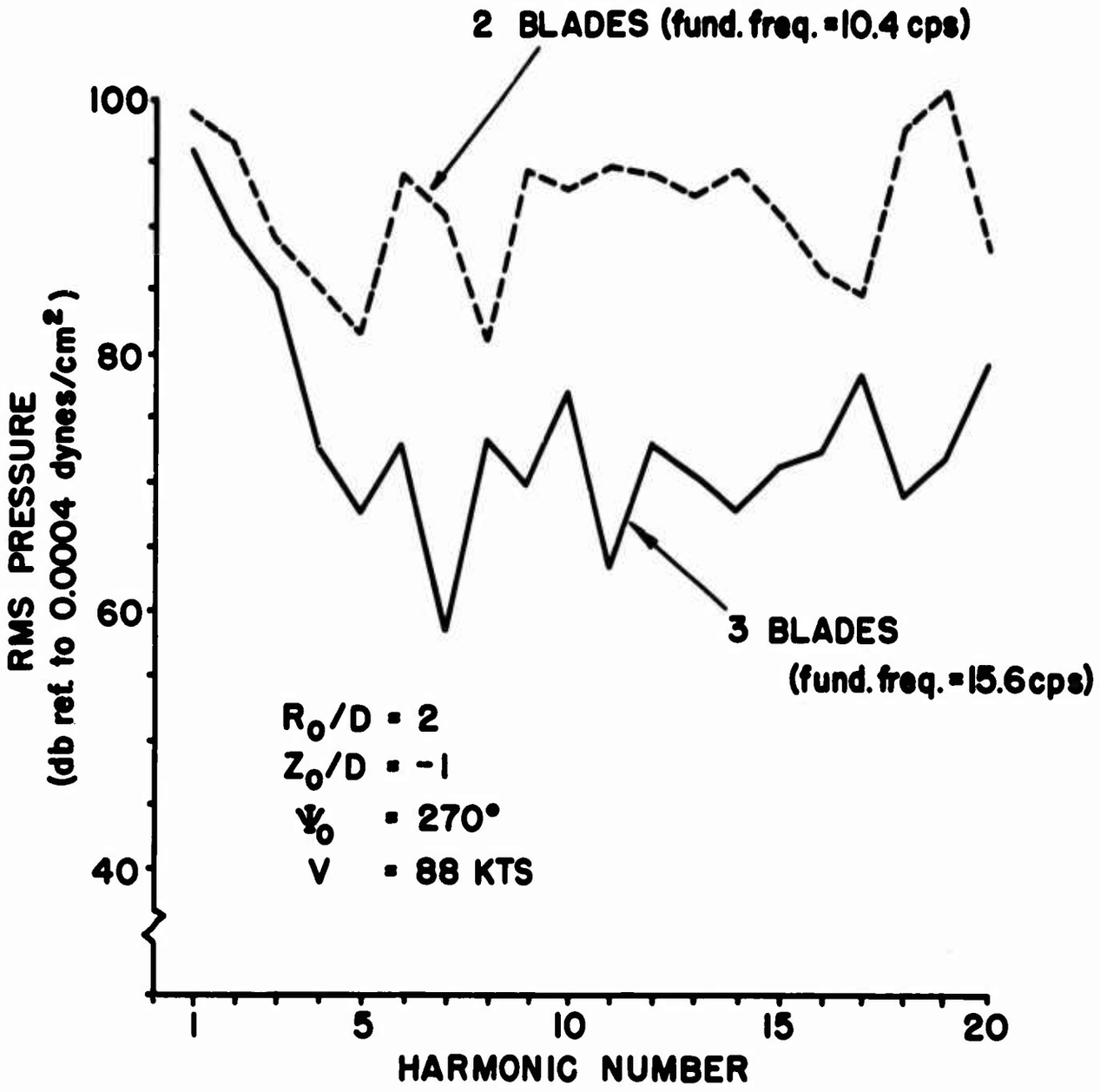

Fig. 38. EFFECT OF NUMBER OF BLADES FOR HU—1 HELICOPTER.

The effect of impulsive downwash was investigated by selective change in the aerodynamic section loading of the H-34 in the 115-knot case. The modification was made over an interval of azimuth approximately 20 degrees on each side of 100° and for fractional blade spans of r/R=0.85,0.90 and 0.95, as shown graphically in Figure 39. This modification was suggested by the data on Figure 7 in Ref. 23. That is, theory indicates sharper variations than experiment. Since data used in the present work was obtained using instrumentation with a break-point of 30 cps, making the ASL more like the theory would tend to correct for "rounding off" of sharp peaks due to instrumentation limitations.

The results of the ASL modification are shown on Figure 40 which indicates that the main effect of this change is to vary the sound level more markedly from one harmonic to another, at least at the one field point used in the comparison.

The final trend studies of the present investigation were associated with setting β, C_D and ϕ equal to zero. This last change, of course, is tantamount to eliminating induced drag. The case investigated was the H-34 in hover; the field point was ψ_o=270, R_o/D=-1, z_o/D=-1. The results indicate no significant effect. Ref. 10 shows the contribution of coning angle to the sound field and indicates that its maximum effect is in the plane of the disc. In the present investigation, with the field point one diameter below the rotor, the effect of coning leaves the sound level unaffected to within 0.5 decibel. This suggests that for typical helicopter rotors, a greatly simplified program could be used with no significant loss of accuracy.

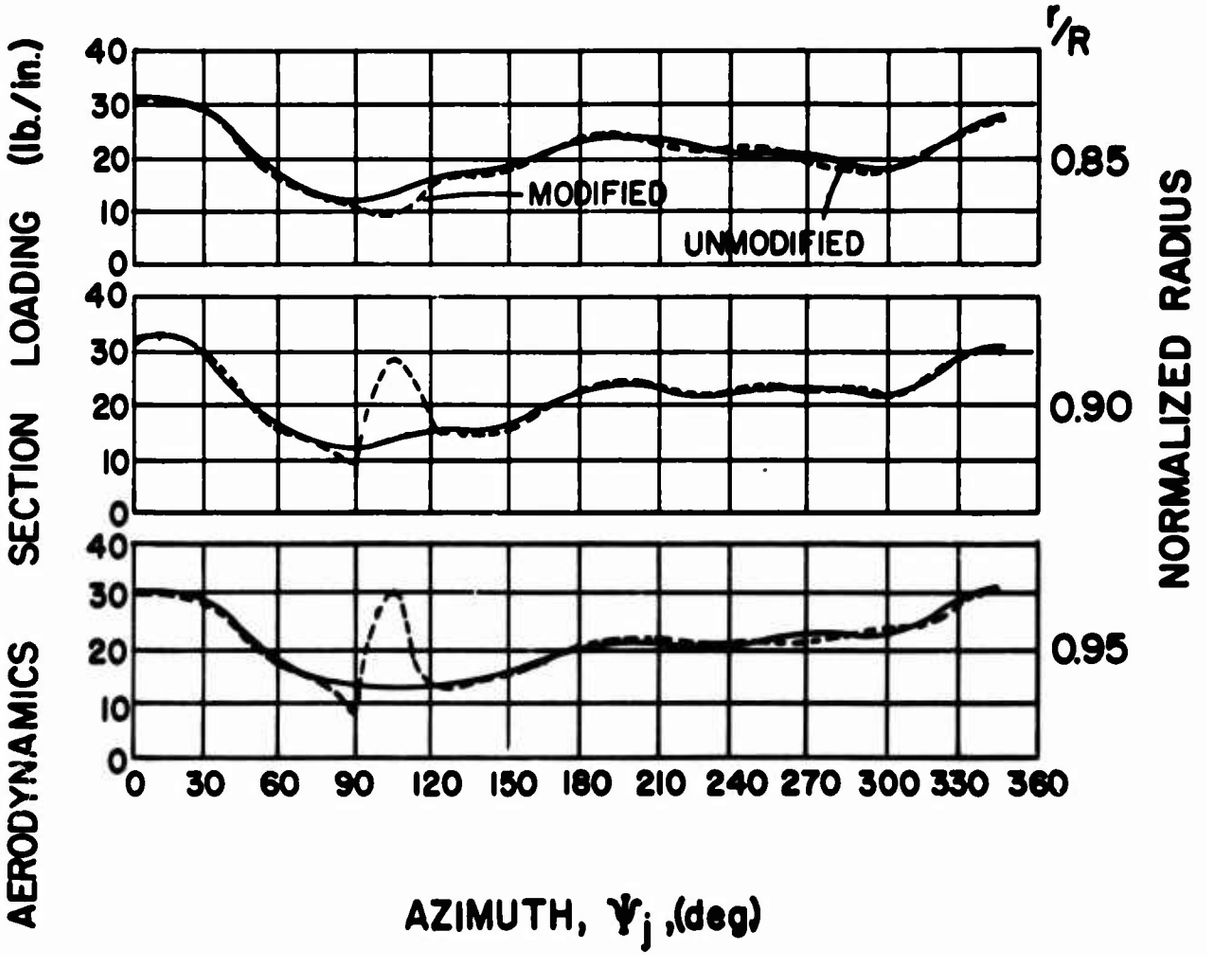

Fig.39. ASL MODIFICATION, H—34 HELICOPTER.

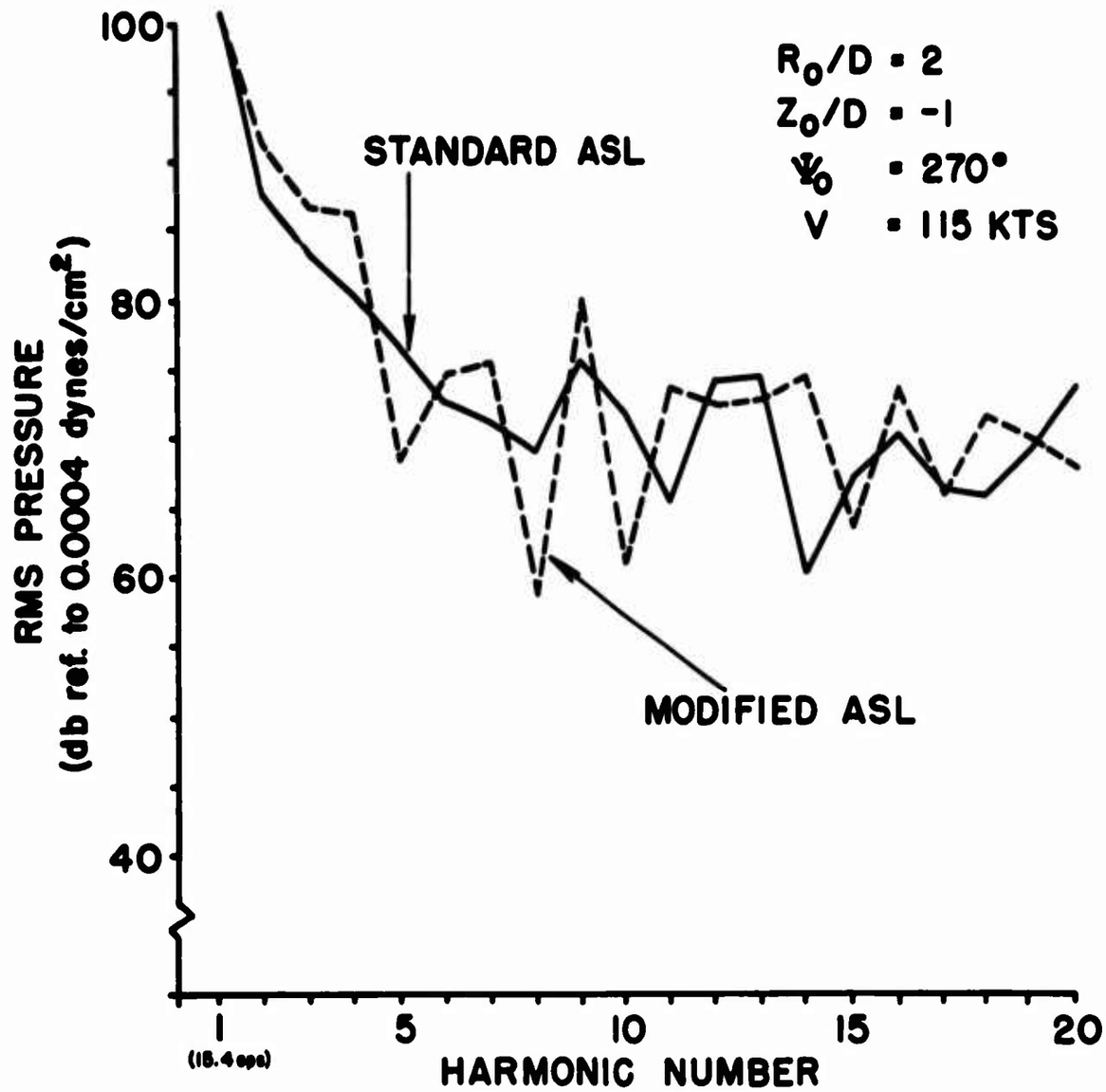

Fig. 40. EFFECT OF IMPULSIVE DOWNWASH FOR H-34 HELICOPTER.

TABLE V
12-PERCENT SYMMETRIC AIRFOIL INPUT DATA

α	M	C_L	C_D	C_N
0.0	0.0	0.0	0.0078	0.0
0.0	0.1	0.0	0.0078	0.0
0.0	0.2	0.0	0.0078	0.0
0.0	0.3	0.0	0.0078	0.0
0.0	0.4	0.0	0.0078	0.0
0.0	0.5	0.0	0.0078	0.0
0.0	0.6	0.0	0.0078	0.0
0.0	0.7	0.0	0.0078	0.0
0.0	1.0	0.0	0.1060	0.0
1.0	0.00	0.11	0.008	0.11012
1.0	0.1	0.11	0.008	0.11012
1.0	0.2	0.14	0.008	0.1401
1.0	0.3	0.11	0.008	0.1101
1.0	0.4	0.11	0.008	0.1101
1.0	0.5	0.13	0.008	0.1301
1.0	0.6	0.11	0.008	0.1101
1.0	0.7	0.15	0.008	0.1501
1.0	1.0	0.02	0.09607	0.02167
2.0	0.0	0.24	0.0083	0.24014
2.0	0.1	0.24	0.0083	0.24014
2.0	0.2	0.25	0.0083	0.25014
2.0	0.3	0.22	0.0083	0.22016
2.0	0.4	0.24	0.0083	0.24014
2.0	0.5	0.24	0.0083	0.24014
2.0	0.6	0.24	0.0083	0.24014
2.0	0.7	0.28	0.0086	0.28013
2.0	1.0	0.04	0.09787	0.04339
3.0	0.0	0.34	0.0086	0.3400
3.0	0.1	0.34	0.0086	0.33998
3.0	0.2	0.35	0.0086	0.34997
3.0	0.3	0.33	0.0086	0.33000
3.0	0.4	0.34	0.0086	0.33998
3.0	0.5	0.365	0.0086	0.36495
3.0	0.6	0.36	0.0086	0.35996
3.0	0.7	0.40	0.0118	0.40007
3.0	1.0	0.075	0.09833	0.08004
4.0	0.0	0.44	0.0092	0.4396
4.0	0.1	0.44	0.0092	0.440
4.0	0.2	0.45	0.0092	0.4496
4.0	0.3	0.43	0.0092	0.4296
4.0	0.4	0.45	0.0092	0.4496
4.0	0.5	0.46	0.0092	0.4595
4.0	0.6	0.47	0.0095	0.4695
4.0	0.7	0.50	0.018	0.5000
4.0	1.0	0.11	0.1108	0.11746
5.0	0.0	0.54	0.0098	0.5388

TABLE V - (Cont'd)

α	M	C_L	C_D	C_N
5.0	0.1	0.54	0.0098	0.53880
5.0	0.2	0.55	0.0098	0.54876
5.0	0.3	0.52	0.0098	0.51887
5.0	0.4	0.54	0.0098	0.53880
5.0	0.5	0.57	0.0098	0.56868
5.0	0.6	0.59	0.013	0.589
5.0	0.7	0.60	0.032	0.600
5.0	1.0	0.20	0.1420	0.21161
6.0	0.0	0.65	0.011	0.6476
6.0	0.1	0.65	0.011	0.6476
6.0	0.2	0.64	0.011	0.6376
6.0	0.3	0.62	0.011	0.6177
6.0	0.4	0.65	0.011	0.6476
6.0	0.5	0.66	0.011	0.657
6.0	0.6	0.68	0.0215	0.678
6.0	0.7	0.66	0.052	0.6618
6.0	1.0	0.26	0.1701	0.27636
7.0	0.0	0.74	0.0123	0.7360
7.0	0.1	0.74	0.0123	0.736
7.0	0.2	0.72	0.0123	0.7161
7.0	0.3	0.72	0.0123	0.7161
7.0	0.4	0.75	0.0123	0.7459
7.0	0.5	0.76	0.0145	0.7561
7.0	0.6	0.78	0.0315	0.778
7.0	0.7	0.68	0.074	0.684
7.0	1.0	0.30	0.2015	0.322
8.0	0.0	0.83	0.0138	0.8238
8.0	0.1	0.83	0.0138	0.8239
8.0	0.2	0.82	0.0138	0.8139
8.0	0.3	0.81	0.0138	0.8040
8.0	0.4	0.85	0.0144	0.8437
8.0	0.5	0.85	0.022	0.845
8.0	0.6	0.835	0.0545	0.8345
8.0	0.7	0.695	0.0945	0.7014
8.0	1.0	0.32	0.2147	0.3468
9.0	0.0	0.91	0.0153	0.9012
9.0	0.1	0.91	0.0153	0.9012
9.0	0.2	0.92	0.0153	0.9111
9.0	0.3	0.92	0.0153	0.9111
9.0	0.4	0.94	0.0183	0.9313
9.0	0.5	0.93	0.037	0.9243
9.0	0.6	0.86	0.076	0.8613
9.0	0.7	0.695	0.116	0.7046
9.0	1.0	0.34	0.236	0.3727
10.0	0.0	1.025	0.0174	1.0125
10.0	0.1	1.025	0.0174	1.0125

TABLE V - (Cont'd)

α	M	C_L	C_D	C_N
10.0	0.2	1.005	0.0174	0.9929
10.0	0.3	1.00	0.0182	0.9880
10.0	0.4	1.02	0.0257	1.00895
10.0	0.5	0.98	0.055	0.97465
10.0	0.6	0.86	0.0975	0.86285
10.0	0.7	0.70	0.1375	0.7132
10.0	1.0	0.36	0.257	0.3991
11.0	0.0	1.1	0.0195	1.0835
11.0	0.1	1.1	0.0195	1.0835
11.0	0.2	1.1	0.0195	1.0835
11.0	0.3	1.1	0.023	1.0841
11.0	0.4	1.11	0.0393	1.097
11.0	0.5	0.99	0.079	0.98686
11.0	0.6	0.84	0.118	0.84705
11.0	0.7	0.695	0.158	0.71236
11.0	1.0	0.38	0.276	0.4257
12.0	0.0	1.2	0.022	1.1784
12.0	0.1	1.2	0.022	1.1783
12.0	0.2	1.19	0.022	1.1685
12.0	0.3	1.18	0.030	1.1603
12.0	0.4	1.13	0.0605	1.1178
12.0	0.5	0.98	0.10	0.9793
12.0	0.6	0.81	0.1395	0.8213
12.0	0.7	0.695	0.179	0.7170
12.0	1.0	0.40	0.297	0.4530
13.0	0.0	1.27	0.0255	1.2432
13.0	0.1	1.27	0.0255	1.2432
13.0	0.2	1.27	0.027	1.24356
13.0	0.3	1.208	0.0443	1.187
13.0	0.4	1.12	0.083	1.11
13.0	0.5	0.94	0.1215	0.94324
13.0	0.6	0.765	0.161	0.7816
13.0	0.7	0.690	0.200	0.71731
13.0	1.0	0.42	0.317	0.4806
14.0	0.0	1.359	0.0385	1.328
14.0	0.1	1.3590	0.0385	1.32795
14.0	0.2	1.299	0.0419	1.27056
14.0	0.3	1.205	0.0715	1.1865
14.0	0.4	1.08	0.1110	1.0748
14.0	0.5	0.89	0.149	0.8996
14.0	0.6	0.728	0.189	0.7521
14.0	0.7	0.682	0.228	0.7169
14.0	1.0	0.44	0.345	0.5104
15.0	0.0	1.378	0.0784	1.3513
15.0	0.1	1.378	0.0784	1.3513
15.0	0.2	1.29	0.0832	1.2675
15.0	0.3	1.18	0.1015	1.16607

TABLE V - (Cont'd)

α	M	C_L	C_D	C_N
15.0	0.4	1.03	0.140	1.0311
15.0	0.5	0.82	0.180	0.8386
15.0	0.6	0.69	0.22	0.72343
15.0	0.7	0.68	0.262	0.72464
15.0	1.0	0.465	0.3837	0.5484
165.0	0.0	-0.5900	0.146	0.6077
165.0	0.1	-0.5900	0.1460	0.6077
165.0	0.2	-0.5520	0.1495	0.5719
165.0	0.3	-0.5350	0.1670	0.5600
165.0	0.4	-0.5250	0.1900	0.5563
165.0	0.5	-0.5100	0.2170	0.5488
165.0	0.6	-0.4700	0.2488	0.5184
165.0	0.7	-0.4750	0.2865	0.5329
165.0	1.0	-0.3800	0.4145	0.4743
166.0	0.0	-0.61	0.134	0.6243
166.0	0.1	-0.6100	0.1340	0.6243
166.0	0.2	-0.5720	0.1380	0.5884
166.0	0.3	-0.5500	0.1530	0.5706
166.0	0.4	-0.5400	0.1728	0.5658
166.0	0.5	-0.5220	0.1970	0.5542
166.0	0.6	-0.4900	0.2250	0.5299
166.0	0.7	-0.4800	0.2595	0.5285
166.0	1.0	-0.3600	0.3770	0.4405
167.0	0.0	-0.62	0.122	0.6316
167.0	0.1	-0.6200	0.1220	0.6316
167.0	0.2	-0.5820	0.1255	0.5978
167.0	0.3	-0.5680	0.1394	0.5876
167.0	0.4	-0.5600	0.1573	0.5842
167.0	0.5	-0.5400	0.1790	0.5700
167.0	0.6	-0.5100	0.2056	0.5473
167.0	0.7	-0.4840	0.2370	0.5280
167.0	1.0	-0.3400	0.3450	0.4158
168.0	0.0	-0.62	0.110	0.6293
168.0	0.1	-0.6200	0.1100	0.6294
168.0	0.2	-0.5950	0.1105	0.6050
168.0	0.3	-0.5800	0.1200	0.5923
168.0	0.4	-0.5720	0.1352	0.5876
168.0	0.5	-0.5500	0.1550	0.5702
168.0	0.6	-0.5200	0.1808	0.5463
168.0	0.7	-0.5000	0.2100	0.5328
168.0	1.0	-0.3250	0.3190	0.3842
169.0	0.0	-0.62	0.098	0.6273
169.0	0.1	-0.6200	0.0980	0.6273
169.0	0.2	-0.6000	0.0980	0.6077
169.0	0.3	-0.5920	0.1000	0.6002
169.0	0.4	-0.5800	0.1122	0.5907
169.0	0.5	-0.5610	0.1295	0.5754

TABLE V - (Cont'd)

α	M	C_L	C_D	C_N
169.0	0.6	-0.5300	0.1532	0.5495
169.0	0.7	-0.5050	0.1858	0.5312
169.0	1.0	-0.3100	0.2980	0.3612
170.0	0.0	-0.619	0.0865	0.6246
170.0	0.1	-0.6190	0.0865	0.6246
170.0	0.2	-0.6000	0.0865	0.6059
170.0	0.3	-0.5900	0.0865	0.5961
170.0	0.4	-0.5800	0.0935	0.5874
170.0	0.5	-0.5650	0.1078	0.5751
170,0	0.6	-0.5400	0.1305	0.5545
170.0	0.7	-0.5080	0.1642	0.5288
170.0	1.0	-0.2920	0.2770	0.3357
171.0	0.0	-0.60	0.0760	0.6045
171.0	0.1	-0.6000	0.0760	0.6045
171.0	0.2	-0.5900	0.0760	0.5946
171.0	0.3	-0.5890	0.0760	0.5936
171.0	0.4	-0.5780	0.0783	0.5831
171.0	0.5	-0.5650	0.0912	0.5723
171.0	0.6	-0.5440	0.1116	0.5548
171.0	0.7	-0.5150	0.1400	0.5306
171.0	1.0	-0.272	0.2535	0.3083
172.0	0.0	-0.56	0.0650	0.5636
172.0	0.1	-0.5600	0.0650	0.5636
172.0	0.2	-0.5700	0.0650	0.5735
172.0	0.3	-0.5700	0.0650	0.5735
172.0	0.4	-0.5700	0.0650	0.5735
172.0	0.5	-0.5600	0.0735	0.5648
172.0	0.6	-0.5450	0.0920	0.5525
172.0	0.7	-0.5150	0.1174	0.5263
172.0	1.0	-0.2550	0.2370	0.2855
173.0	0.0	-0.51	0.0560	0.5131
173.0	0.1	-0.5100	0.0560	0.5131
173.0	0.2	-0.5320	0.0560	0.5349
173.0	0.3	-0.5400	0.0560	0.5428
173.0	0.4	-0.5450	0.0560	0.5478
173.0	0.5	-0.5500	0.0585	0.5531
173.0	0.6	-0.5400	0.0720	0.5448
173.0	0.7	-0.5080	0.0935	0.5156
173.0	1.0	-0.2320	0.2180	0.2569
174.0	0.0	-0.424	0.0465	0.4265
174.0	0.1	-0.4240	0.0465	0.4265
174.0	0.2	-0.4650	0.0465	0.4673
174.0	0.3	-0.4800	0.0465	0.4822
174.0	0.4	-0.5200	0.0465	0.5220
174.0	0.5	-0.5210	0.0465	0.5230
174.0	0.6	-0.5300	0.0520	0.5325
174.0	0.7	-0.5000	0.0703	0.5046

TABLE V - (Cont'd)

α	M	C_L	C_D	C_N
174.0	1.0	-0.2100	0.2055	0.2303
175.0	0.0	-0.38	0.0380	0.3819
175.0	0.1	-0.3800	0.0380	0.3819
175.0	0.2	-0.4000	0.0380	0.4018
175.0	0.3	-0.4080	0.0380	0.4098
175.0	0.4	-0.4480	0.0380	0.4496
175.0	0.5	-0.4600	0.0380	0.4616
175.0	0.6	-0.5000	0.0410	0.5017
175.0	0.7	-0.4800	0.0565	0.4831
175.0	1.0	-0.1840	0.1940	0.2002
176.0	0.0	-0.31	0.0300	0.3113
176.0	0.1	-0.3100	0.0300	0.3113
176.0	0.2	-0.3350	0.0300	0.3363
176.0	0.3	-0.3350	0.0300	0.3363
176.0	0.4	-0.3800	0.0300	0.3812
176.0	0.5	-0.3900	0.0300	0.3912
176.0	0.6	-0.4400	0.0310	0.4411
176.0	0.7	-0.4350	0.0425	0.4369
176.0	1.0	-0.1550	0.1835	0.1674
177.0	0.0	-0.24	0.0240	0.2409
177.0	0.1	-0.2400	0.0240	0.2409
177.0	0.2	-0.2500	0.0240	0.2509
177.0	0.3	-0.2600	0.0240	0.2609
177.0	0.4	-0.2920	0.0240	0.2928
177.0	0.5	-0.3050	0.0240	0.3058
177.0	0.6	-0.3450	0.0240	0.3458
177.0	0.7	-0.3500	0.0322	0.3512
177.0	1.0	-0.1150	0.1740	0.1239
178.0	0.0	-0.16	0.0205	0.1606
178.0	0.1	-0.1600	0.0205	0.1606
178.0	0.2	-0.1680	0.0205	0.1686
178.0	0.3	-0.1750	0.0205	0.1756
178.0	0.4	-0.2050	0.0205	0.2056
178.0	0.5	-0.2080	0.0205	0.2086
178.0	0.6	-0.2400	0.0205	0.2406
178.0	0.7	-0.2500	0.0220	0.2506
178.0	1.0	-0.0800	0.1660	0.0857
179.0	0.0	-0.09	0.0170	0.0903
179.0	0.1	-0.0900	0.0170	0.0903
179.0	0.2	-0.0800	0.0170	0.0803
179.0	0.3	-0.0840	0.0170	0.0843
179.0	0.4	-0.1000	0.0170	0.1003
179.0	0.5	-0.1000	0.0170	0.1003
179.0	0.6	-0.1350	0.0170	0.1353
179.0	0.7	-0.1300	0.0173	0.1303
179.0	1.0	-0.0350	0.1620	0.0378

TABLE V - (Cont'd)

α	M	C_L	C_D	C_N
180.0	0.0	0.0	0.0150	0.0
180.0	0.1	0.0	0.0150	0.0
180.0	0.2	0.0	0.0150	0.0
180.0	0.3	0.0	0.0150	0.0
180.0	0.4	0.0	0.0150	0.0
180.0	0.5	0.0	0.0150	0.0
180.0	0.6	0.0	0.0150	0.0
180.0	0.7	0.0	0.0150	0.0
180.0	1.0	0.0	0.1585	0.0

TABLE VI

15 PERCENT SYMMETRIC AIRFOIL INPUT DATA

α	M	C_L	C_D	C_N
0.0	0.0	0.0	.0086	0.0
0.0	0.1	0.0	.0086	0.0
0.0	0.2	0.0	.0086	0.0
0.0	0.3	0.0	.0086	0.0
0.0	0.4	0.0	.0086	0.0
0.0	0.5	0.0	.0087	0.0
0.0	0.6	0.0	.0087	0.0
0.0	0.7	0.0	.0088	0.0
0.0	1.0	0.0	.1068	0.0
1.0	0.0	.1028	.0088	.1030
1.0	0.1	.1028	.0088	.1030
1.0	0.2	.1009	.0090	.1010
1.0	0.3	.1006	.0090	.1008
1.0	0.4	.1076	.0090	.1008
1.0	0.5	.1170	.0090	.1171
1.0	0.6	.1375	.0091	.1376
1.0	0.7	.1440	.0094	.1441
1.0	1.0	.0250	.1036	.0268
2.0	0.0	.2057	.0092	.2059
2.0	0.1	.2057	.0092	.2059
2.0	0.2	.2018	.0092	.2019
2.0	0.3	.2012	.0092	.2014
2.0	0.4	.2152	.0092	.2154
2.0	0.5	.2365	.0092	.2367
2.0	0.6	.2650	.0092	.2652
2.0	0.7	.2790	.0103	.2792
2.0	1.0	.0550	.1060	.0587
3.0	0.0	.3086	.0094	.3086
3.0	0.1	.3086	.0094	.3086
3.0	0.2	.3026	.0094	.3027
3.0	0.3	.3019	.0094	.3020
3.0	0.4	.3228	.0096	.3229
3.0	0.5	.3510	.0096	.3510
3.0	0.6	.3725	.0096	.3725
3.0	0.7	.4150	.0150	.4152
3.0	1.0	.0925	.1074	.0980
4.0	0.0	.4114	.0100	.4111
4.0	0.1	.4114	.0100	.4111
4.0	0.2	.4036	.0100	.4033
4.0	0.3	.4025	.0100	.4022
4.0	0.4	.4305	.0100	.4302
4.0	0.5	.4605	.0100	.4601
4.0	0.6	.4630	.0108	.4626
4.0	0.7	.5250	.0216	.5252
4.0	1.0	.1400	.1166	.1478
5.0	0.0	.5143	.0106	.5133

TABLE VI - (Cont'd

α	M	C_L	C_D	C_N
5.0	0.1	.5143	.0106	.5133
5.0	0.2	.5044	.0106	.5034
5.0	0.3	.5032	.0108	.5022
5.0	0.4	.5381	.0108	.5370
5.0	0.5	.5800	.0108	.5787
5.0	0.6	.5975	.0156	.5966
5.0	0.7	.6050	.0346	.6057
5.0	1.0	.2125	.1430	.2242
6.0	0.0	.6172	.0118	.6150
6.0	0.1	.6172	.0118	.6150
6.0	0.2	.6053	.0118	.6032
6.0	0.3	.6038	.0118	.6017
6.0	0.4	.6458	.0118	.6434
6.0	0.5	.6895	.0127	.6883
6.0	0.6	.6900	.0249	.6888
6.0	0.7	.6575	.0528	.6594
6.0	1.0	.2650	.1710	.2814
7.0	0.0	.7200	.0132	.7162
7.0	0.1	.7200	.0132	.7162
7.0	0.2	.7062	.0132	.7025
7.0	0.3	.7044	.0132	.7008
7.0	0.4	.7534	.0132	.7494
7.0	0.5	.7675	.0172	.7639
7.0	0.6	.7800	.0356	.7785
7.0	0.7	.6810	.0750	.6851
7.0	1.0	.3075	.2024	.3299
8.0	0.0	.8100	.0146	.8042
8.0	0.1	.8100	.0146	.8042
8.0	0.2	.8070	.0146	.8012
8.0	0.3	.8050	.0146	.7992
8.0	0.4	.8600	.0154	.8538
8.0	0.5	.8550	.0271	.8505
8.0	0.6	.8340	.0572	.8338
8.0	0.7	.6975	.0905	.7033
8.0	1.0	.3300	.2156	.3568
9.0	0.0	.9100	.0162	.9013
9.0	0.1	.9100	.0162	.9013
9.0	0.2	.9050	.0162	.8964
9.0	0.3	.9050	.0162	.8964
9.0	0.4	.9500	.0212	.9416
9.0	0.5	.9300	.0415	.9250
9.0	0.6	.8550	.0772	.8566
9.0	0.7	.7000	.1168	.7096
9.0	1.0	.3525	.2368	.3852
10.0	0.0	1.0125	.0182	1.0003
10.0	0.1	1.0125	.0182	1.0003

TABLE VI - (Cont'd)

α	M	C_L	C_D	C_N
10.0	0.2	1.0050	.0184	.9929
10.0	0.3	1.0000	.0195	.9882
10.0	0.4	1.0200	.0317	1.0100
10.0	0.5	.9740	.0604	.9697
10.0	0.6	.8605	.0985	.8645
10.0	0.7	.7050	.1385	.7183
10.0	1.0	.3750	.2578	.4141
11.0	0.0	1.0950	.0204	1.0788
11.0	0.1	1.0950	.0204	1.0788
11.0	0.2	1.1000	.0204	1.0837
11.0	0.3	1.1000	.0256	1.0847
11.0	0.4	1.0950	.0448	1.0834
11.0	0.5	.9925	.0804	.9896
11.0	0.6	.8450	.1192	.8522
11.0	0.7	.7030	.1588	.7204
11.0	1.0	.3950	.2768	.4406
12.0	0.0	1.2050	.0228	1.1834
12.0	0.1	1.2050	.0228	1.1834
12.0	0.2	1.1950	.0232	1.1694
12.0	0.3	1.1750	.0348	1.1566
12.0	0.4	1.1175	.0636	1.1063
12.0	0.5	.9800	.1015	.9797
12.0	0.6	.8150	.1406	.8264
12.0	0.7	.7000	.1802	.7222
12.0	1.0	.4150	.2978	.4679
13.0	0.0	1.2900	.0264	1.2629
13.0	0.1	1.2900	.0264	1.2629
13.0	0.2	1.2675	.0301	1.2418
13.0	0.3	1.2050	.0496	1.1853
13.0	0.4	1.1300	.0844	1.0948
13.0	0.5	.9350	.1228	.9386
13.0	0.6	.7775	.1616	.7939
13.0	0.7	.6950	.2008	.7223
13.0	1.0	.4375	.3178	.4978
14.0	0.0	1.3570	.0394	1.3262
14.0	0.1	1.3570	.0394	1.3262
14.0	0.2	1.2970	.0472	1.2699
14.0	0.3	1.2025	.0750	1.1849
14.0	0.4	1.0650	.1121	1.0605
14.0	0.5	.8850	.1506	.8952
14.0	0.6	.7425	.1896	.7663
14.0	0.7	.6875	.2288	.7224
14.0	1.0	.4460	.3458	.5164
15.0	0.0	1.3725	.0788	1.3461
15.0	0.1	1.3725	.0796	1.3461
15.0	0.2	1.2850	.0890	1.2643
15.0	0.3	1.1800	.1086	1.1679

TABLE VI - (Cont'd)

α	M	C_L	C_D	C_N
15.0	0.4	1.0050	.1421	1.0075
15.0	0.5	.8250	.1811	.8438
15.0	0.6	.7100	.2214	.7431
15.0	0.7	.6805	.2626	.7253
15.0	1.0	.4815	.3846	.5646
165.0	0.0	-.5911	.1468	-.6090
165.0	0.1	-.5911	.1476	-.6092
165.0	0.2	-.5498	.1574	-.5718
165.0	0.3	-.5300	.1764	-.5576
165.0	0.4	-.5122	.1992	-.5464
165.0	0.5	-.5131	.2247	-.5538
165.0	0.6	-.4836	.2540	-.5329
165.0	0.7	-.4782	.2892	-.5367
165.0	1.0	-.3978	.4154	-.4917
166.0	0.0	-.6091	.1348	-.6236
166.0	0.1	-.6091	.1350	-.6237
166.0	0.2	-.5711	.1434	-.5888
166.0	0.3	-.5488	.1606	-.5714
166.0	0.4	-.5325	.1814	-.5606
166.0	0.5	-.5280	.2046	-.5618
166.0	0.6	-.5018	.2301	-.5426
166.0	0.7	-.4853	.2620	-.5343
166.0	1.0	-.3764	.3778	-.4566
167.0	0.0	-.6248	.1228	-.6365
167.0	0.1	-.6248	.1228	-.6365
167.0	0.2	-.5875	.1282	-.6013
167.0	0.3	-.5626	.1438	-.5806
167.0	0.4	-.5600	.1625	-.5810
167.0	0.5	-.5372	.1842	-.5648
167.0	0.6	-.5132	.2088	-.5471
167.0	0.7	-.4855	.2374	-.5265
167.0	1.0	-.3542	.3458	-.4229
168.0	0.0	-.6226	.1108	-.6320
168.0	0.1	-.6226	.1108	-.6320
168.0	0.2	-.6005	.1118	-.6106
168.0	0.3	-.5785	.1240	-.5916
168.0	0.4	-.5688	.1410	-.5856
168.0	0.5	-.5492	.1612	-.5707
168.0	0.6	-.5232	.1854	-.5503
168.0	0.7	-.4936	.2128	-.5270
168.0	1.0	-.3372	.3198	-.3963
169.0	0.0	-.6228	.0988	-.6303
169.0	0.1	-.6228	.0988	-.6303
169.0	0.2	-.6000	.0988	-.6078
169.0	0.3	-.5920	.1034	-.6009
169.0	0.4	-.5722	.1176	-.5841
169.0	0.5	-.5624	.1365	-.5781

TABLE VI - (Cont'd)

α	M	C_L	C_D	C_N
169.0	0.6	-.5300	.1604	-.5509
169.0	0.7	-.5086	.1890	-.5353
169.0	1.0	-.3181	.2988	-.3693
170.0	0.0	-.6075	.0874	-.6134
170.0	0.1	-.6075	.0874	-.6134
170.0	0.2	-.5970	.0874	-.6031
170.0	0.3	-.5900	.0880	-.5963
170.0	0.4	-.5800	.0978	-.5882
170.0	0.5	-.5627	.1141	-.5740
170.0	0.6	-.5403	.1366	-.5558
170.0	0.7	-.5086	.1668	-.5298
170.0	1.0	-.3021	.2778	-.3458
171.0	0.0	-.5935	.0768	-.5982
171.0	0.1	-.5935	.0768	-.5982
171.0	0.2	-.5868	.0768	-.5915
171.0	0.3	-.5858	.0768	-.5906
171.0	0.4	-.5842	.0808	-.5896
171.0	0.5	-.5670	.0956	-.5750
171.0	0.6	-.5472	.1160	-.5586
171.0	0.7	-.5126	.1426	-.5286
171.0	1.0	-.2820	.2544	-.3183
172.0	0.0	-.5532	.0658	-.5569
172.0	0.1	-.5532	.0658	-.5569
172.0	0.2	-.5700	.0658	-.5736
172.0	0.3	-.5665	.0658	-.5702
172.0	0.4	-.5767	.0662	-.5803
172.0	0.5	-.5700	.0772	-.5752
172.0	0.6	-.5444	.0962	-.5524
172.0	0.7	-.5118	.1209	-.5237
172.0	1.0	-.2630	.2378	-.2935
173.0	0.0	-.4914	.0568	-.4946
173.0	0.1	-.4914	.0568	-.4946
173.0	0.2	-.5254	.0568	-.5284
173.0	0.3	-.5366	.0568	-.5396
173.0	0.4	-.5474	.0568	-.5503
173.0	0.5	-.5628	.0614	-.5661
173.0	0.6	-.5400	.0767	-.5453
173.0	0.7	-.5088	.0984	-.5170
173.0	1.0	-.2409	.2188	-.2658
174.0	0.0	-.4330	.0474	-.4355
174.0	0.1	-.4330	.0474	-.4355
174.0	0.2	-.4659	.0474	-.4683
174.0	0.3	-.4770	.0474	-.4794
174.0	0.4	-.5223	.0474	-.5244
174.0	0.5	-.5290	.0476	-.5311
174.0	0.6	-.5378	.0578	-.5409
174.0	0.7	-.4981	.0780	-.5035

TABLE VI - (Cont'd)

α	M	C_L	C_D	C_N
174.0	1.0	-.2140	.2064	-.2344
175.0	0.0	-.3697	.0388	-.3717
175.0	0.1	-.3697	.0388	-.3717
175.0	0.2	-.3966	.0388	-.3984
175.0	0.3	-.4025	.0388	-.4044
175.0	0.4	-.4520	.0388	-.4537
175.0	0.5	-.4680	.0388	-.4697
175.0	0.6	-.5241	.0448	-.5260
175.0	0.7	-.4840	.0635	-.4877
175.0	1.0	-.1902	.1948	-.2065
176.0	0.0	-.3114	.0308	-.3127
176.0	0.1	-.3114	.0308	-.3127
176.0	0.2	-.3321	.0308	-.3334
176.0	0.3	-.3280	.0308	-.3293
176.0	0.4	-.3817	.0308	-.3829
176.0	0.5	-.3938	.0308	-.3950
176.0	0.6	-.4428	.0325	-.4440
176.0	0.7	-.4568	.0478	-.4590
176.0	1.0	-.1669	.1844	-.1794
177.0	0.0	-.2336	.0248	-.2345
177.0	0.1	-.2336	.0248	-.2345
177.0	0.2	-.2484	.0248	-.2494
177.0	0.3	-.2584	.0248	-.2593
177.0	0.4	-.2913	.0248	-.2922
177.0	0.5	-.3182	.0248	-.3190
177.0	0.6	-.3725	.0250	-.3733
177.0	0.7	-.3724	.0367	-.3739
177.0	1.0	-.1418	.1748	-.1508
178.0	0.0	-.1654	.0214	-.1660
178.0	0.1	-.1654	.0214	-.1660
178.0	0.2	-.1586	.0214	-.1660
178.0	0.3	-.1789	.0214	-.1795
178.0	0.4	-.1908	.0214	-.1915
178.0	0.5	-.2158	.0214	-.2164
178.0	0.6	-.2765	.0214	-.2771
178.0	0.7	-.2527	.0272	-.2535
178.0	1.0	-.1100	.1668	-.1158
179.0	0.0	-.0876	.0178	-.0878
179.0	0.1	-.0876	.0178	-.0878
179.0	0.2	-.0793	.0178	-.0796
179.0	0.3	-.0844	.0178	-.0847
179.0	0.4	-.1004	.0178	-.1007
179.0	0.5	-.1026	.0178	-.1029
179.0	0.6	-.1435	.0178	-.1438
179.0	0.7	-.1356	.0212	-.1360
179.0	1.0	-.0438	.1628	-.0466

TABLE VI - (Cont'd)

α	M	C_L	C_D	C_N
180.0	0.0	-0.0	.0158	-0.0
180.0	0.1	-0.0	.0158	-0.0
180.0	0.2	-0.0	.0158	-0.0
180.0	0.3	-0.0	.0158	-0.0
180.0	0.4	-0.0	.0158	-0.0
180.0	0.5	-0.0	.0158	-0.0
180.0	0.6	-0.0	.0158	-0.0
180.0	0.7	-0.0	.0181	-0.0
180.0	1.0	-0.0	.1594	-0.0

TABLE VII
18-PERCENT SYMMETRIC AIRFOIL INPUT DATA

α	M	C_L	C_D	C_N
0.0	0.0	0.0	.0095	0.0
0.0	0.1	0.0	.0095	0.0
0.0	0.2	0.0	.0095	0.0
0.0	0.3	0.0	.0095	0.0
0.0	0.4	0.0	.0095	0.0
0.0	0.5	0.0	.0095	0.0
0.0	0.6	0.0	.0095	0.0
0.0	0.7	0.0	.0096	0.0
0.0	1.0	0.0	.1075	0.0
1.0	0.0	.1000	.0097	.1002
1.0	0.1	.1000	.0097	.1002
1.0	0.2	.1000	.0098	.1002
1.0	0.3	.1000	.0098	.1002
1.0	0.4	.1081	.0098	.1083
1.0	0.5	.1200	.0099	.1202
1.0	0.6	.1600	.0099	.1601
1.0	0.7	.1500	.0105	.1502
1.0	1.0	.0300	.1110	.0319
2.0	0.0	.2000	.0100	.2002
2.0	0.1	.2000	.0100	.2002
2.0	0.2	.2000	.0100	.2002
2.0	0.3	.2000	.0100	.2002
2.0	0.4	.2162	.0100	.2164
2.0	0.5	.2450	.0101	.2452
2.0	0.6	.3000	.0101	.3002
2.0	0.7	.2820	.0120	.2822
2.0	1.0	.0700	.1140	.0739
3.0	0.0	.3000	.0103	.3001
3.0	0.1	.3000	.0103	.3001
3.0	0.2	.3000	.0103	.3001
3.0	0.3	.3000	.0103	.3001
3.0	0.4	.3243	.0104	.3244
3.0	0.5	.3600	.0104	.3601
3.0	0.6	.4000	.0104	.4000
3.0	0.7	.4400	.0183	.4404
3.0	1.0	.1100	.1165	.1159
4.0	0.0	.4000	.0109	.3998
4.0	0.1	.4000	.0109	.3998
4.0	0.2	.4000	.0109	.3998
4.0	0.3	.4000	.0109	.3998
4.0	0.4	.4324	.0109	.4321
4.0	0.5	.4650	.0109	.4646
4.0	0.6	.4660	.0123	.4657
4.0	0.7	.5500	.0253	.5504
4.0	1.0	.1500	.1223	.1582
5.0	0.0	.5000	.0115	.4991

TABLE VII - (Cont'd)

α	M	C_L	C_D	C_N
5.0	0.1	.5000	.0115	.4991
5.0	0.2	.5000	.0115	.4991
5.0	0.3	.5000	.0116	.4991
5.0	0.4	.5405	.0116	.5395
5.0	0.5	.5900	.0116	.5888
5.0	0.6	.6250	.0184	.6242
5.0	0.7	.6100	.0372	.6109
5.0	1.0	.2150	.1440	.2267
6.0	0.0	.6000	.0127	.5980
6.0	0.1	.6000	.0127	.5980
6.0	0.2	.6000	.0127	.5980
6.0	0.3	.6000	.0127	.5980
6.0	0.4	.6486	.0127	.6464
6.0	0.5	.7000	.0144	.6977
6.0	0.6	.7000	.0284	.6991
6.0	0.7	.6550	.0538	.6570
6.0	1.0	.2700	.1718	.2865
7.0	0.0	.7000	.0140	.6965
7.0	0.1	.7000	.0140	.6965
7.0	0.2	.7000	.0140	.6965
7.0	0.3	.7000	.0141	.6965
7.0	0.4	.7567	.0141	.7528
7.0	0.5	.7850	.0199	.7816
7.0	0.6	.7800	.0398	.7790
7.0	0.7	.6820	.0760	.6862
7.0	1.0	.3150	.2032	.3374
8.0	0.0	.8000	.0155	.7944
8.0	0.1	.8000	.0155	.7944
8.0	0.2	.8000	.0155	.7944
8.0	0.3	.8000	.0155	.7944
8.0	0.4	.8700	.0165	.8638
8.0	0.5	.8700	.0322	.8660
8.0	0.6	.8330	.0600	.8332
8.0	0.7	.7000	.0865	.7052
8.0	1.0	.3400	.2164	.3668
9.0	0.0	.9000	.0170	.8916
9.0	0.1	.9000	.0170	.8916
9.0	0.2	.9000	.0171	.8916
9.0	0.3	.9000	.0171	.8916
9.0	0.4	.9600	.0240	.9519
9.0	0.5	.9300	.0460	.9257
9.0	0.6	.8550	.0784	.8567
9.0	0.7	.7050	.1175	.7147
9.0	1.0	.3650	.2377	.3977
10.0	0.0	1.0000	.0191	.9881
10.0	0.1	1.0000	.0191	.9881

TABLE VII - (Cont'd)

α	M	C_L	C_D	C_N
10.0	0.2	1.0000	.0192	.9881
10.0	0.3	1.0000	.0208	.9884
10.0	0.4	1.0200	.0378	1.0111
10.0	0.5	.9700	.0635	.9663
10.0	0.6	.8610	.0995	.8652
10.0	0.7	.7100	.1395	.7234
10.0	1.0	.3900	.2587	.4290
11.0	0.0	1.1000	.0212	1.0838
11.0	0.1	1.1000	.0212	1.0838
11.0	0.2	1.1000	.0212	1.0838
11.0	0.3	1.1000	.0285	1.0852
11.0	0.4	1.0800	.0505	1.0698
11.0	0.5	.9950	.0818	.99233
11.0	0.6	.8450	.1200	.8524
11.0	0.7	.7080	.1596	.7254
11.0	1.0	.4100	.2777	.4555
12.0	0.0	1.2100	.0237	1.1885
12.0	0.1	1.2100	.0237	1.1885
12.0	0.2	1.2000	.0245	1.1789
12.0	0.3	1.1720	.0395	1.1546
12.0	0.4	1.1150	.0667	1.1045
12.0	0.5	.9750	.1030	.9751
12.0	0.6	.8200	.1420	.8610
12.0	0.7	.7050	.1814	.7273
12.0	1.0	.4300	.2987	.4832
13.0	0.0	1.3000	.0272	1.2728
13.0	0.1	1.3000	.0272	1.2728
13.0	0.2	1.2750	.0332	1.2498
13.0	0.3	1.2000	.0549	1.1816
13.0	0.4	1.1100	.0858	1.1009
13.0	0.5	.9300	.1240	.9341
13.0	0.6	.7900	.1626	.8063
13.0	0.7	.7000	.2015	.7274
13.0	1.0	.4550	.3187	.5150
14.0	0.0	1.3550	.0402	1.3245
14.0	0.1	1.3550	.0402	1.3245
14.0	0.2	1.2950	.0532	1.2694
14.0	0.3	1.2000	.0785	1.1834
14.0	0.4	1.0500	.1132	1.0462
14.0	0.5	.8900	.1520	.9003
14.0	0.6	.7600	.1906	.7835
14.0	0.7	.6950	.2295	.7299
14.0	1.0	.4800	.3467	.5496
15.0	0.0	1.3750	.0797	1.3488
15.0	0.1	1.3750	.0808	1.3491
15.0	0.2	1.2800	.0950	1.2610
15.0	0.3	1.1800	.1157	1.1697

TABLE VII - (Cont'd)

α	M	C_L	C_D	C_N
15.0	0.4	.9800	.1440	.9839
15.0	0.5	.8300	.1820	.8488
15.0	0.6	.7300	.2224	.7627
15.0	0.7	.6850	.2632	.7298
15.0	1.0	.5030	.3854	.5856
165.0	0.0	-.5922	.1477	-.6103
165.0	0.1	-.5922	.1493	-.6107
165.0	0.2	-.5477	.1652	-.5718
165.0	0.3	-.5300	.1858	-.5600
165.0	0.4	-.4995	.2085	-5364
165.0	0.5	-.5162	.2326	-.5588
165.0	0.6	-.4972	.2594	-.5474
165.0	0.7	-.4813	.2918	-.5404
165.0	1.0	-.4155	.4162	-.5091
166.0	0.0	-.6082	.1357	-.6230
166.0	0.1	-.6082	.1360	-.6230
166.0	0.2	-.5702	.1486	-.5892
166.0	0.3	-.5477	.1679	-.5721
166.0	0.4	-.5250	.1900	-.5554
166.0	0.5	-.5310	.2125	-.5666
166.0	0.6	-.5137	.2352	-.5553
166.0	0.7	-.4906	.2644	-.5400
166.0	1.0	-.3927	.3787	-.4727
167.0	0.0	-.6297	.1237	-.6414
167.0	0.1	-.6297	.1237	-.6414
167.0	0.2	-.5910	.1310	-.6053
167.0	0.3	-.5603	.1482	-.5793
167.0	0.4	-.5600	.1677	-.5834
167.0	0.5	-.5343	.1895	-.5632
167.0	0.6	-.5215	.2120	-.5558
167.0	0.7	-.4890	.2392	-.5303
167.0	1.0	-.3683	.3467	-.4369
168.0	0.0	-.6252	.1117	-.6348
168.0	0.1	-.6252	.1117	-.6348
168.0	0.2	-.6030	.1130	-.6133
168.0	0.3	-.5770	.1280	-.5910
168.0	0.4	-.5675	.1468	-.5856
168.0	0.5	-.5464	.1675	-.5693
168.0	0.6	-.5264	.1900	-.5544
168.0	0.7	-.4971	.2156	-.5311
168.0	1.0	-.3494	.3207	-.4084
169.0	0.0	-.6257	.0997	-.6332
169.0	0.1	-.6257	.0997	-.6332
169.0	0.2	-.6000	.0997	-.6080
169.0	0.3	-.5920	.1068	-.6015
169.0	0.4	-.5643	.1230	-.5774
169.0	0.5	-.5638	.1435	-.5808

TABLE VII - (Cont'd)

α	M	C_L	C_D	C_N
169.0	0.6	-.5300	.1675	-.5522
169.0	0.7	-.5122	.1922	-.5395
169.0	1.0	-.3302	.2997	-.3813
170.0	0.0	-.6000	.0882	-.6062
170.0	0.1	-.6000	.0882	-.6062
170.0	0.2	-.5941	.0882	-.6004
170.0	0.3	-.5900	.0895	-.5966
170.0	0.4	-.5800	.1020	-.5889
170.0	0.5	-.5604	.1205	-.5728
170.0	0.6	-.5406	.1426	-.5572
170.0	0.7	-.5122	.1695	-.5339
170.0	1.0	-.3142	.2787	-.3578
171.0	0.0	-.5870	.0777	-.5919
171.0	0.1	-.5870	.0777	-.5919
171.0	0.2	-.5835	.0777	-.5885
171.0	0.3	-.5825	.0777	-.5874
171.0	0.4	-.5903	.0834	-.5961
171.0	0.5	-.5670	.1000	-.5757
171.0	0.6	-.5440	.1204	-.5561
171.0	0.7	-.5151	.1453	-.5315
171.0	1.0	-.2920	.2552	-.3283
172.0	0.0	-.5463	.0667	-.5503
172.0	0.1	-.5463	.0667	-.5503
172.0	0.2	-.5650	.0667	-.5688
172.0	0.3	-.5630	.0667	-.5668
172.0	0.4	-.5834	.0673	-.5871
172.0	0.5	-.5800	.0808	-.5856
172.0	0.6	-.5437	.1005	-.5524
172.0	0.7	-.5137	.1244	-.5260
172.0	1.0	-.2709	.2387	-.3015
173.0	0.0	-.4777	.0577	-.4812
173.0	0.1	-.4777	.0577	-.4812
173.0	0.2	-.5208	.0577	-.5240
173.0	0.3	-.5333	.0577	-.5364
173.0	0.4	-.5499	.0577	-.5528
173.0	0.5	-.5757	.0643	-.5792
173.0	0.6	-.5400	.0814	-.5459
173.0	0.7	-.5095	.1033	-.5183
173.0	1.0	-.2468	.2197	-.2717
174.0	0.0	-.4209	.0482	-.4236
174.0	0.1	-.4209	.0482	-.4236
174.0	0.2	-.4618	.0482	-.4643
174.0	0.3	-.4741	.0482	-.4765
174.0	0.4	-.5246	.0482	-.5268
174.0	0.5	-.5371	.0488	-.5393
174.0	0.6	-.5456	.0636	-.5493
174.0	0.7	-.4962	.0857	-.5024

TABLE VII - (Cont'd)

α	M	C_L	C_D	C_N
174.0	1.0	-.2181	.2072	-.2386
175.0	0.0	-.3594	.0397	-.3615
175.0	0.1	-.3594	.0397	-.3615
175.0	0.2	-.3931	.0397	-.3951
175.0	0.3	-.4000	.0397	-.4019
175.0	0.4	-.4540	.0397	-.4557
175.0	0.5	-.4761	.0397	-.4777
175.0	0.6	-.5482	.0486	-.5503
175.0	0.7	-.4880	.0705	-.4923
175.0	1.0	-.1925	.1957	-.2088
176.0	0.0	-.3027	.0317	-.3042
176.0	0.1	-.3027	.0317	-.3042
176.0	0.2	-.3292	.0317	-.3306
176.0	0.3	-.3259	.0317	-.3273
176.0	0.4	-.3834	.0317	-.3847
176.0	0.5	-.3977	.0317	-.3989
176.0	0.6	-.4457	.0340	-.4470
176.0	0.7	-.4785	.0532	-.4810
176.0	1.0	-.1788	.1852	-.1913
177.0	0.0	-.2271	.0257	-.2281
177.0	0.1	-.2271	.0257	-.2281
177.0	0.2	-.2469	.0257	-.2479
177.0	0.3	-.2567	.0257	-.2577
177.0	0.4	-.2926	.0257	-.2935
177.0	0.5	-.3263	.0257	-.3272
177.0	0.6	-.4000	.0260	-.4008
177.0	0.7	-.3949	.0412	-.3965
177.0	1.0	-.1687	.1757	-.1777
178.0	0.0	-.1608	.0222	-.1615
178.0	0.1	-.1608	.0222	-.1615
178.0	0.2	-.1572	.0222	-.1579
178.0	0.3	-.1778	.0222	-.1785
178.0	0.4	-.1917	.0222	-.1924
178.0	0.5	-.2235	.0222	-.2241
178.0	0.6	-.3130	.0222	-.3136
178.0	0.7	-.2554	.0324	-.2564
178.0	1.0	-.1400	.1677	-.1458
179.0	0.0	-.0851	.0187	-.0854
179.0	0.1	-.0851	.0187	-.0854
179.0	0.2	-.0786	.0187	-.0789
179.0	0.3	-.0839	.0187	-.0842
179.0	0.4	-.1009	.0187	-.1012
179.0	0.5	-.1053	.0187	-.1056
179.0	0.6	-.1670	.0187	-.1673
179.0	0.7	-.1413	.0252	-.1417
179.0	1.0	-.0525	.1637	-.0553

TABLE VII - (Cont'd)

α	M	C_L	C_D	C_N
180.0	0.0	-0.0	.0167	0.0
180.0	0.1	-0.0	.0167	0.0
180.0	0.2	-0.0	.0167	0.0
180.0	0.3	-0.0	.0167	0.0
180.0	0.4	-0.0	.0167	0.0
180.0	0.5	-0.0	.0167	0.0
180.0	0.6	-0.0	.0167	0.0
180.0	0.7	-0.0	.0212	0.0

REFERENCES

1. Loewy, Robert G., Aural Detection of Helicopters in Tactical Situations, Journal of the American Helicopter Society, Vol. 8, No. 4, October 1963.

2. Sternfeld, Harry, Jr., and J. Everette Forehand, Helicopter Noise, Its Evaluation and Treatment, Proceedings of the American Helicopter Society Seventeenth Annual Forum, Washington, D. C., May 3-5, 1961.

3. Gutin, L., On the Sound Field of a Rotating Propeller, NACA TM 1195, 1948. (From Phys. Zeitschr. der Sowjetunion, Bd. 9, Heft 1, 1936, pp. 57-71).

4. Deming, Arthur F., Propeller Rotation Noise Due to Torque and Thrust, National Advisory Committee for Aeronautics Technical Note No. 747, January 1940.

5. Garrick, E. I. and C. E. Watkins, A Theoretical Study of the Effect of Forward Speed on the Free-Space Sound-Pressure Field Around Propellers, National Advisory Committee for Aeronautics Technical Note 3018, October 1953.

6. Franken, P. A., E. M. Kervin, Jr., et al, Methods of Flight Vehicle Noise Prediction, TR 58-343, Wright Air Development Center, Dayton, Ohio, November 1958.

7. A Study of the Origin and Means of Reducing Helicopter Noise, TCREC Technical Report 62-73, U. S. Army Transportation Research Command*, Fort Eustis, Virginia, November 1962.

8. Miller, R. H., On the Computation of Airloads Acting on Rotor Blades in Forward Flight, Journal of the American Helicopter Society, Vol. 7, No. 2, April 1962.

9. Piziali, R. A. and F. A. DuWaldt, A Method for Computing Rotary Wind Airload Distributions in Forward Flight, TCREC TR 62-44, U. S. Army Transportation Research Command*, Fort Eustis, Virginia, November 1962.

10. Lowson, M. V., Basic Mechanisms of Noise Generation by Helicopters, V/STOL Aircraft, and Ground Effect Machines, Wyle Laboratories Report No. WR 65-9, May 1965.

11. Rabbott, J. P., Jr., and G. B. Churchill, Experimental Investigation of the Aerodynamic Loading on a Helicopter Rotor Blade in Forward Flight, NACA RM L56107, October 1956.

*Now U. S. Army Aviation Materiel Laboratories

12. Gessow, A., and G. C. Myers, Aerodynamics of the Helicopter, MacMillan Company, New York, 1952.

13. Hubbard, H. H., and D. J. Maglieri, Noise Characteristics of Helicopter Rotors at Tip Speeds up to 900 1/sec, Journal of Acoustic Society of America, Vol. 32, No. 9, September 1960.

14. Hildebrand, Francis B., Advanced Calculus for Applications, Prentice-Hall, Inc., Englewood Cliffs, New Jersey, 1962.

15. Nikolsky, A. A., Helicopter Analysis, John Wiley & Sons, Inc., New York, New York, 1951.

16. Scheiman, James, A Tabulation of Helicopter Rotor-Blade Differential Pressures, Stresses, and Motions as Measured in Flight, NASA Technical Memorandum NASA TM X-952, March 1964.

17. Measurement of Dynamic Air Loads on A Full-Scale Semirigid Rotor, TCREC Technical Report 62-42, U. S. Army Transportation Research Command , Fort Eustis, Virginia, December 1962.

18. Scheiman, James and Henry Kelley, Comparison of Flight Measured Helicopter Rotor Blade Chordwise Pressure Distributions and Two-Dimensional Airfoil Characteristics, NASA, Langley Field, Hampton, Virginia, (date unknown).

19. Sternfeld, H., Jr., R. H. Spencer and E. G. Schaeffer, Study to Establish Realistic Acoustic Design Criteria for Future Army Aircraft, Vertol Division, The Boeing Company, Report No. 192, June 1961.

20. Peterson, A. P. G., and L. L. Beranek, Handbook of Noise Measurement and Measurement of Vibration, General Radio Company, Cambridge, Mass., 3rd Edition, 1956.

21. Stowell, E. Z., and A. F. Deming, Vortex Noise from Rotating Cylindrical Rods, NACA TN 519, February 1935.

22. Yudin, E. Y., On the Vortex Sound from Rotating Rods, (Translation), NACA TM 1136, March 1947.

Unclassified

Security Classification

DOCUMENT CONTROL DATA - R&D

(Security classification of title, body of abstract and indexing annotation must be entered when the overall report is classified)

1. ORIGINATING ACTIVITY (Corporate author) Rochester Applied Science Associates, Inc. 1595 Elmwood Avenue Rochester, New York 14620	2a. REPORT SECURITY CLASSIFICATION Unclassified 2b. GROUP NA

3. REPORT TITLE

A THEORY FOR PREDICTING THE ROTATIONAL NOISE OF LIFTING ROTORS IN FORWARD FLIGHT INCLUDING A COMPARISON WITH EXPERIMENT

4. DESCRIPTIVE NOTES (Type of report and inclusive dates)

Final Report

5. AUTHOR(S) (Last name, first name, initial)

Loewy, Robert G.
Sutton, Lawrence R.

6. REPORT DATE	7a. TOTAL NO. OF PAGES	7b. NO. OF REFS
January 1966	99	22

8a. CONTRACT OR GRANT NO. DA 44-177-AMC-204(T) b. PROJECT NO. Task 1P121401A14801 c. d.	9a. ORIGINATOR'S REPORT NUMBER(S) USAAVLABS Technical Report 65-82 9b. OTHER REPORT NO(S) (Any other numbers that may be assigned this report) RASA Report 65-10

10. AVAILABILITY/LIMITATION NOTICES

Distribution of this document is unlimited.

11. SUPPLEMENTARY NOTES	12. SPONSORING MILITARY ACTIVITY
	U.S. ARMY AVIATION MATERIAL LABORATORIES Fort Eustis, Virginia

13. ABSTRACT

A theory and resultant calculations are presented, predicting the noise generated by a lifting rotor in forward flight. With suitable adjustments in parameters, this theory reproduced (by numerical integration) the closed form results of Garrick and Watkins in their investigation of noise produced by a propeller. The theory presented here accounts for (1) asymmetry of inflow, lift, and drag; (2) non-linear section characteristics, compressibility, and reverse flow; (3) first harmonic and steady rigid blade flapping and pitching; (4) rotor shaft tilt; and (5) chordwise distribution of lift and drag forces. Sound pressure levels were evaluated for up to 20 harmonics at a general field point translating with the rotor hub, for the H-34 and HU-1 helicopters. A comparison with experiment is also presented.

DD FORM 1 JAN 64 1473

Unclassified

Security Classification

Unclassified

Security Classification

14. KEY WORDS	LINK A		LINK B		LINK C	
	ROLE	WT	ROLE	WT	ROLE	WT
Rotational Noise Theory Lifting Rotors H-34/HU-1 Helicopters Various Forward Speeds Trend Studies Sound Levels Fourier Analysis Numerical Integration Near and Far Field						

INSTRUCTIONS

1. ORIGINATING ACTIVITY: Enter the name and address of the contractor, subcontractor, grantee, Department of Defense activity or other organization *(corporate author)* issuing the report.

2*a*. REPORT SECURITY CLASSIFICATION: Enter the overall security classification of the report. Indicate whether "Restricted Data" is included. Marking is to be in accordance with appropriate security regulations.

2*b*. GROUP: Automatic downgrading is specified in DoD Directive 5200.10 and Armed Forces Industrial Manual. Enter the group number. Also, when applicable, show that optional markings have been used for Group 3 and Group 4 as authorized.

3. REPORT TITLE: Enter the complete report title in all capital letters. Titles in all cases should be unclassified. If a meaningful title cannot be selected without classification, show title classification in all capitals in parenthesis immediately following the title.

4. DESCRIPTIVE NOTES: If appropriate, enter the type of report, e.g., interim, progress, summary, annual, or final. Give the inclusive dates when a specific reporting period is covered.

5. AUTHOR(S): Enter the name(s) of author(s) as shown on or in the report. Enter last name, first name, middle initial. If military, show rank and branch of service. The name of the principal author is an absolute minimum requirement.

6. REPORT DATE: Enter the date of the report as day, month, year; or month, year. If more than one date appears on the report, use date of publication.

7*a*. TOTAL NUMBER OF PAGES: The total page count should follow normal pagination procedures, i.e., enter the number of pages containing information.

7*b*. NUMBER OF REFERENCES: Enter the total number of references cited in the report.

8*a*. CONTRACT OR GRANT NUMBER: If appropriate, enter the applicable number of the contract or grant under which the report was written.

8*b*, 8*c*, & 8*d*. PROJECT NUMBER: Enter the appropriate military department identification, such as project number, subproject number, system numbers, task number, etc.

9*a*. ORIGINATOR'S REPORT NUMBER(S): Enter the official report number by which the document will be identified and controlled by the originating activity. This number must be unique to this report.

9*b*. OTHER REPORT NUMBER(S): If the report has been assigned any other report numbers *(either by the originator or by the sponsor)*, also enter this number(s).

10. AVAILABILITY/LIMITATION NOTICES: Enter any limitations on further dissemination of the report, other than those imposed by security classification, using standard statements such as:

(1) "Qualified requesters may obtain copies of this report from DDC."

(2) "Foreign announcement and dissemination of this report by DDC is not authorized."

(3) "U. S. Government agencies may obtain copies of this report directly from DDC. Other qualified DDC users shall request through _____."

(4) "U. S. military agencies may obtain copies of this report directly from DDC. Other qualified users shall request through _____."

(5) "All distribution of this report is controlled. Qualified DDC users shall request through _____."

If the report has been furnished to the Office of Technical Services, Department of Commerce, for sale to the public, indicate this fact and enter the price, if known.

11. SUPPLEMENTARY NOTES: Use for additional explanatory notes.

12. SPONSORING MILITARY ACTIVITY: Enter the name of the departmental project office or laboratory sponsoring *(paying for)* the research and development. Include address.

13. ABSTRACT: Enter an abstract giving a brief and factual summary of the document indicative of the report, even though it may also appear elsewhere in the body of the technical report. If additional space is required, a continuation sheet shall be attached.

It is highly desirable that the abstract of classified reports be unclassified. Each paragraph of the abstract shall end with an indication of the military security classification of the information in the paragraph, represented as *(TS), (S), (C), or (U)*.

There is no limitation on the length of the abstract. However, the suggested length is from 150 to 225 words.

14. KEY WORDS: Key words are technically meaningful terms or short phrases that characterize a report and may be used as index entries for cataloging the report. Key words must be selected so that no security classification is required. Idenfiers, such as equipment model designation, trade name, military project code name, geographic location, may be used as key words but will be followed by an indication of technical context. The assignment of links, rules, and weights is optional.

Unclassified

Security Classification